AFGL-TR-81-0266
ENVIRONMENTAL RESEARCH PAPERS, NO. 763

Comparison of Ionospheric Scintillation Statistics From the North Atlantic and Alaskan Sectors of the Auroral Oval Using the Wideband Satellite

SUNANDA BASU
SANTIMAY BASU
ROBERT C. LIVINGSTON
HERBERT E. WHITNEY
EILEEN MACKENZIE

15 September 1981

SPACE PHYSICS DIVISION PROJECT 4643
AIR FORCE GEOPHYSICS LABORATORY
HANSCOM AFB, MASSACHUSETTS 01731

AIR FORCE SYSTEMS COMMAND, USAF

This report has been reviewed by the ESD Public Affairs Office (PA) and is releasable to the National Technical Information Service (NTIS).

This technical report has been reviewed and is approved for publication.

FOR THE COMMANDER

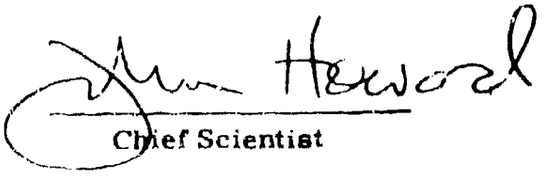

Chief Scientist

Qualified requestors may obtain additional copies from the Defense Technical Information Center. All others should apply to the National Technical Information Service.

Unclassified

SECURITY CLASSIFICATION OF THIS PAGE (When Data Entered)

REPORT DOCUMENTATION PAGE

1. REPORT NUMBER AFGL-TR-81-0266	2. GOVT ACCESSION NO AD-A111 [illegible]
4. TITLE (and Subtitle) COMPARISON OF IONOSPHERIC SCINTILLATION STATISTICS FROM THE NORTH ATLANTIC AND ALASKAN SECTORS OF THE AURORAL OVAL USING THE WIDEBAND SATELLITE	5. TYPE OF REPORT & PERIOD COVERED Scientific Interim. 6. PERFORMING ORG. REPORT NUMBER ERP No. 776
7. AUTHOR(s) Sunanda Basu*, Santimay Basu*, Robert C. Livingston**, Herbert E. Whitney, Eileen MacKenzie*	8. CONTRACT OR GRANT NUMBER(s)
9. PERFORMING ORGANIZATION NAME AND ADDRESS Air Force Geophysics Laboratory (PHY) Hanscom AFB Massachusetts 01731	10. PROGRAM ELEMENT, PROJECT, TASK AREA & WORK UNIT NUMBERS 46430505 62101F
11. CONTROLLING OFFICE NAME AND ADDRESS Air Force Geophysics Laboratory (PHY) Hanscom AFB Massachusetts 01731	12. REPORT DATE 15 September 1981 13. NUMBER OF PAGES 134
14. MONITORING AGENCY NAME & ADDRESS(if different from Controlling Office)	15. SECURITY CLASS. (of this report) Unclassified 15a. DECLASSIFICATION DOWNGRADING SCHEDULE

16. DISTRIBUTION STATEMENT (of this Report)

Approved for public release; distribution unlimited.

17. DISTRIBUTION STATEMENT (of the abstract entered in Block 20, if different from Report)

18. SUPPLEMENTARY NOTES

This work was partially sponsored by the Defense Nuclear Agency, Subtask 125AAXHX and the Space Division, Project 2029 under contract F19628-81-K-0011.

*Emmanuel College, Boston, Mass. **SRI International, Menlo Park, Calif.

19. KEY WORDS (Continue on reverse side if necessary and identify by block number)

Amplitude scintillation
Phase scintillation
F-region irregularities
High-latitude irregularities
Signal statistics
Auroral region
Alaskan sector
Atlantic sector
Magnetic index
Ionospheric scintillation statistics

20. ABSTRACT (Continue on reverse side if necessary and identify by block number)

Phase and amplitude scintillation measurements made at 138 MHz at two widely separated auroral stations, Goose Bay, Labrador, and Anchorage, Alaska, are presented. The phase coherent transmissions obtained from the sun-synchronous Wideband satellite were used for this purpose. The data were obtained for part of the year 1979 during a high sunspot epoch and was terminated by the failure of the Wideband satellite in August, 1979. The primary objective of the report is the presentation of scintillation statistics

DD FORM 1 JAN 73 1473

Unclassified

SECURITY CLASSIFICATION OF THIS PAGE When Data Entered

20. Abstract (Continued)

in a manner required for communications system planning. The morphology at the two stations was found to be significantly different with more nighttime scintillations observed at Goose Bay, while many more daytime scintillations were observed at Anchorage during the same season. The report establishes the existence of L-shell aligned sheets in the daytime in addition to the well-established similar geometry at night. The existence of sheetlike irregularities during the daytime well-equatorward of the auroral oval is significant both from modeling and physical standpoints.

Preface

This report was made possible by the contributions of many individuals and organizations. M. D. Cousins of SRI International was responsible for instrumentation and installation; Canadian Marconi Company for running the Goose Bay observational program; and N. Scotti of Bedford Research Associates for computer analysis.

Contents

Illustrations

Tables

Comparison of Ionospheric Scintillation Statistics From the North Atlantic and Alaskan Sectors of the Auroral Oval Using the Wideband Satellite

1. INTRODUCTION

In recent years, measurements using different techniques have shown that the earth's ionosphere contains electron density irregularities covering many decades of scale sizes. By using different techniques to probe the irregularities much progress has been achieved in the understanding of equatorial irregularities that can produce the largest effects on transionospheric propagation. Such correlated studies that combine equatorial scintillation measurements with rocket and satellite in situ, radar and airglow observations have been reviewed (Basu and Kelley, 1979[1]; Basu and Basu, 1981[2]). While the magnitude of the amplitude and phase perturbations of the signal is the largest at the equator, the high-latitude environment certainly affects the propagation channel for a much larger percentage of time. The object of this report is to describe the morphology of medium-scale irregularities (tens of km to few hundred m) in two sectors of the auroral oval as obtained from phase and amplitude scintillation measurements at 138 MHz using the orbiting Wideband satellite. It has been well-known for over a decade that

(Received for publication 15 September 1981)

1. Basu, S. and Kelley, M.C. (1979) A review of recent observations of equatorial scintillations and their relationship to current theories of F-region irregularity generation, Radio Sci. 14:471.

2. Basu, S. and Basu, S. (1981) Equatorial scintillations – a review, J. Atmos. Terr. Phys. 43:473.

amplitude scintillations can degrade the performance of satellite communication links (Aarons et al, 1969[3]; Aarons and Allen, 1971[4]). More recently, it has become clear that naturally-occurring phase scintillation can impair the performance of satellite systems that use synthetic aperture processing to achieve high angular resolution (Brown, 1976[5]).

In view of the simplicity of amplitude measurements, there exists a relatively good global coverage of such observations. On the other hand, phase scintillation measurements have been quite sparse because phase coherent transmissions and/or complex receiving systems are required. The first phase measurements were made by utilizing the 150- and 400-MHz transmissions from the U.S. Navy navigation system of satellites. In this experiment, the characteristics of phase scintillation at VHF with respect to the UHF frequency were determined for a sub-auroral location (Wand and Evans, 1975[6]; Crane, 1976[7]). Since the launch of the orbiting Wideband satellite in May, 1976, SRI International has utilized the phase coherent transmissions (10 spectral lines between VHF and S-band) to make phase scintillation measurements at VHF, UHF, and L-band with reference to S-band transmissions that, under most conditions, remain unperturbed by the ionosphere. The instrument characteristics and initial data-processing procedures have been described by Fremouw et al (1978).[8]

Morphological studies of phase and amplitude scintillation from Poker Flat (65^{0} invariant latitude) for the period 1976-78 have been presented by Rino and Matthews (1980)[9] and Fremouw et al (1980).[10] The most important feature in

3. Aarons, J., Mullen, J.P., and Whitney, H.E. (1969) The scintillation boundary, J. Geophys. Res. 74:884.

4. Aarons, J. and Allen, R.S. (1971) Scintillation boundary during quiet and disturbed magnetic conditions, J. Geophys. Res. 76:170. AFCRL-71-0101, AD 718 923.

5. Brown, W.D. (1976) Effects of atmospheric induced phase errors in synthetic aperture radar, Report SAND76-0520, Sandia Laboratory, Albuquerque, New Mexico.

6. Wand, R.H. and Evans, J.V. (1975) Morphology of ionospheric scintillation in the auroral zone, Proceedings of Symposium on Effect of the Ionosphere on Space Systems and Communications, J.M. Goodman (ed.), U.S. Govt. Printing Office, Washington, D.C.

7. Crane, R.K. (1976) Spectra of ionospheric scintillation, J. Geophys. Res. 81:2041.

8. Fremouw, E.J., Leadabrand, R.L., Livingston, R.C., Cousins, M.D., Rino, C.L., Fair, B.C., and Long, R.A. (1978) Early results from the DNA Wideband satellite experiment – complex-signal scintillation, Radio Sci. 13:167-187.

9. Rino, C.L. and Matthews, S.J. (1980) On the morphology of auroral zone radio wave scintillation, J. Geophys. Res. 85:4139.

10. Fremouw, E.J., Lansinger, J.M., and Miller, D.A. (1980) Further geophysical analysis of coherent satellite scintillation data, Annual Report, PD-NW-81-237R, Contract No. F49620-78-C-0014, Physical Dynamics, Inc., Bellevue, Washington.

the nighttime phase and amplitude data reported by these authors is the existence of a geometric enhancement caused by the presence of sheetlike irregularities aligned with the magnetic L-shells in the auroral oval (Fremouw et al, 1977[11]; Rino et al, 1978[12]). However, no seasonal variation was found as shown in Figure 1 (Fremouw and Lansinger, 1979[13]).

On the other hand, as shown in Figure 2, nighttime amplitude scintillation data from ATS-3 taken at Narssarssuaq, Greenland (350 km subionospheric intersection at 64° invariant latitude, very close to Goose Bay overhead) had shown a consistent seasonal pattern with the occurrence and magnitude of scintillations being high in the summer and low during the winter solstice (Basu, 1975[14]; Basu and Aarons, 1980[15]). Basu (1975)[14] had established that this seasonal behavior of scintillations during quiet times, namely a winter minimum and summer maximum, is in close agreement with the variation of the auroral electrojet index AL (Davis and Sugiura, 1966[16]) in the same sector of the auroral oval. Following the suggestion of Boller and Stolov (1970,[17] 1974[18]) it was proposed by Basu that the varying geometry of the plasma sheet with the dipole tilt angle may cause a seasonal modulation of particle precipitation and, hence, of scintillations. If this hypothesis is correct, no such marked seasonal variation should be observed in the Alaskan and Scandinavian sectors of the oval. Thus, it is encouraging to note that no marked seasonal variation was observed in the Alaskan sector.

It was hoped that a Wideband station in the North Atlantic sector of the oval would determine whether the seasonal variation shown by the amplitude scintillation

11. Fremouw, E.J., Rino, C.L., Livingston, R.C., and Cousins, M.D. (1977) A persistent subauroral scintillation enhancement observed in Alaska, Geophys. Res. Lett. 4:539.

12. Rino, C.L., Livingston, R.C., and Matthews, S.J. (1978) Evidence for sheet-like auroral ionospheric irregularities, Geophys. Res. Lett. 5:1039.

13. Fremouw, E.J. and Lansinger, J.M. (1979) Continued geophysical analysis of coherent satellite scintillation data, Annual Report, PD-NW-79-213R, Contract F49620-78-C-0014, Physical Dynamics, Inc., Bellevue, Washington.

14. Basu, Sunanda (1975) Universal time seasonal variations of auroral zone magnetic activity and VHF scintillations, J. Geophys. Res. 80:4725-4728. AFGL-TR-76-0114, AD A025 579.

15. Basu, S., and Aarons, J. (1980) The morphology of high-latitude VHF scintillation near 70°W, Radio Sci. 15:59. AFGL-TR-80-0145, AD A084 298.

16. Davis, T.N. and Sugiura, M. (1966) Auroral electrojet activity index AE and its universal time variations, J. Geophys. Res. 71:785-801.

17. Boller, B.R. and Stolov, H.L. (1970) Kelvin-Helmholtz instability and the semi-annual variation of geomagnetic activity, J. Geophys. Res. 75:6073.

18. Boller, B.R. and Stolov, H.L. (1974) Investigation of the association of magnetopause instability with interplanetary sector structure, J. Geophys. Res. 79:673.

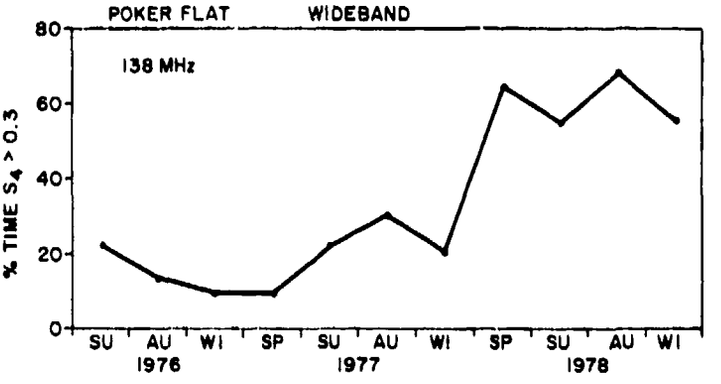

Figure 1. Seasonal Variation of Amplitude Scintillation in the Alaskan Sector as Obtained from Wideband Data Taken at Poker Flat, Alaska

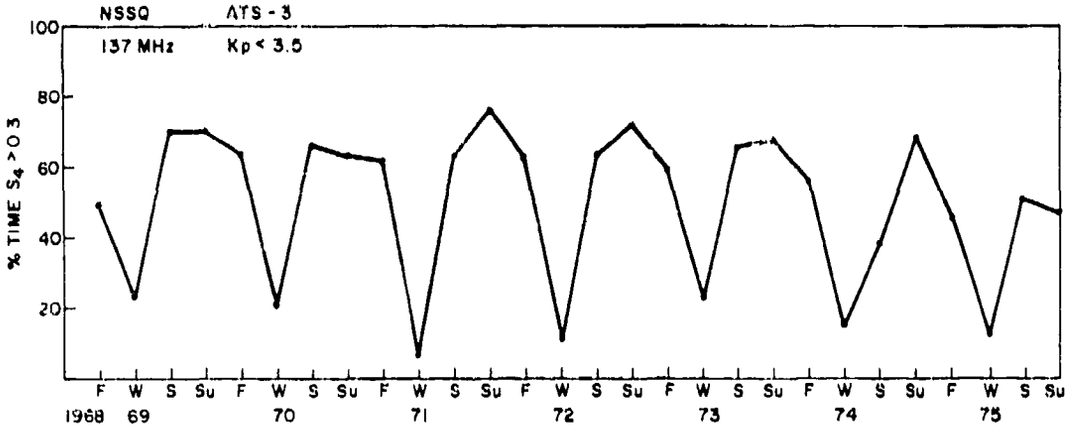

Figure 2. Seasonal Variation of Amplitude Scintillations in the North Atlantic Sector as Obtained from ATS-3 Data Taken at Narssarssuaq, Greenland

is also observed in the phase scintillation data. Furthermore, the data would be able to confirm the existence of sheetlike irregularities observed most noticeably in the phase data in the Alaskan sector. On the basis of amplitude scintillation data from the North Atlantic sector Martin and Aarons (1977)[19] had earlier postulated the existence of sheetlike irregularities.

---

19. Martin, E. and Aarons, J. (1977) F-layer scintillations and the aurora, J. Geophys. Res. 82:2717-2722. AFGL-TR-77-0182, AD A043 623.

With the above dual objectives in mind, modified Wideband receivers known as the Micro-Wideband system started operation in January, 1979, at Goose Bay, Labrador and at Anchorage, Alaska, so that a comparison of scintillation behavior in the two sectors on same days could be made. Table 1 gives the geographic and magnetic coordinates of the two stations. It was hoped that Anchorage being a few degrees lower in latitude than Poker Flat would be better able to resolve the plasmaspheric component of scintillations that was observed at low elevation angles to the south of Poker Flat (Rino and Matthews, 1980[9]). It had been proposed to keep the Goose Bay Wideband station operational to provide a long-term comparison with Poker Flat data. Unfortunately the failure of the Wideband satellite early in August, 1979, terminated the Goose Bay measurements only after an approximately six-month operation while the Anchorage receiver was operated from January to April, 1979. It is this limited data set from these two stations that will form the basis of the report. The positions of Goose Bay with respect to the Q=3 auroral oval at midnight and noon are shown in Figure 3 on an invariant latitude – magnetic local time grid. From Table 1 we find that Anchorage is about 4° further equatorward of the Goose Bay position so that it is south of the auroral oval at midnight even for moderate magnetic activity ($Q \sim 3$).

Table 1. Goose Bay and Anchorage Coordinates

	Geographic Coordinates	Invariant Latitude	L Value
Goose Bay	53.3°N; 60.3°W	64.17°	5.2
Anchorage	61.2°N; 149.9°W	60.44°	4.11

2. RECEIVING SYSTEM

The Micro-Wideband system differs from the original Wideband system in that it receives only the four lowest coherent frequencies of the Wideband-beacon satellite: 138 MHz, 378 MHz, 390 MHz, and 402 MHz. By locking onto the 402-MHz signal and synthesizing the necessary references in the receiver, both phase and amplitude measurements can be made at the three lower frequencies. To do this, the quadrature components of the signal at each of these frequencies are recorded as a function of time, and each record is digitized at the rate of 100 samples per sec (Livingston, 1979[20]).

---

20. Livingston, R.C. (1979) Micro-Wideband analysis summary output – Wideband beacon, Technical Memorandum, SRI International, Menlo Park, California.

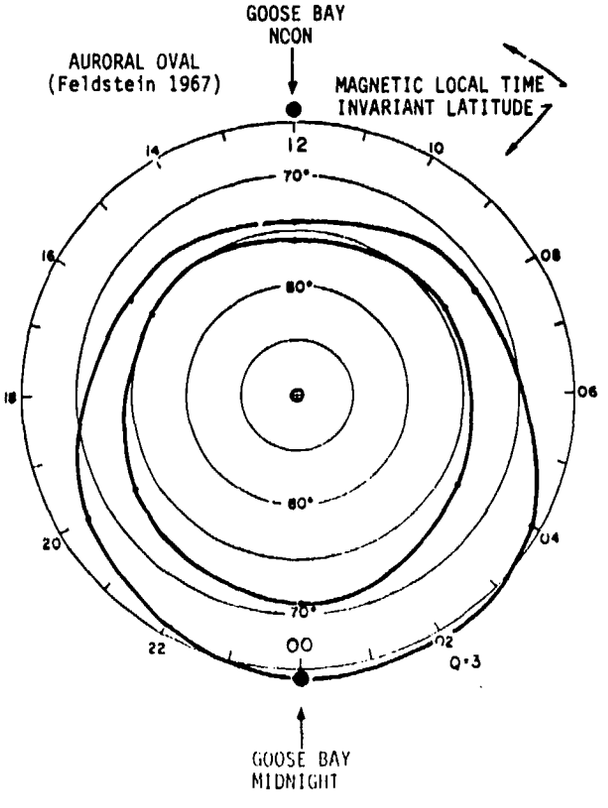

Figure 3. The Position of the Goose Bay Station at Magnetic Midnight and Noon with Respect to the Q=3 Auroral Oval

As with the original Wideband data (Fremouw et al, 1978[8]), the generation of summary statistics is preceded by separating the long-term, deterministic trend from the scintillation components. This is done by initially smoothing the intensity and phase, using a 6-pole, low-pass Butterworth filter with a cutoff of 0.1 Hz. The smoothed phase is subtracted from the raw phase, while the raw intensity is divided by the smoothed intensity. This results in a continuous data record of zero mean phase and unity mean intensity. The detrending process has little effect on the intensity spectrum, which is already cutoff by the ionosphere at frequencies higher than 0.1 Hz by Fresnel filtering. Any low frequency trends, such as antenna pattern variations, are removed. The phase spectrum, on the other hand, displays large spectral intensities at frequencies well below

21. Feldstein, Y.I. and Starkov, G.V. (1967) Dynamics of auroral belt and polar geomagnetic disturbances, Planet. Space Sci. 15:209.

the 0.1 Hz cutoff. Following the SRI convention, fluctuations that occur in the domain greater than 0.1 Hz are called scintillation and those less than 0.1 Hz are called trend. These definitions are arbitrary, but convenient.

3. DEFINITION OF STATISTICAL PARAMETERS

In this section the different parameters that quantize the phase and amplitude scintillation measurements will be defined so that, particularly in the case of phase measurements, the effects of the data filtering on the phase scintillation magnitudes may be understood. The terminology and method of calculation of statistical parameters are as follows:

3.1 RMS Phase Deviation

Standard deviation of detrended phase component is calculated as

$$\sigma_\phi = (\langle\phi^2\rangle - \langle\phi\rangle^2)^{1/2} \tag{1}$$

in radians, as measured at the receiver output, and not corrected for the finite reference frequency. Note that this parameter is dependent upon the detrend cutoff frequency. Before the median σ_ϕ values, as shown in the next section, were calculated they were corrected for the finite receiver reference frequency of 402 MHz in the following manner. Assuming a f^{-2} dependence of the phase variance as has been displayed by the Wideband data, the measured phase deviation is related to the true value of σ_ϕ as

$$\sigma_{\phi_{meas}} = \sigma_\phi(1 - n^{-2}) \quad , \tag{2}$$

where n is the ratio of the reference frequency to the measurement frequency. For Micro-Wideband, the measured VHF phase deviation is not drastically altered at 0.88 of its true value. However, the UHF deviations are decreased to 0.12 and 0.06 of their true magnitudes at 378 MHz and 390 MHz, respectively. Thus, even under strong scatter conditions the observed UHF phase deviations are small and unreliable. For this reason only the 138-MHz phase (and amplitude) data are presented in the next section.

3.2 Phase Spectral Slope and Strength

We assume a power-law form of the phase power spectrum, as has been displayed by Wideband data, in the form

$$\Phi_\phi(f) = T_\phi f^{p_\phi} \quad , \tag{3}$$

where p_ϕ is the slope, and T_ϕ is the strength in mks units. These parameters are extracted from a linear least-squares fit to the plot of log of phase power spectral density vs log of frequency over the range of 0.5 to 5 Hz, as demonstrated in Figure 4. The T_ϕ values given in the next section are the spectral strengths obtained at 1 Hz.

The advantage of using T_ϕ and p_ϕ is that they characterize the phase disturbance independent of the detrend cutoff, unlike σ_ϕ. Generally the T_ϕ and p_ϕ are consistent with σ_ϕ, although σ_ϕ can include energy outside of the slope-fit range. It is therefore recommended that σ_ϕ, T_ϕ, and p_ϕ all be considered together. The spectral strengths, T_ϕ and $T_{\phi_{meas}}$, are related as follows:

$$T_{\phi_{meas}} = T_\phi(1 - n^{-2})^2 \quad . \tag{4}$$

3.3 S_4 Scintillation Index

The normalized standard deviation of intensity is given by

$$S_4 = \left[\left(\langle I^2\rangle - \langle I\rangle^2\right)/\langle I\rangle^2\right]^{1/2} \quad , \tag{5}$$

which ranges from 0 to above 1.2 from quiet to strong scatter conditions. The S_4 index was first introduced by Briggs and Parkin (1963).[22]

3.4 Intensity Spectral Slope and Strength

Except under weak scatter conditions, the intensity power spectrum will not be power law. This characterization is of the high-frequency end (5 to 40 Hz) of the intensity spectrum which may or may not be linear:

$$\Phi_I(f) = T_I f^{p_I} \quad , \tag{6}$$

where p_I is the slope, and T_I the strength of the intensity spectrum. The fit is illustrated in Figure 5. As with T_ϕ of Eq. (3), T_I is given in mks units and is evaluated at 1 Hz by extrapolation of the linear least-squares fit of the spectrum between 5 and 40 Hz.

---

22. Briggs, B.H. and Parkin, I.A. (1963) On the variation of radio star and satellite scintillation with zenith angle, J. Atmos. Terr. Phys. 25:339.

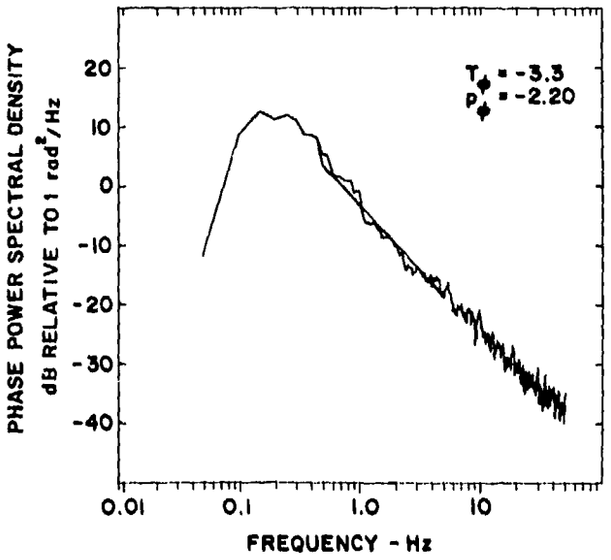

Figure 4. Sample Power Spectrum of Phase Scintillations Obtained With the Micro-Wideband System (Day 90, 050320-050339 UT) ϕ = 3.2 radians, T_ϕ = -3.3 dB, p_ϕ = -2.2

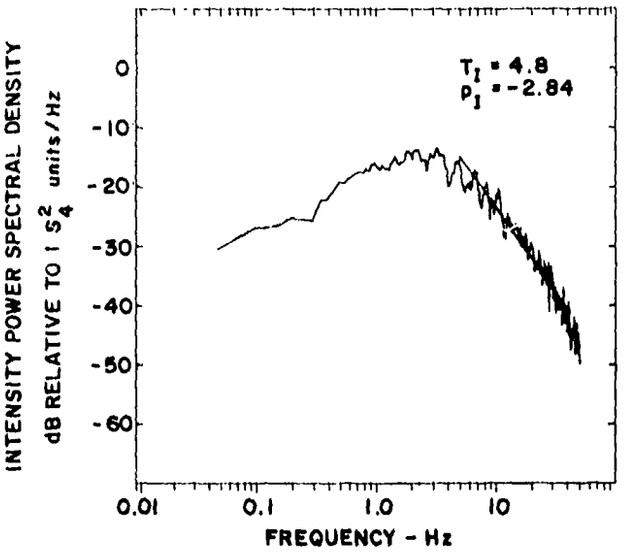

Figure 5. Sample Power Spectrum of Amplitude Scintillations Corresponding to Phase Spectrum Shown in Figure 4. S_4 = 0.62, T_I = 4.8 dB, p_I = -2.8

4. RESULTS

With the user in mind, the statistical results of the spatial and temporal variation of 20-sec values of phase and amplitude scintillation parameters observed t the Goose Bay and Anchorage stations will be given in the form of a large number of graphs. To bring out the importance of the geometry of observations, we shall present both the nighttime and daytime data in three groups sorted according to different UT time intervals. Because of the sun-synchronous nature of the satellite orbit (inclination 99°) the three UT groupings in each category represent passes in three distinct corridors with the earliest time interval corresponding to passes to the east, the middle interval to overhead passes, and the latest times to passes in the west. Figures 6 and 7 show typical nighttime and daytime subionospheric tracks (at 350 km altitude) of the Wideband satellite in each of the three corridors for the Goose Bay station. The magnetic midnight at Goose Bay is 0310 UT while the local time is UT-4 hours. Thus the nighttime passes occur approximately during premidnight, midnight, and postmidnight hours, respectively, while the morning passes occur within the morning to noon local time sector. The nighttime passes progress from north to south and vice versa for the daytime passes. Figures 8 and 9 show such typical passes for Anchorage, where magnetic midnight is 1115 UT and local time is UT-10 hours.

The basic format chosen for presenting the data is in the form of subionospheric invariant latitude plots of the scintillation parameters. The invariant latitude, as is well-known, is defined by

$$\Lambda = \cos^{-1} L^{-1/2} \quad , \tag{7}$$

where L is the McIlwain (1961)[23] L-parameter. Twenty-second values of σ_ϕ, T_ϕ, p_ϕ, S_4, T_I, and p_I as defined in the last section are sorted into 1° invariant latitude bins for Kp < 3.5 (2° bins for Kp > 3.5) and the 50, 90, and 99 percentile occurrence statistics are computed. The 99 percentile occurrence is labeled as a "worst case" situation when the number of data points in the bin is less than 100. Only the 50 percentile curve is extended to cover latitude bins having at least five points. The lowest and highest number of 20-sec values per latitude bin are specified on the graphs to give an idea of the size of the data base.

---

23. McIlwain, C. E. (1961) Coordinates for mapping the distribution of magnetically trapped particles, J. Geophys. Res. 66:3681.

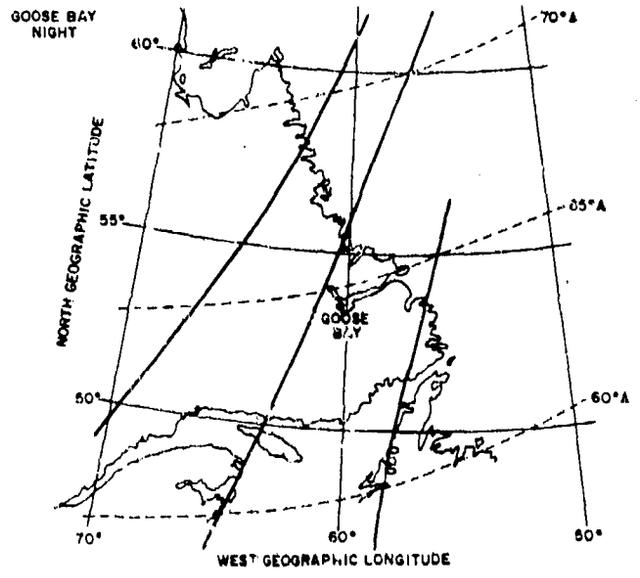

Figure 6. Subionospheric Tracks at 350 km Altitude of Typical Nighttime Wideband Passes in the Eastern, Overhead and Western Corridors Observed in the Goose Bay Sector

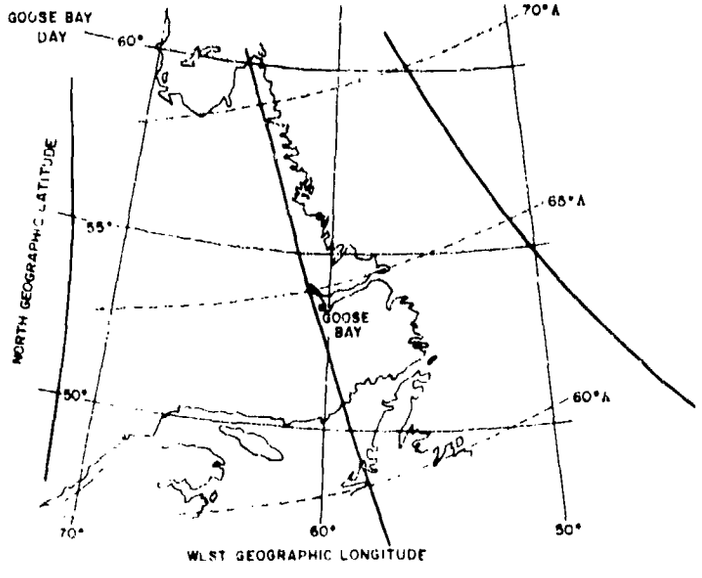

Figure 7. Subionospheric Tracks at 350 km Altitude of Typical Daytime Wideband Passes in the Eastern, Overhead, and Western Corridors Observed in the Goose Bay Sector

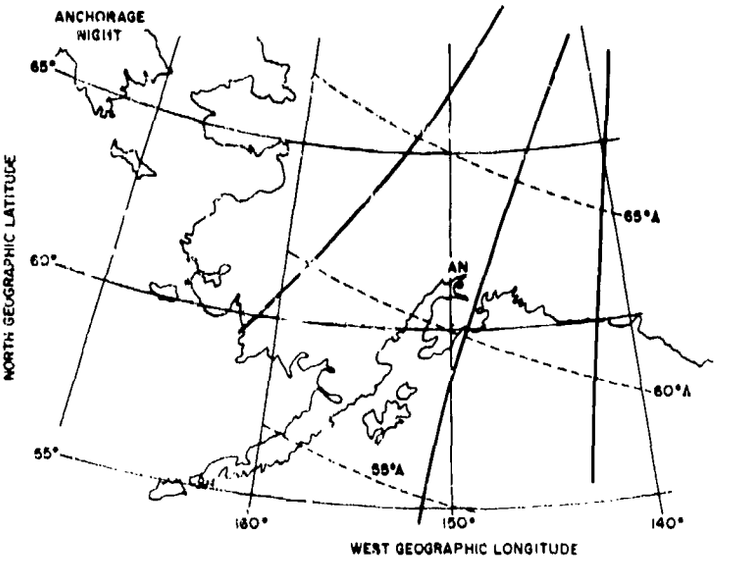

Figure 8. Subionospheric Tracks at 350 km Altitude of Typical Nighttime Wideband Passes in the Eastern, Overhead, and Western Corridors Observed in the Anchorage Sector

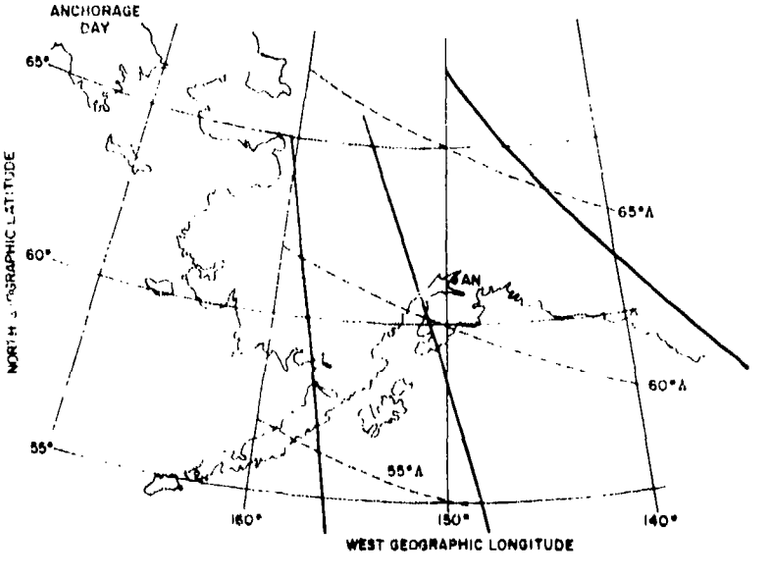

Figure 9. Subionospheric Tracks at 350 km Altitude of Typical Daytime Wideband Passes in the Eastern, Overhead, and Western Corridors Observed in the Anchorage Sector

4.1 Nighttime Phase Statistics at Goose Bay

The phase scintillation σ_ϕ in radians for magnetically quiet (Kp < 3.5) nighttime 138-MHz Goose Bay Wideband passes is plotted on a semilogarithmic scale vs invariant latitude in Figures 10a, 11a, and 12a for the three corridors previously defined. Similar graphs for the disturbed cases (Kp > 3.5) are shown in Figures 10b, 11b, and 12b. A logarithmic scale was chosen to accommodate the large range of phase scintillation values observed. The major point of interest is the geometrical enhancement in the 63-64° latitude bin in the quiet cases and in the 63-65° bin in the disturbed cases. For the overhead geometry the "worst case" phase fluctuation may be as large as 20 rad in the region of geometrical enhancement. However, the median values are generally less than a rad outside of the enhancement region. This enhancement for Goose Bay is most marked for the eastern and, of course, the overhead corridors. It is interesting to note that the magnetic azimuth of the propagation vector changes with altitude in the western corridor where the geometrical enhancement is least. Thus in the western corridor the ray path does not align itself along a particular L-shell over a large altitude range, thereby tending to smear out the geometrical enhancement. Indeed, a smearing effect is observed in Figure 12a, with a plateau of relatively high values being observed near the geometrical enhancement region rather than one prominent peak.

The paucity of data makes the latitude coverage during magnetically disturbed conditions much smaller. The lower-latitude end shows a relatively greater enhancement of phase scintillations at such times.

It has been pointed out in the last section that σ_ϕ depends on the detrend interval used for filtering the raw data. Figures 13a, 13b, 14a, 14b, 15a, and 15b give the respective T_ϕ values at 1 Hz that are free of any filtering effects. Thus, these values in conjunction with p_ϕ values shown in Figures 16a, 16b, 17a, 17b, 18a, and 18b can be used to estimate σ_ϕ according to the specific system integration requirements. Only the overhead values of T_ϕ under both quiet and disturbed conditions shown in Figures 14a and 14b show a geometrical enhancement. This tends to indicate that the geometrical enhancement seen in σ_ϕ in the eastern corridor comes from spectral frequencies between 0.1-1 Hz.

The median p_ϕ curves uniformly show a value slightly exceeding 2, actually between 2.2-2.3 rather than a value of 3, which is to be expected from a one-dimensional in-situ spectral index of 2 reported earlier (Dyson et al, 1974[24];

---

24. Dyson, P.L., McClure, J.P., and Hanson, W.B. (1974) In-situ measurements of the spectral characteristics of ionospheric irregularities, J. Geophys. Res. 79:1497.

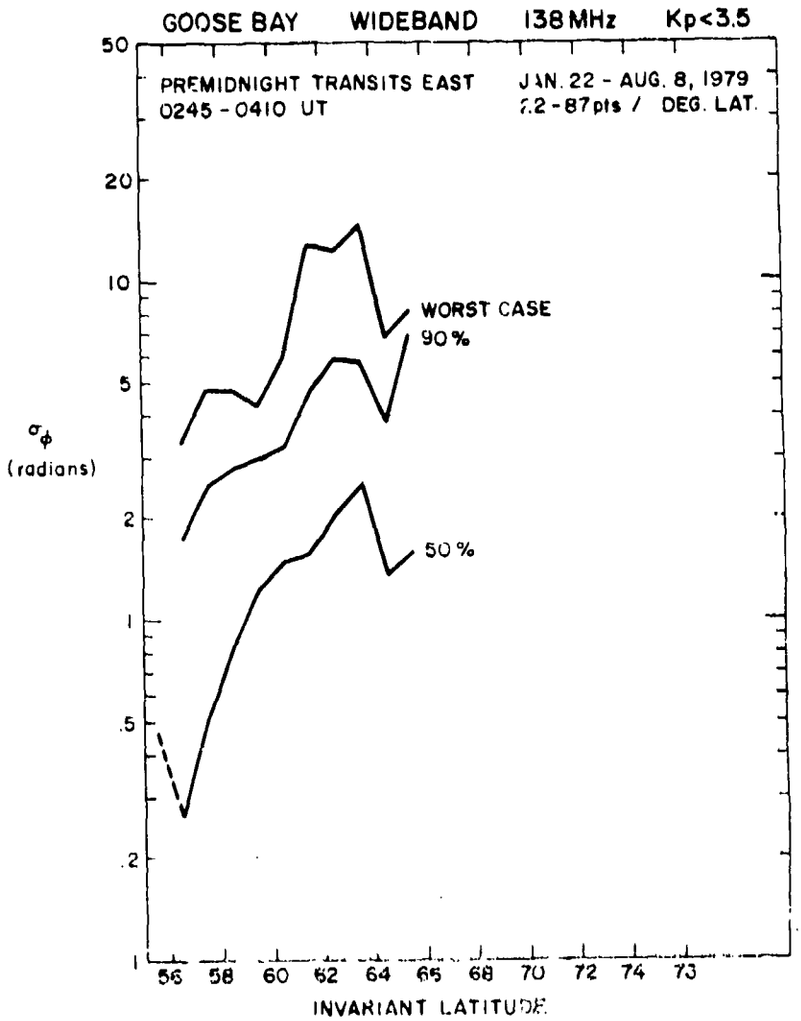

Figure 10a. Phase Scintillation Index σ_ϕ vs. Invariant Latitude for Nighttime Transits East of Goose Bay Under Quiet Magnetic Condition.

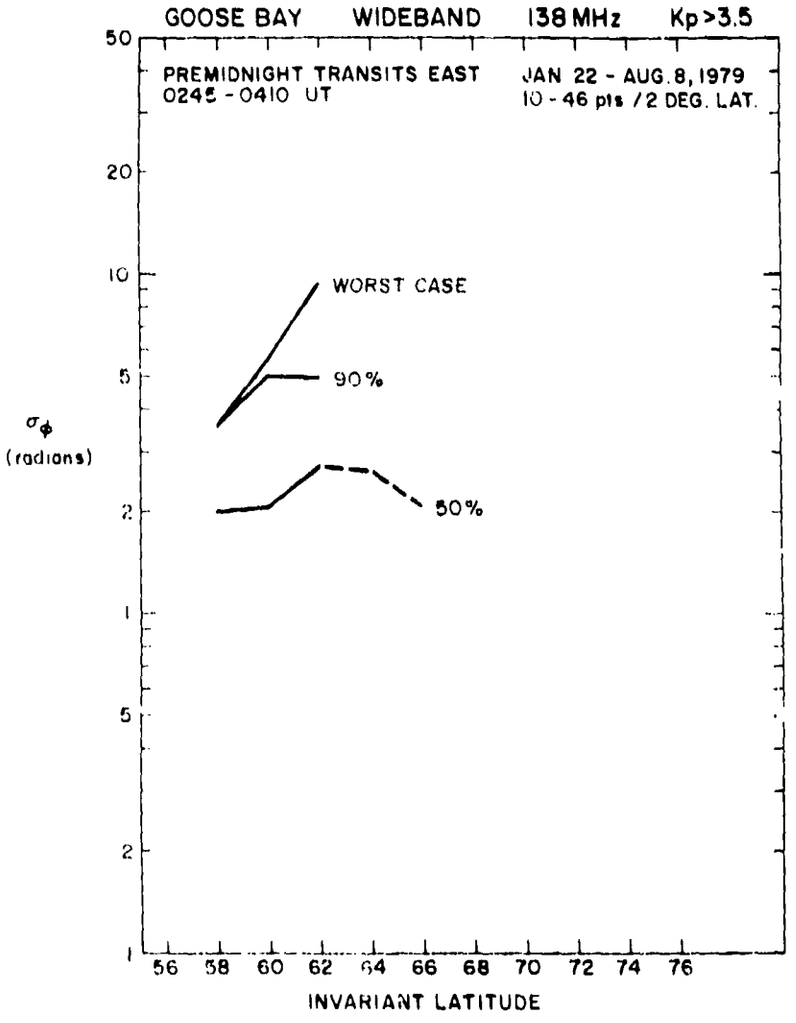

Figure 10b. Phase Scintillation Index σ_ϕ vs. Invariant Latitude for Nighttime Transits East of Goose Bay Under Disturbed Magnetic Conditions

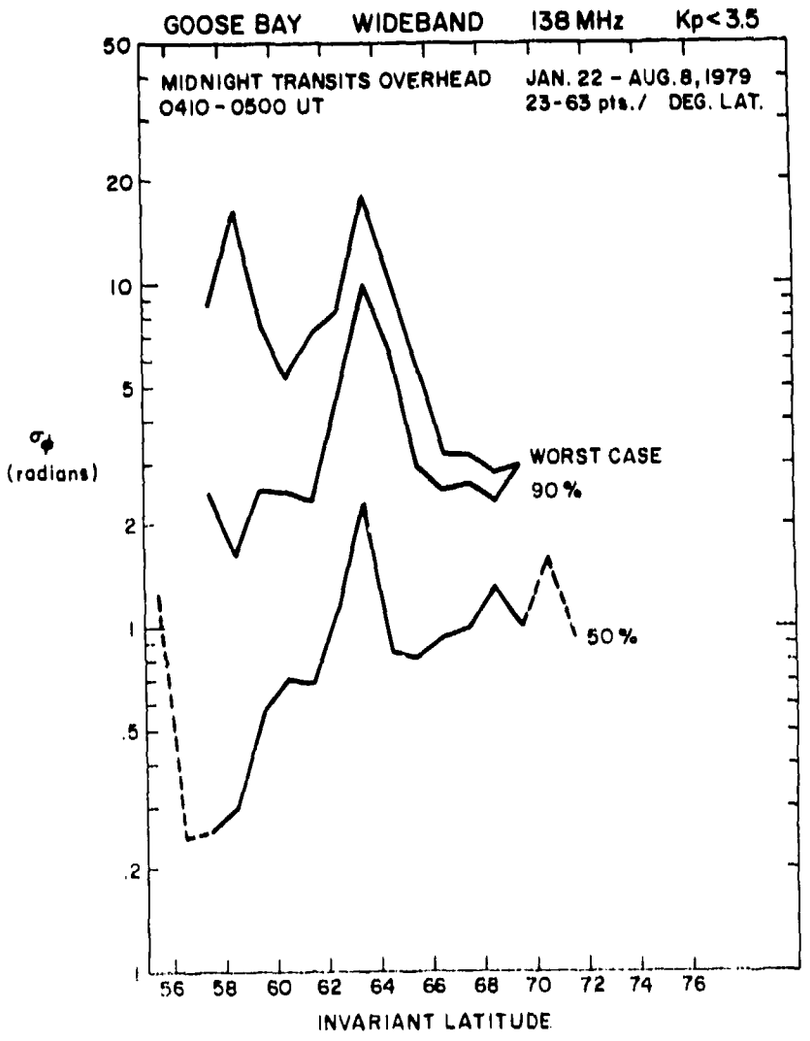

Figure 11a. Phase Scintillation Index σ_ϕ vs. Invariant Latitude for Nighttime Transits Overhead of Goose Bay Under Quiet Magnetic Conditions

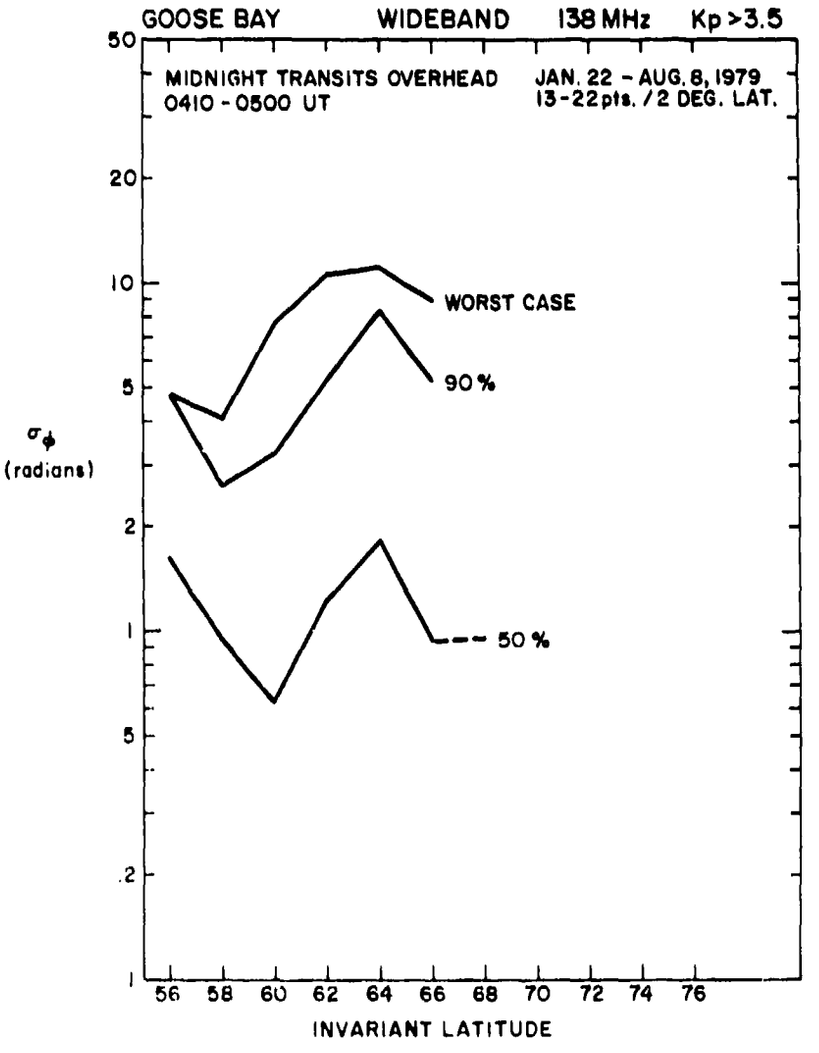

Figure 11b. Phase Scintillation Index σ_ϕ vs. Invariant Latitude for Nighttime Transits Overhead of Goose Bay Under Disturbed Magnetic Conditions

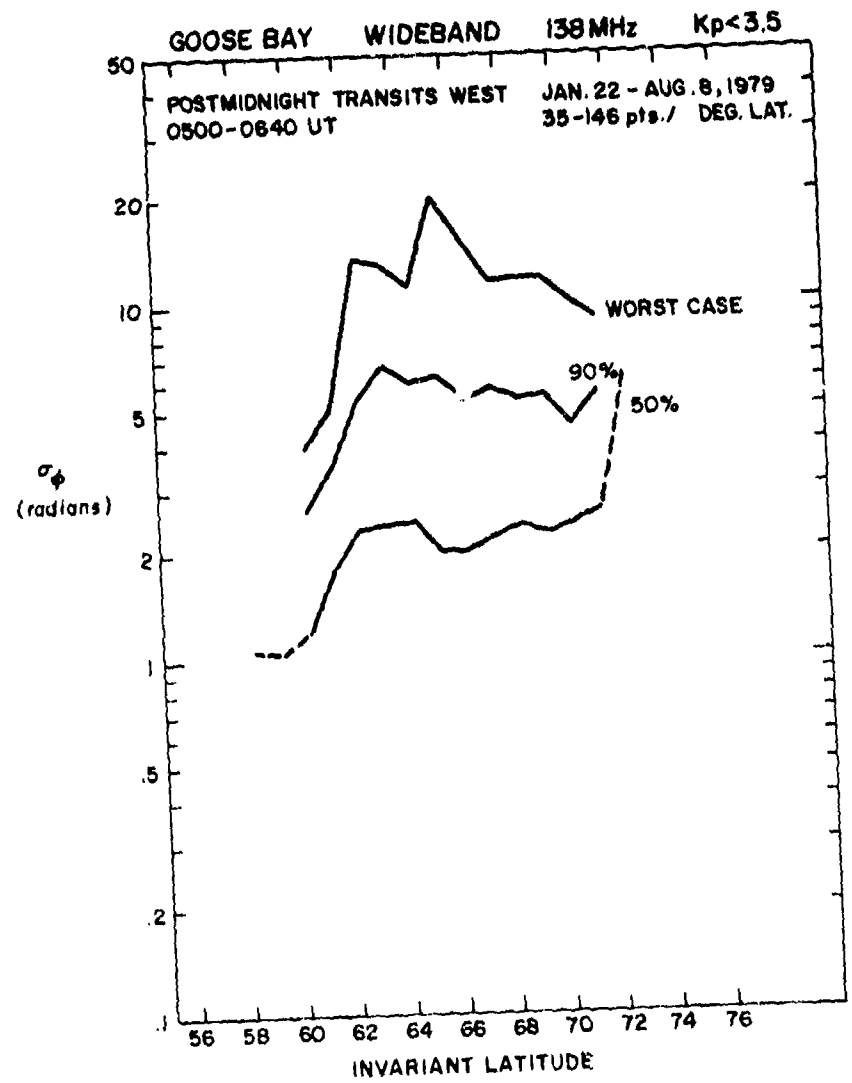

Figure 12a. Phase Scintillation Index σ_ϕ vs. Invariant Latitude for Nighttime Transits West of Goose Bay Under Quiet Magnetic Conditions

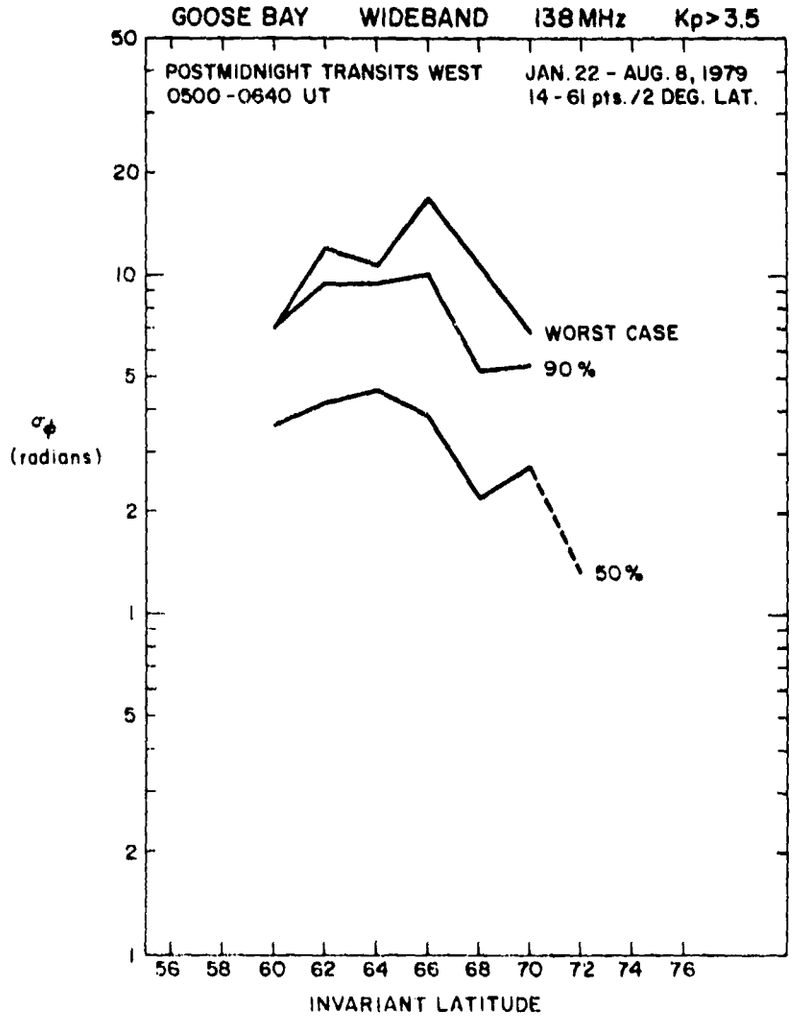

Figure 12b. Phase Scintillation Index σ_ϕ vs. Invariant Latitude for Nighttime Transits West of Goose Bay Under Disturbed Magnetic Conditions

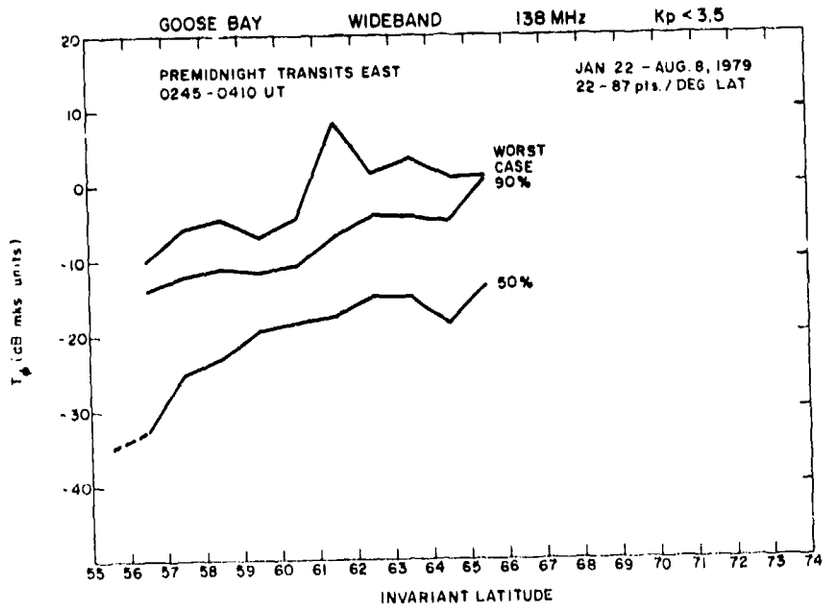

Figure 13a. Spectral Strength T_ϕ of Phase at 1 Hz vs. Invariant Latitude for Nighttime Transits East of Goose Bay Under Quiet Magnetic Conditions

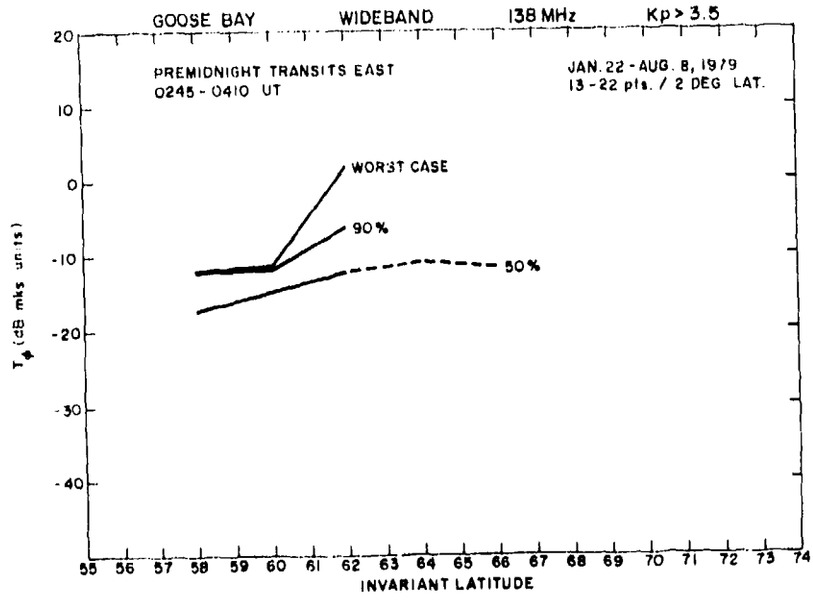

Figure 13b. Spectral Strength T_ϕ of Phase at 1 Hz vs. Invariant Latitude for Nighttime Transits East of Goose Bay Under Disturbed Magnetic Conditions

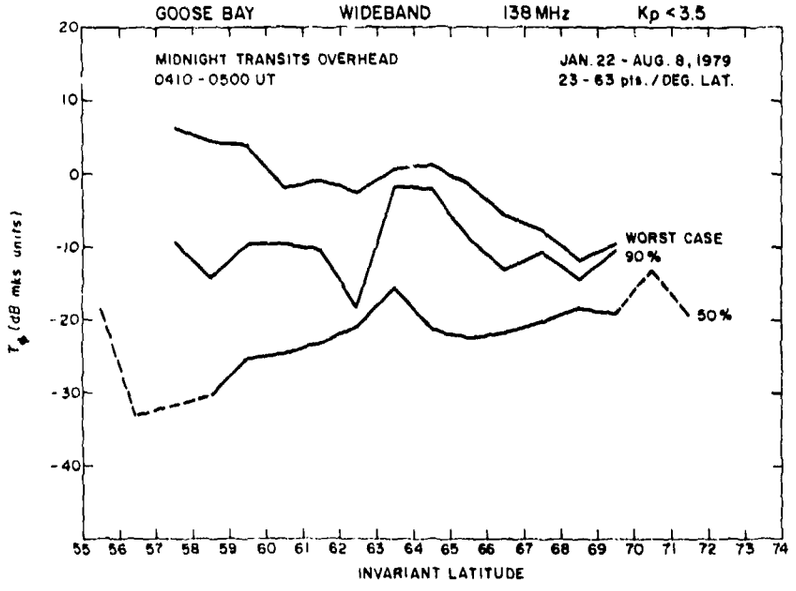

Figure 14a. Spectral Strength T_ϕ of Phase at 1 Hz vs. Invariant Latitude for Nighttime Transits Overhead of Goose Bay Under Quiet Magnetic Conditions

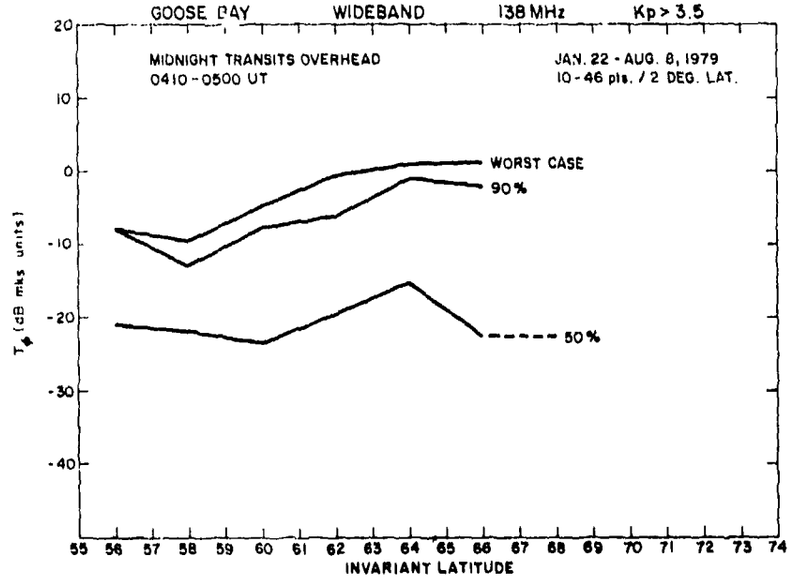

Figure 14b. Spectral Strength T_ϕ of Phase at 1 Hz vs. Invariant Latitude for Nighttime Transits Overhead of Goose Bay Under Disturbed Magnetic Conditions

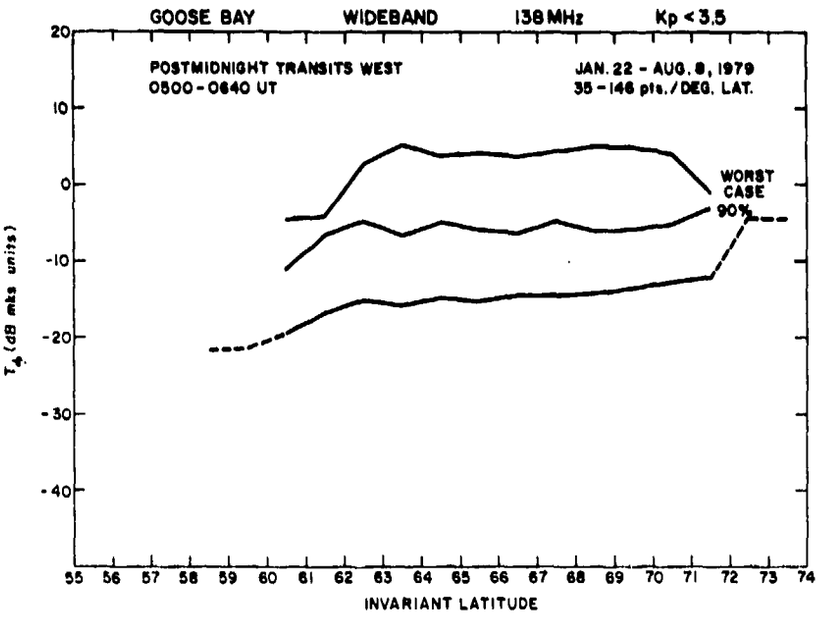

Figure 15a. Spectral Strength T_ϕ of Phase at 1 Hz vs. Invariant Latitude for Nighttime Transits West of Goose Bay Under Quiet Magnetic Conditions

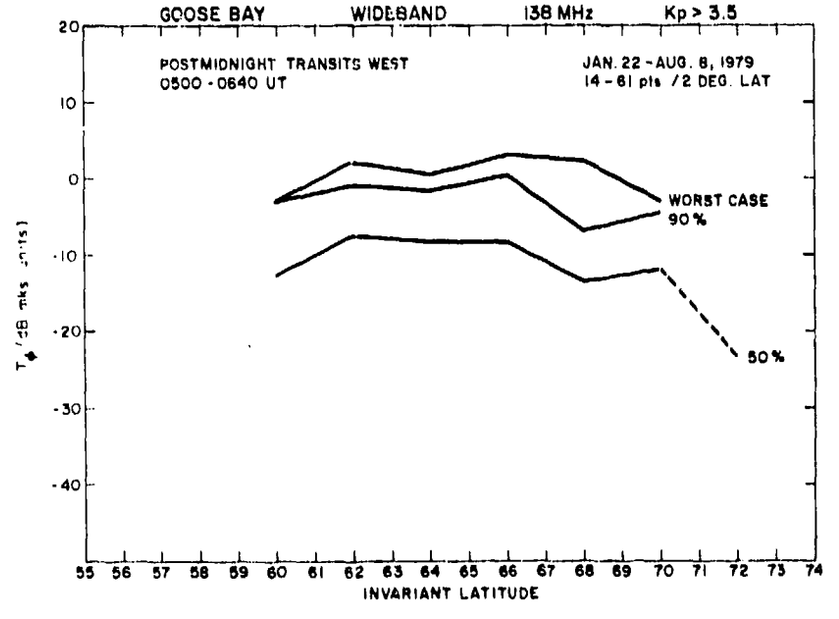

Figure 15b. Spectral Strength T_ϕ of Phase at 1 Hz vs. Invariant Latitude for Nighttime Transits West of Goose Bay Under Disturbed Magnetic Conditions

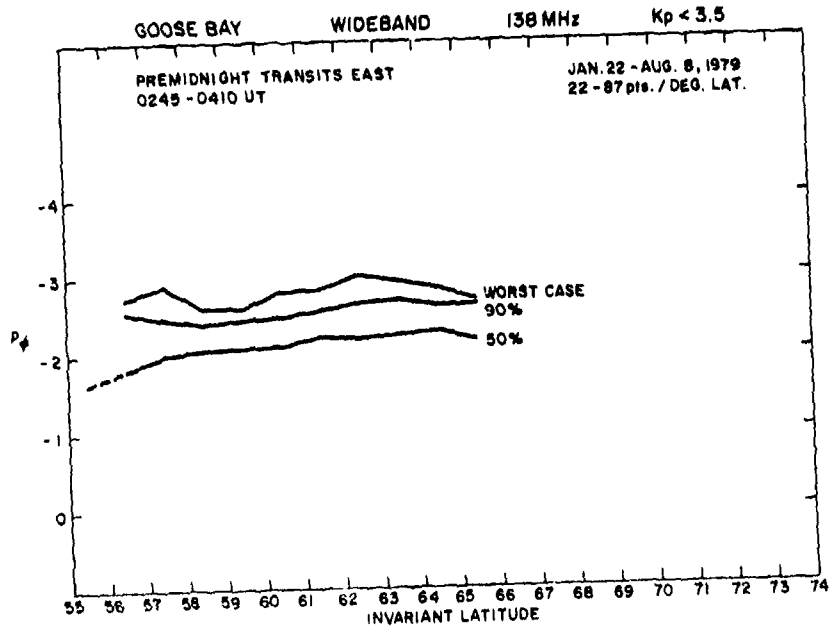

Figure 16a. Phase Spectral Index p_ϕ vs. Invariant Latitude for Nighttime Transits East of Goose Bay Under Quiet Magnetic Conditions

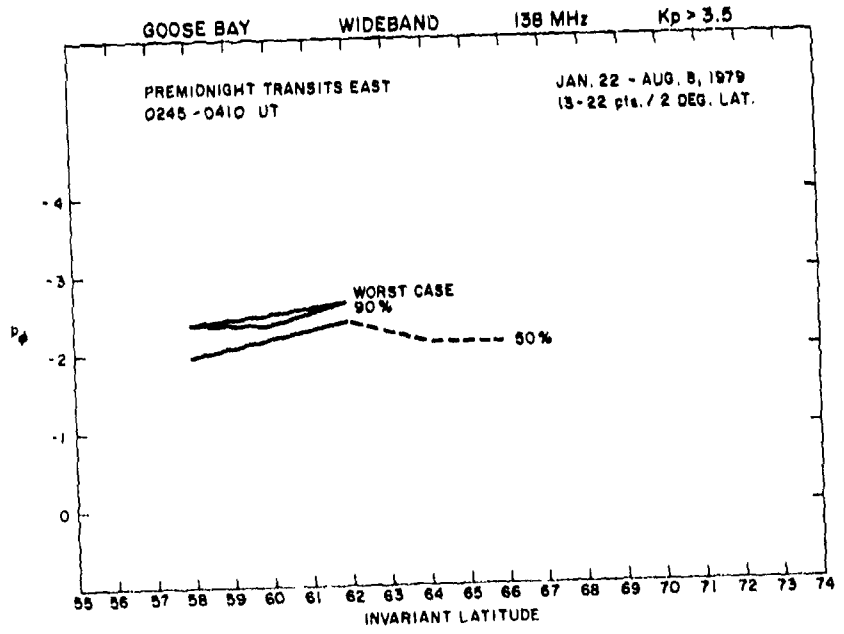

Figure 16b. Phase Spectral Index p_ϕ vs. Invariant Latitude for Nighttime Transits East of Goose Bay Under Disturbed Magnetic Conditions

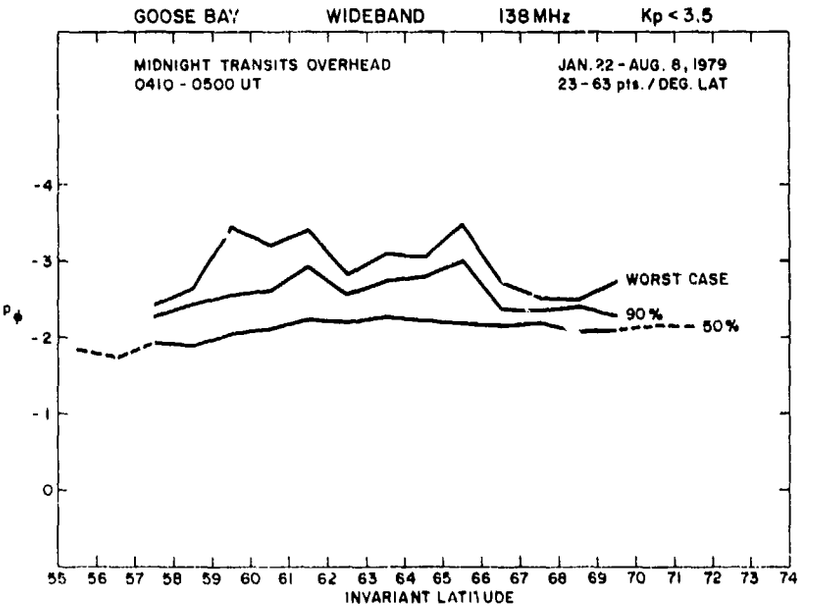

Figure 17a. Phase Spectral Index p_ϕ vs. Invariant Latitude for Nighttime Transits Overhead of Goose Bay Under Quiet Magnetic Conditions

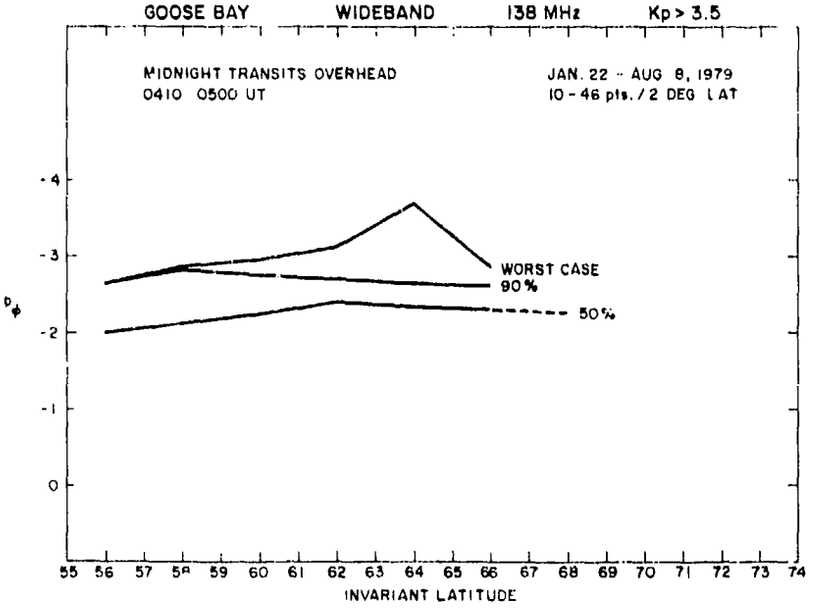

Figure 17b. Phase Spectral Index p_ϕ vs. Invariant Latitude for Nighttime Transits Overhead of Goose Bay Under Disturbed Magnetic Conditions

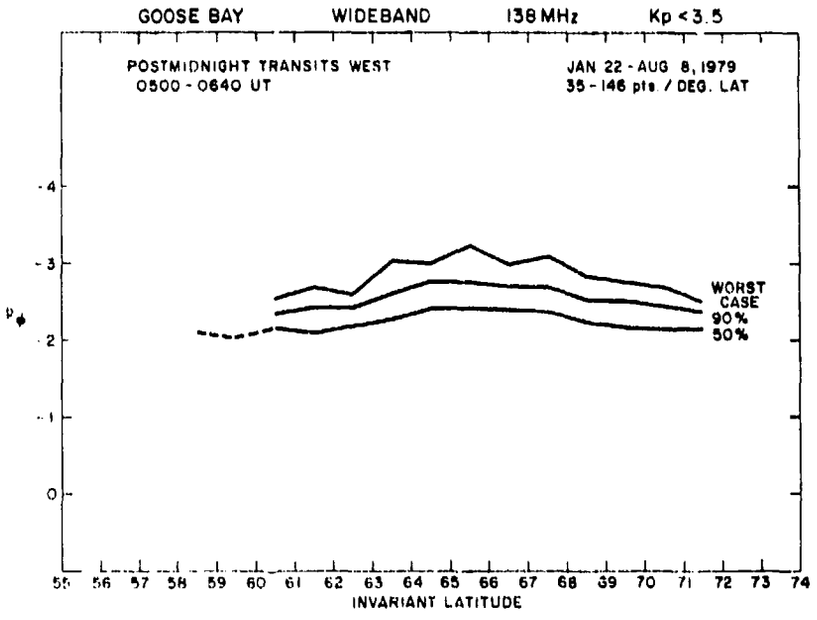

Figure 18a. Phase Spectral Index p_ϕ vs. Invariant Latitude for Nighttime Transits West of Goose Bay Under Quiet Magnetic Conditions

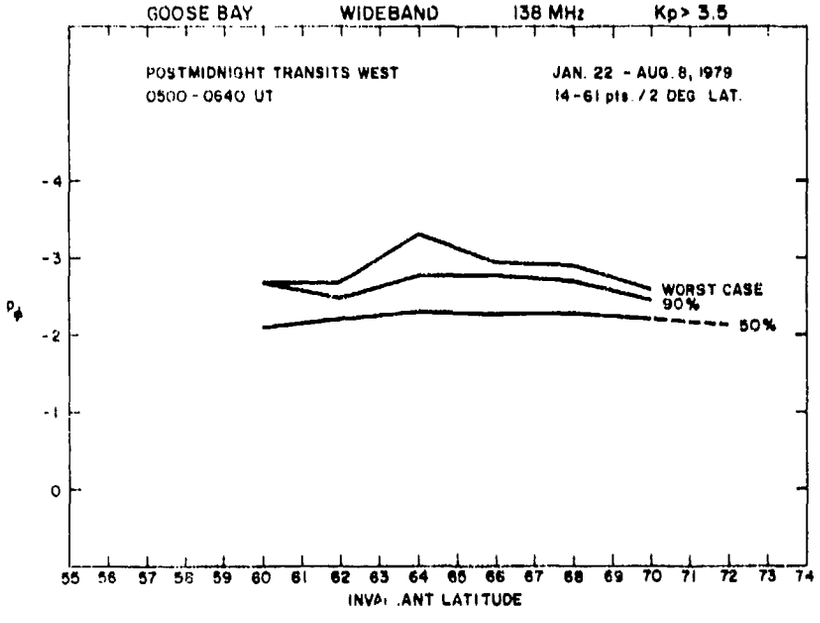

Figure 18b. Phase Spectral Index p_ϕ vs. Invariant Latitude for Nighttime Transits West of Goose Bay Under Disturbed Magnetic Conditions

Phelps and Sagalyn, 1976[25]). They are consistent however with the p_ϕ values obtained at Poker Flat over a 2-year period (Rino, 1979[26]). However, contrary to these observations, no significant enhancement of p_ϕ is seen in the region of the geometrical enhancement of σ_ϕ (Figure 3 of Fremouw and Lansinger, 1979[13]).

4.2 Nighttime Intensity Statistics at Goose Bay

Since the geometrical enhancement is not very marked in the S_4 index, these data give us a better insight into the actual latitude variation of the strength of turbulence C_s (Rino, 1979[26]) of the irregularities. Thus in the premidnight quiet situation (Figure 19a), median S_4 increases from 0.2 at 56°Λ to 0.6 at 66°Λ, that is, a factor of 3 increase in 10° latitude, most of which is caused by an increase of the strength of irregularities with latitude. In the worst case situation it is possible to have saturated amplitude scintillations at 138 MHz throughout the latitude interval during both quiet and disturbed magnetic conditions as observed in Figures 19a, 19b, 20a, 20b, 21a, and 21b. The primary effect of magnetic disturbances seems to be to raise the level of scintillations at the low-latitude end of the Wideband coverage.

The overhead quiet scintillation curve, Figure 20a shows an interesting increase of S_4 at the low-latitude end near 55°Λ. Unfortunately the number of points there are between 5-10. Therefore we cannot conclusively identify it as the plasmaspheric component of scintillations. A similar phenomenon was observed at Poker Flat (Rino and Matthews, 1980[9]).

The intensity spectral strength parameter, T_I, and slope, p_I, are shown in Figures 22a, 22b, 23a, 23b, 24a, and 24b and 25a, 25b, 26a, 26b, 27a and 27b, respectively, for the sake of completeness. Actually these parameters are of limited use as T_I and p_I are contaminated by noise at the low-latitude end when S_4 is low, which is to be expected. However, these parameters are also contaminated by multiple scattering effects when S_4 is high and the roll-off frequency shown in Figure 5 moves to the high-frequency end (Whitney and Basu, 1977[27]). Thus, only the middle portions of the curves between 60-64°Λ are of some use in providing information on the temporal structure of scintillations. Within this range, median

---

25. Phelps, A.D.R. and Sagalyn, R.C. (1976) Plasma density irregularities in the high-latitude top side ionosphere, J. Geophys. Res. 81:515. AFGL-TR-76-0077, AD A024 248.

26. Rino, C.L. (1979) A power law phase screen model for ionospheric scintillation, 1. Weak scatter, Radio Sci. 14:1135.

27. Whitney, H.E. and Basu, S. (1977) The effect of ionospheric scintillation on VHF/UHF satellite communications, Radio Sci. 12:123. AFGL-TR-77-0067, AD A037 520.

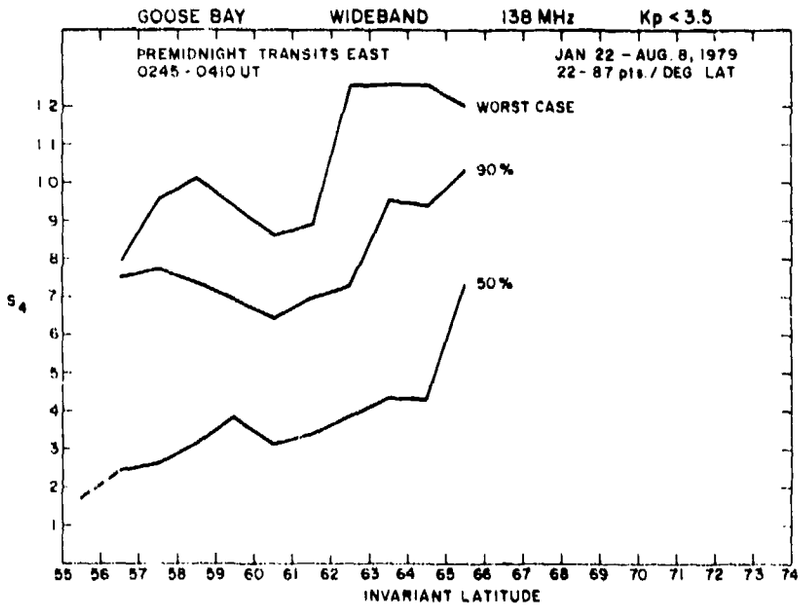

Figure 19a. Intensity Scintillation Index S_4 vs. Invariant Latitude for Nighttime Transits East of Goose Bay Under Quiet Magnetic Conditions

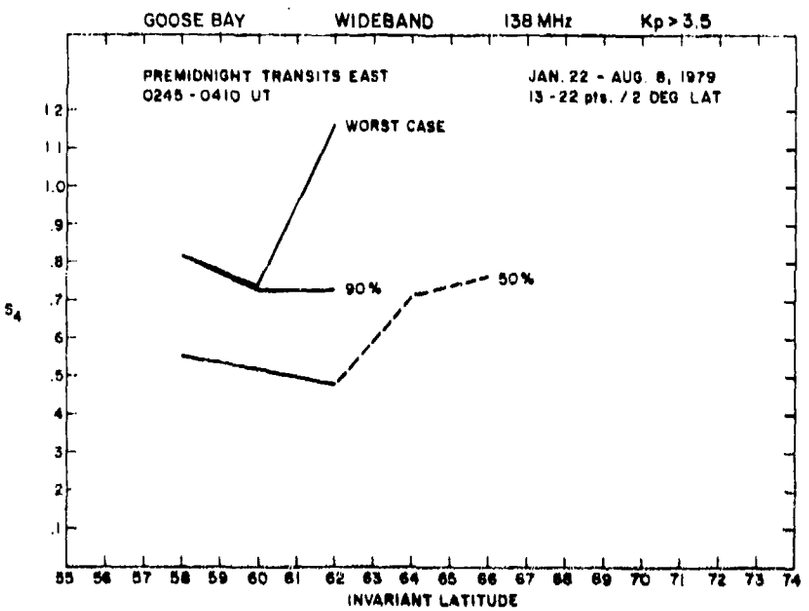

Figure 19b. Intensity Scintillation Index S_4 vs. Invariant Latitude for Nighttime Transits East of Goose Bay Under Disturbed Magnetic Conditions

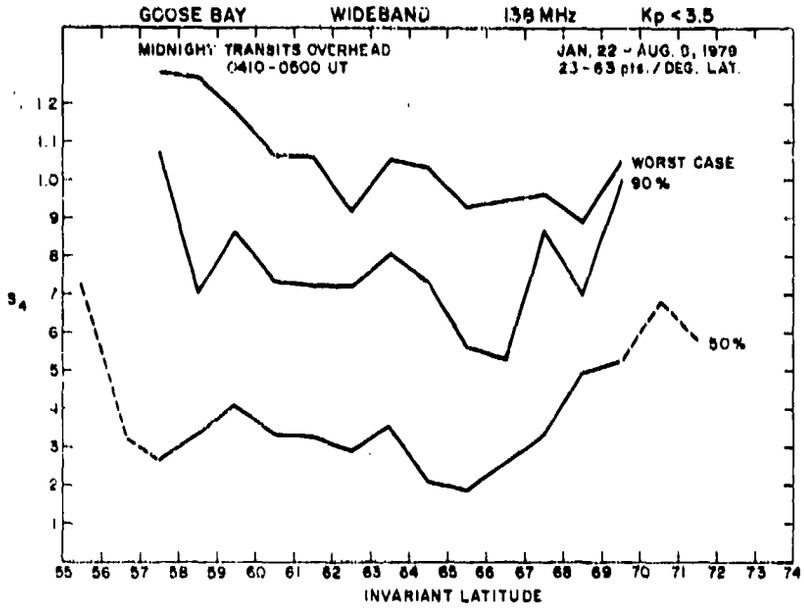

Figure 20a. Intensity Scintillation Index S_4 vs. Invariant Latitude for Nighttime Transits Overhead of Goose Bay Under Quiet Magnetic Conditions

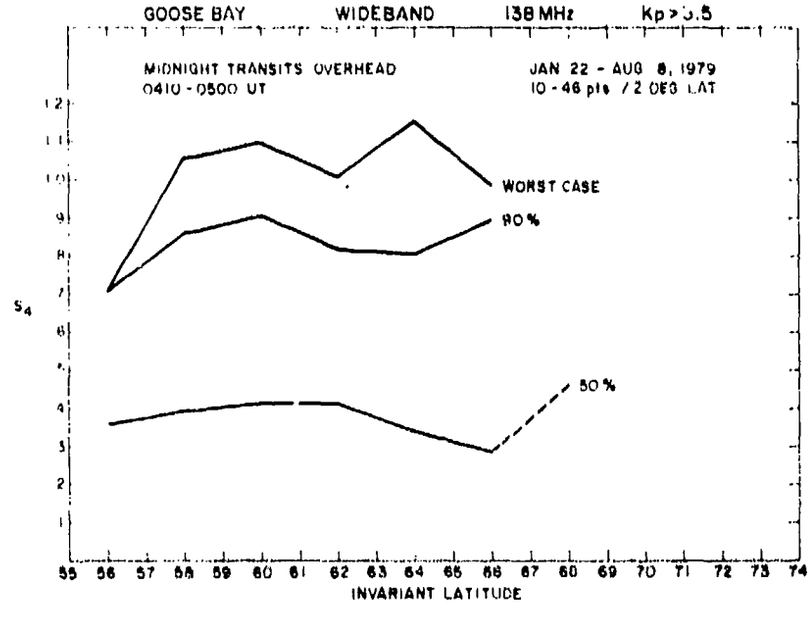

Figure 20b. Intensity Scintillation Index S_4 vs. Invariant Latitude for Nighttime Transits Overhead of Goose Bay Under Disturbed Magnetic Conditions

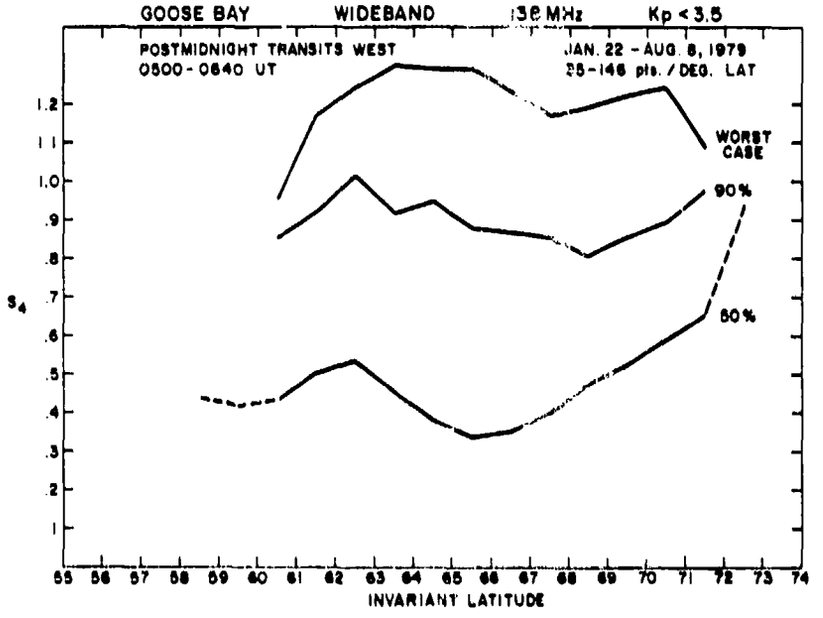

Figure 21a. Intensity Scintillation Index S_4 vs. Invariant Latitude for Nighttime Transits West of Goose Bay Under Quiet Magnetic Conditions

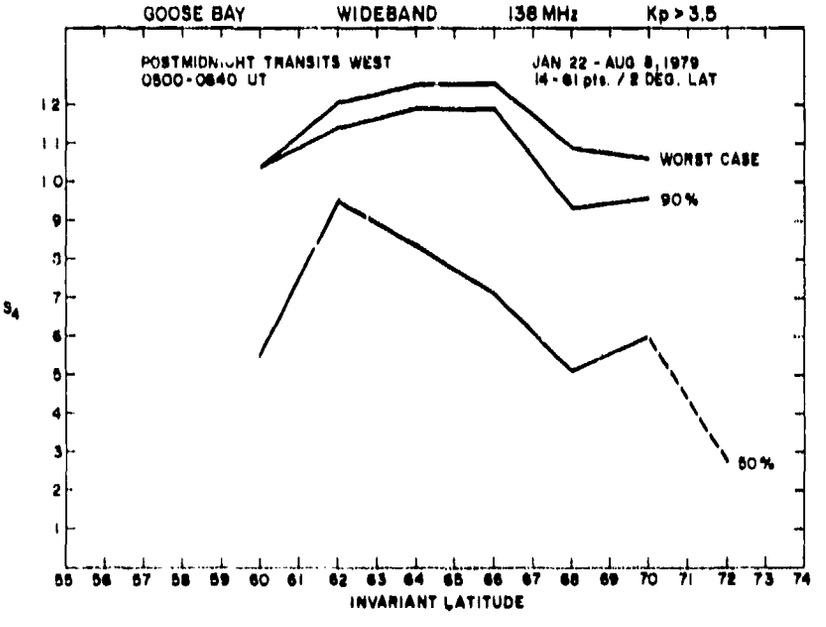

Figure 21b. Intensity Scintillation Index S_4 vs. Invariant Latitude for Nighttime Transits West of Goose Bay Under Disturbed Magnetic Conditions

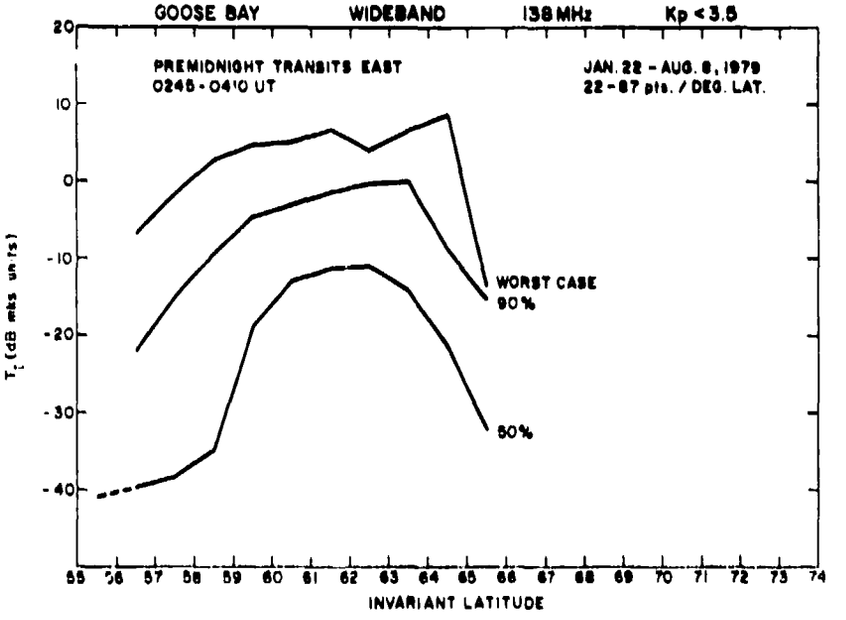

Figure 22a. Spectral Strength T_I of Intensity at 1 Hz vs. Invariant Latitude for Nighttime Transits East of Goose Bay Under Quiet Magnetic Conditions

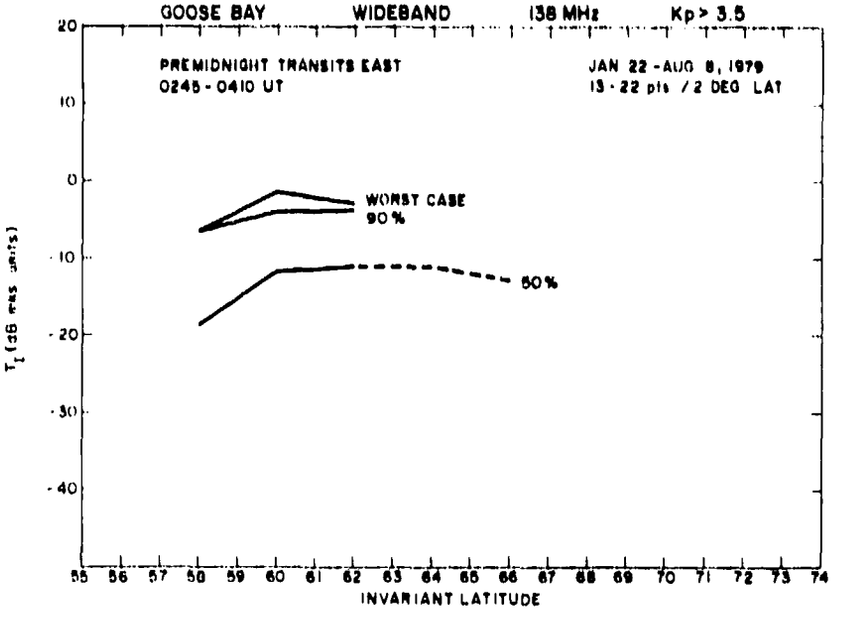

Figure 22b. Spectral Strength T_I of Intensity at 1 Hz vs. Invariant Latitude for Nighttime Transits East of Goose Bay Under Disturbed Magnetic Conditions

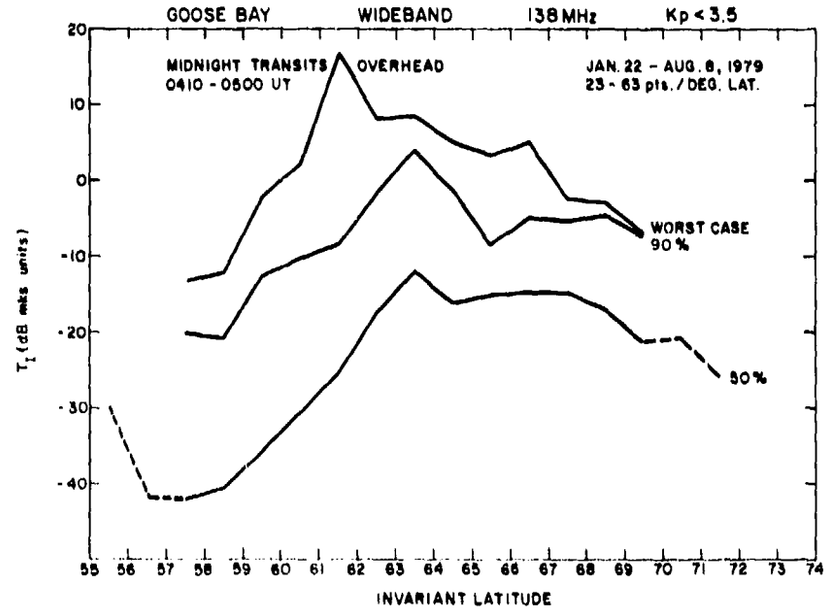

Figure 23a. Spectral Strength T_I of Intensity at 1 Hz vs. Invariant Latitude for Nighttime Transits Overhead of Goose Bay Under Quiet Magnetic Conditions

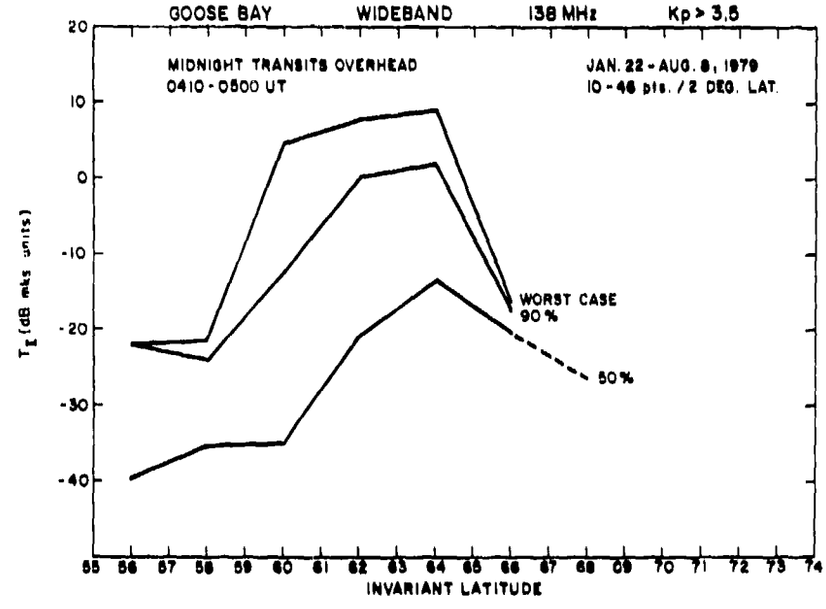

Figure 23b. Spectral Strength T_I of Intensity at 1 Hz vs. Invariant Latitude for Nighttime Transits Overhead of Goose Bay Under Disturbed Magnetic Conditions

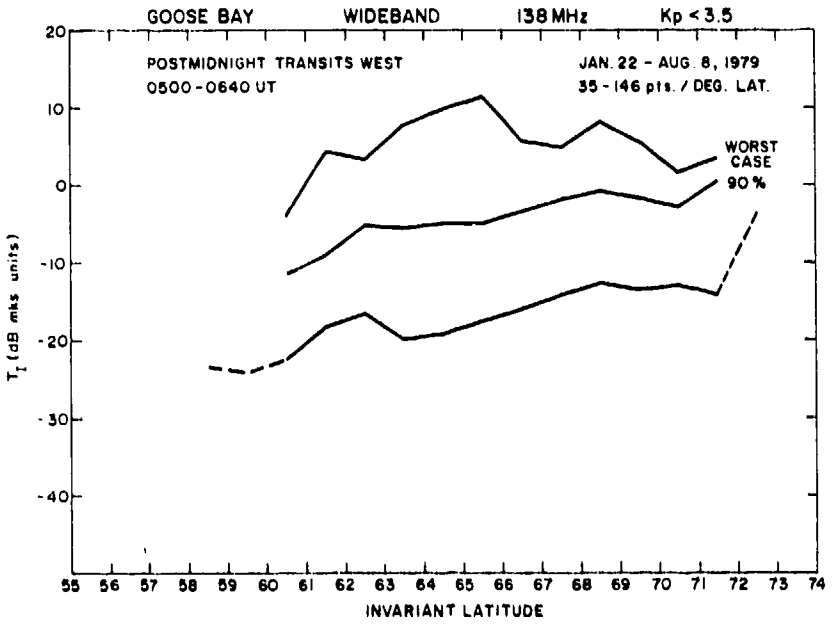

Figure 24a. Spectral Strength T_I of Intensity at 1 Hz vs. Invariant Latitude for Nighttime Transits West of Goose Bay Under Quiet Magnetic Conditions

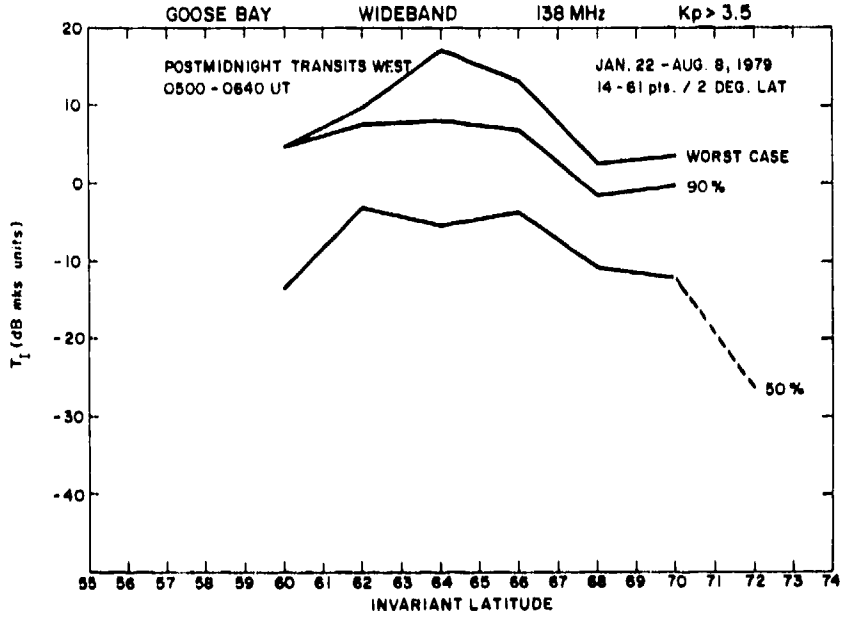

Figure 24b. Spectral Strength T_I of Intensity at 1 Hz vs. Invariant Latitude for Nighttime Transits West of Goose Bay Under Disturbed Magnetic Conditions

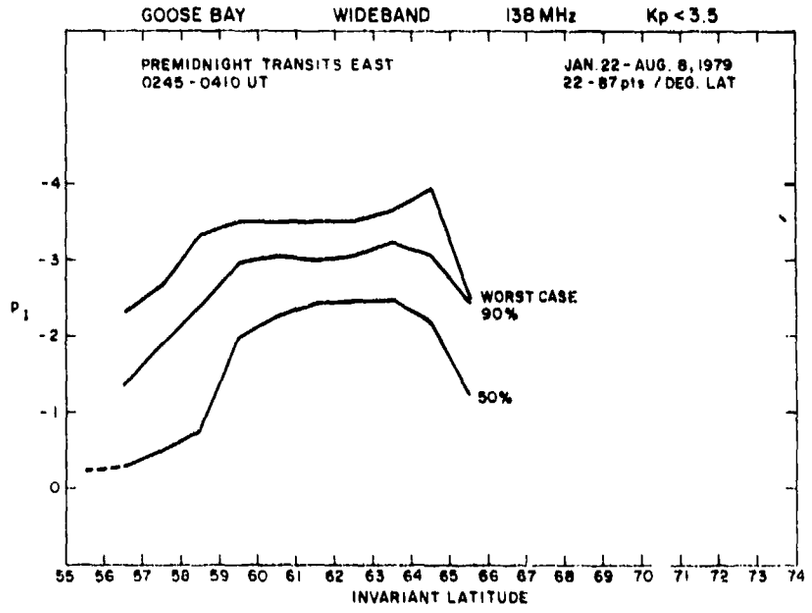

Figure 25a. Intensity Spectral Index p_I vs. Invariant Latitude for Nighttime Transits East of Goose Bay Under Quiet Magnetic Conditions

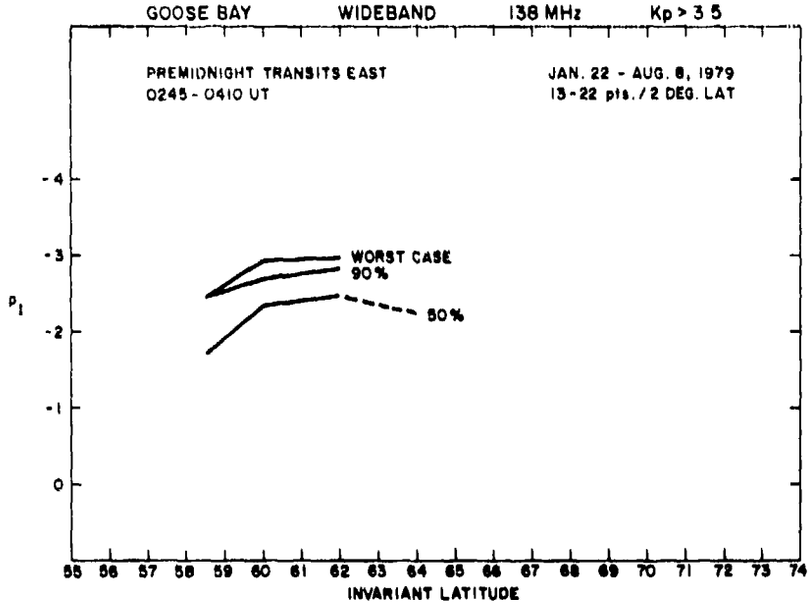

Figure 25b. Intensity Spectral Index p_I vs. Invariant Latitude for Nighttime Transits East of Goose Bay Under Disturbed Magnetic Conditions

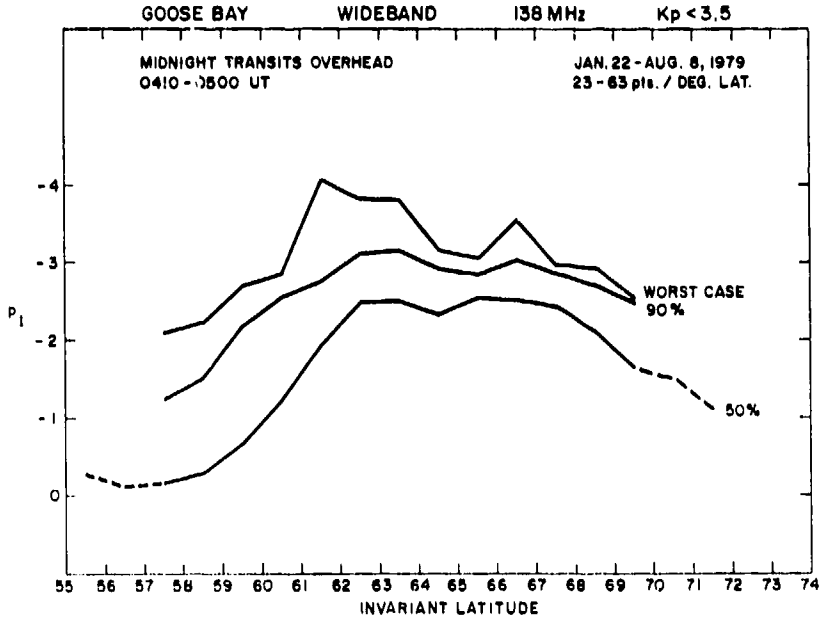

Figure 26a. Intensity Spectral Index p_I vs. Invariant Latitude for Nighttime Transits Overhead of Goose Bay Under Quiet Magnetic Conditions

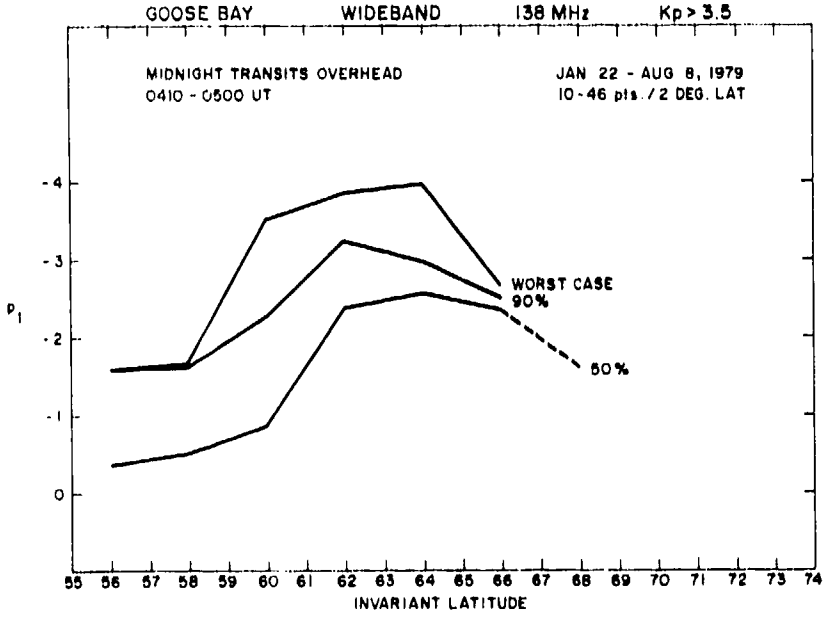

Figure 26b. Intensity Spectral Index p_I vs. Invariant Latitude for Nighttime Transits Overhead of Goose Bay Under Disturbed Magnetic Conditions

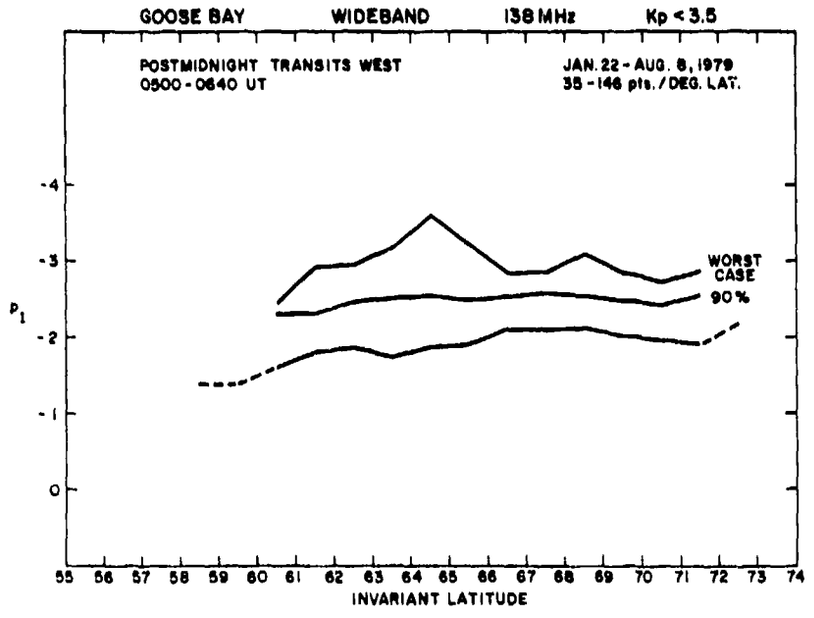

Figure 27a. Intensity Spectral Index p_I vs. Invariant Latitude for Nighttime Transits West of Goose Bay Under Quiet Magnetic Conditions

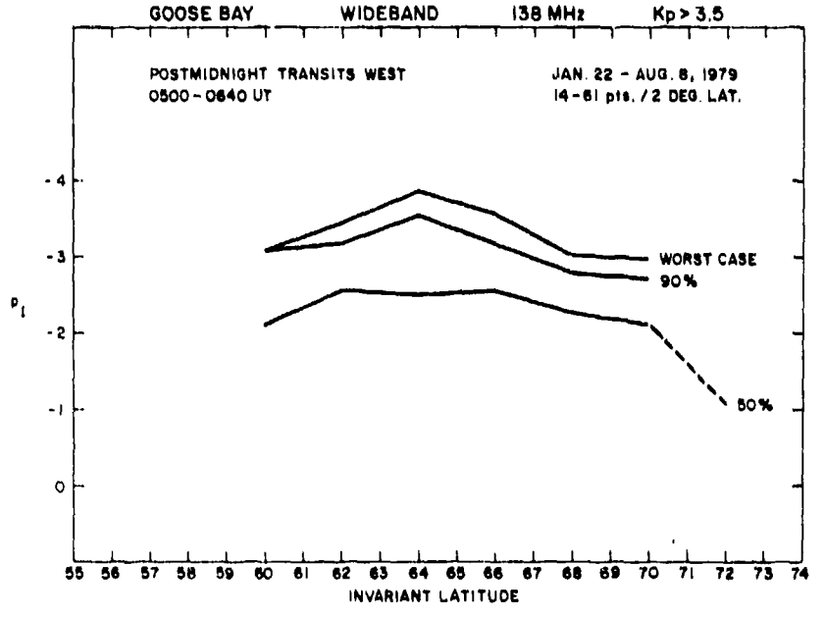

Figure 27b. Intensity Spectral Index p_I vs. Invariant Latitude for Nighttime Transits West of Goose Bay Under Disturbed Magnetic Conditions

p_I and p_ϕ agree numerically as they should in the weak-scatter regime (Rufenach, 1975[28]).

4.3 Daytime Phase Statistics at Goose Bay

In keeping with the greatly equatorward position of the Goose Bay station with respect to the daytime auroral oval, we see little phase scintillations during magnetically quiet times as shown by the median curves in Figures 28a, 29a, and 30a. Scintillations increase poleward of 68°Λ. The overhead transits show a geometrical enhancement near 64°Λ during both quiet and disturbed times (Figures 29a and 29b) while the two other corridors do not have a prominent enhancement (Figures 28a, 28b, 30a, and 30b). This led Rino and Matthews (1980)[9] and Fremouw and Lansinger (1981)[29] to postulate that the daytime irregularities are in the form of field-aligned rods and not L-shell aligned sheets. However, a small enhancement is visible in the eastern corridor (Figures 28a and 28b) as with the nighttime date. The limited nature of the data base precludes any definitive conclusions. The 90 percentile and worst case values can be as large as 5-10 rad even during quiet daytime hours.

The T_ϕ parameters in the various categories (Figures 31a, 31b, 32a, 32b, 33a, and 33b) behave very much like their σ_ϕ counterparts, displaying similar geometrical characteristics as discussed previously. The daytime T_ϕ values are at least 10 dB below the nighttime values as may be observed by comparing Figure 14a with Figure 32a.

The median p_ϕ values are shown in Figures 34a, 34b, 35a, 35b, 36a, and 36b. They are also lower than the nighttime values probably because of the low σ_ϕ magnitudes that, in turn, are associated with a more noiselike spectrum.

4.4 Daytime Intensity Statistics at Goose Bay

The S_4 indices observed at Goose Bay during the daytime are indeed very low. During quiet magnetic conditions (Figures 37a, 38a, and 39a) the median value of S_4 is everywhere less than 0.3 and is about 0.1 close to overhead. No geometrical enhancement is observed in the median for overhead passes but is evident at the 90 and higher percentiles. Magnetic disturbances (Figures 37b, 38b, and 39b) cause S_4 values on the order of 0.5 at latitudes greater than 68°Λ and also give rise to noticeable geometrical enhancements.

---

28. Rufenach, C.L. (1975) Ionospheric scintillation by a random phase screen: spectral approach, Radio Sci. 10:155.

29. Fremouw, E.J. and Lansinger, J.M. (1981) Recent high latitude improvement in a computer based scintillation model, Proceedings of Ionospheric Effects Symposium, Alexandria, Virginia.

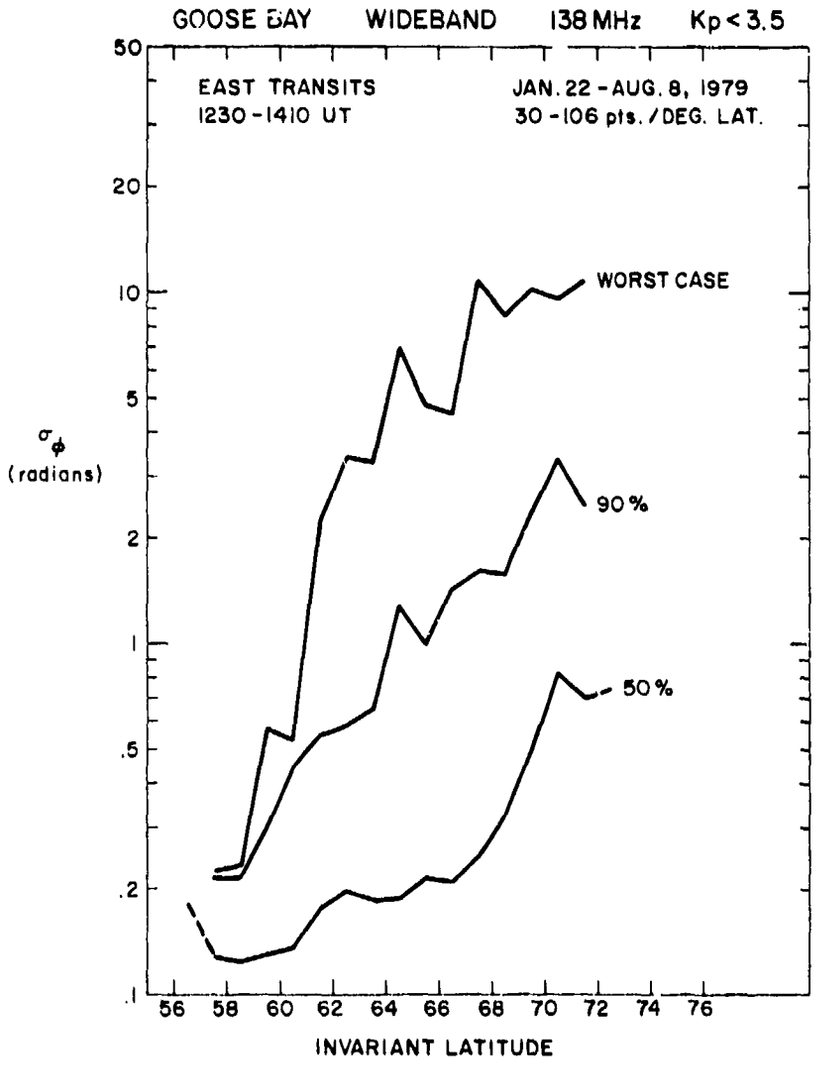

Figure 28a. Phase Scintillation Index σ_ϕ vs. Invariant Latitude for Daytime Transits East of Goose Bay Under Quiet Magnetic Conditions

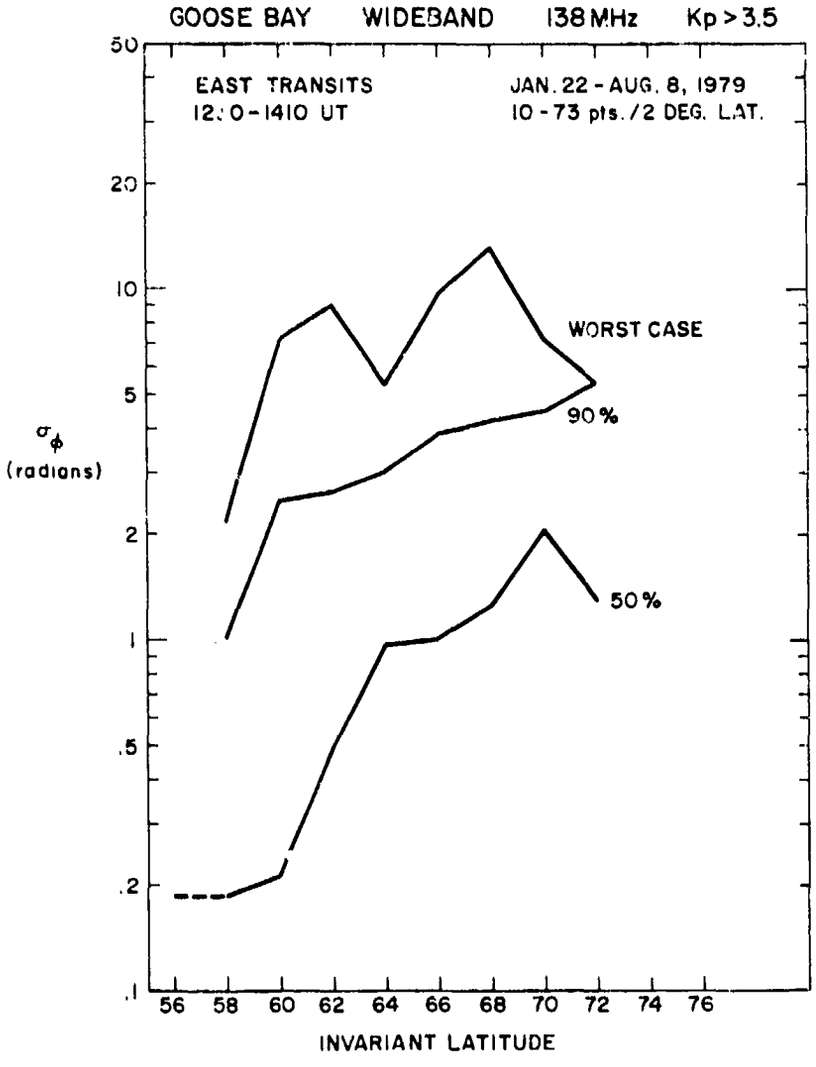

Figure 28b. Phase Scintillation Index σ_ϕ vs. Invariant Latitude for Daytime Transits East of Goose Bay Under Disturbed Magnetic Conditions

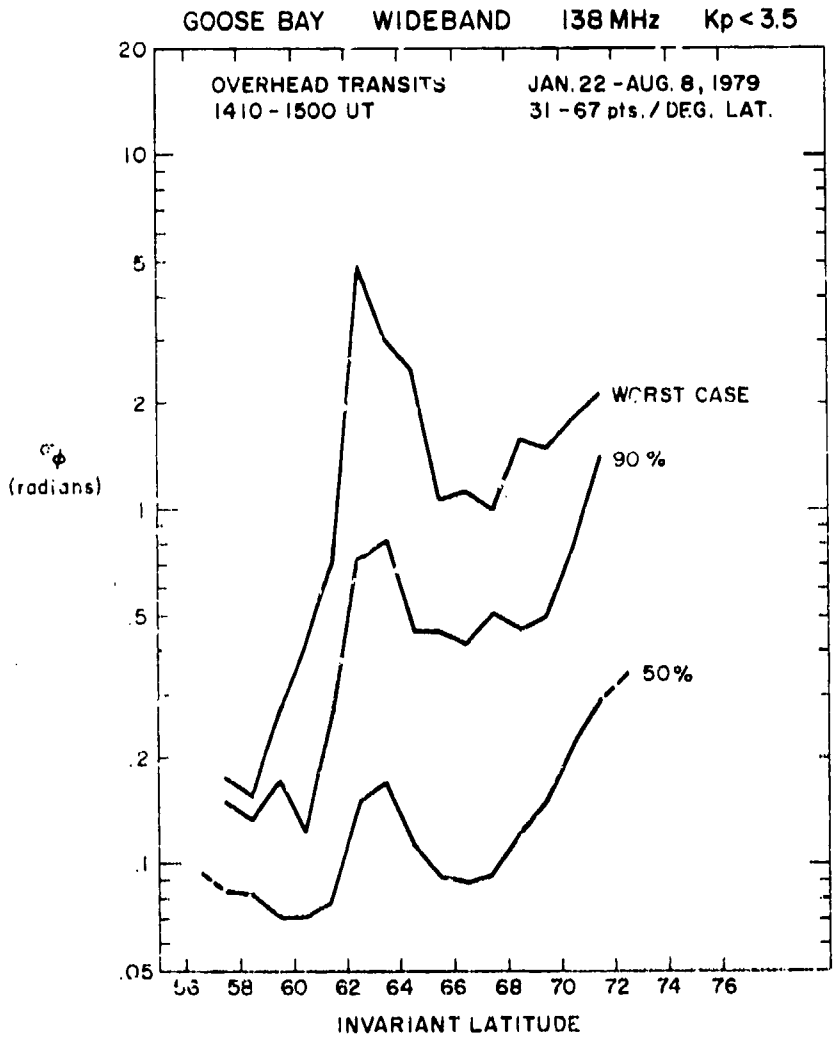

Figure 29a. Phase Scintillation Index σ_ϕ vs. Invariant Latitude for Daytime Transits Overhead of Goose Bay Under Quiet Magnetic Conditions

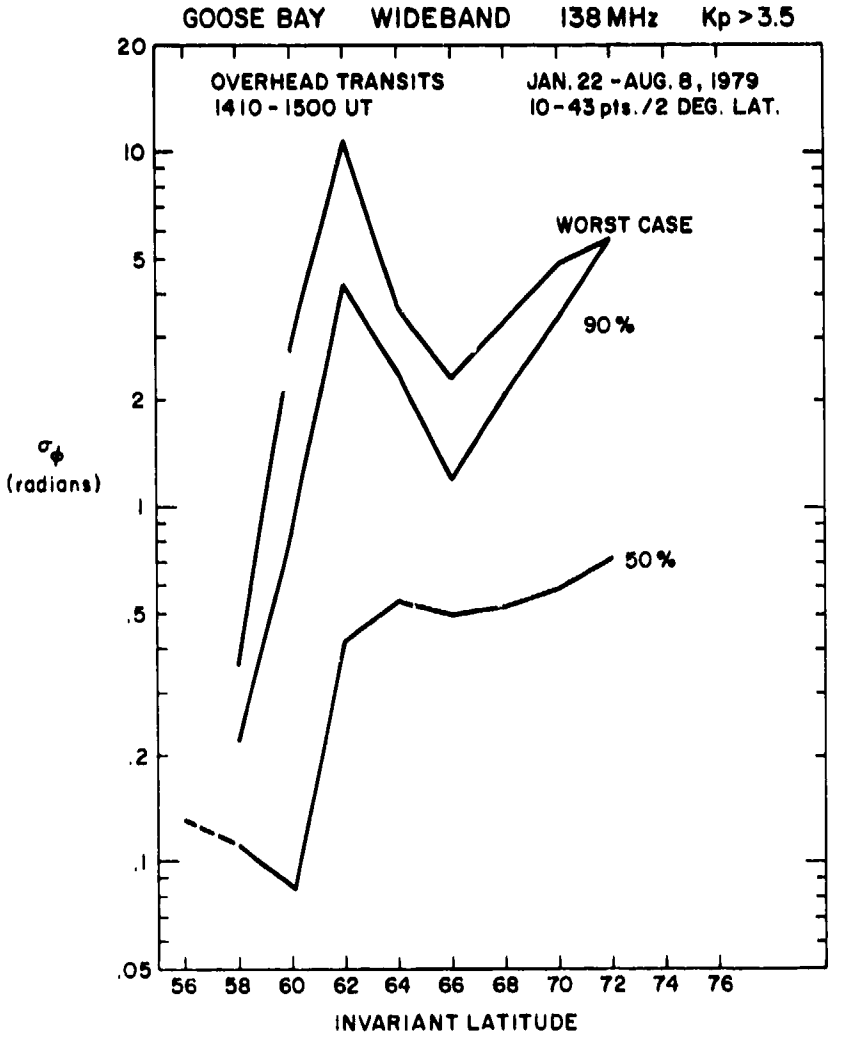

Figure 29b. Phase Scintillation Index σ_ϕ vs. Invariant Latitude for Daytime Transits Overhead of Goose Bay Under Disturbed Magnetic Conditions

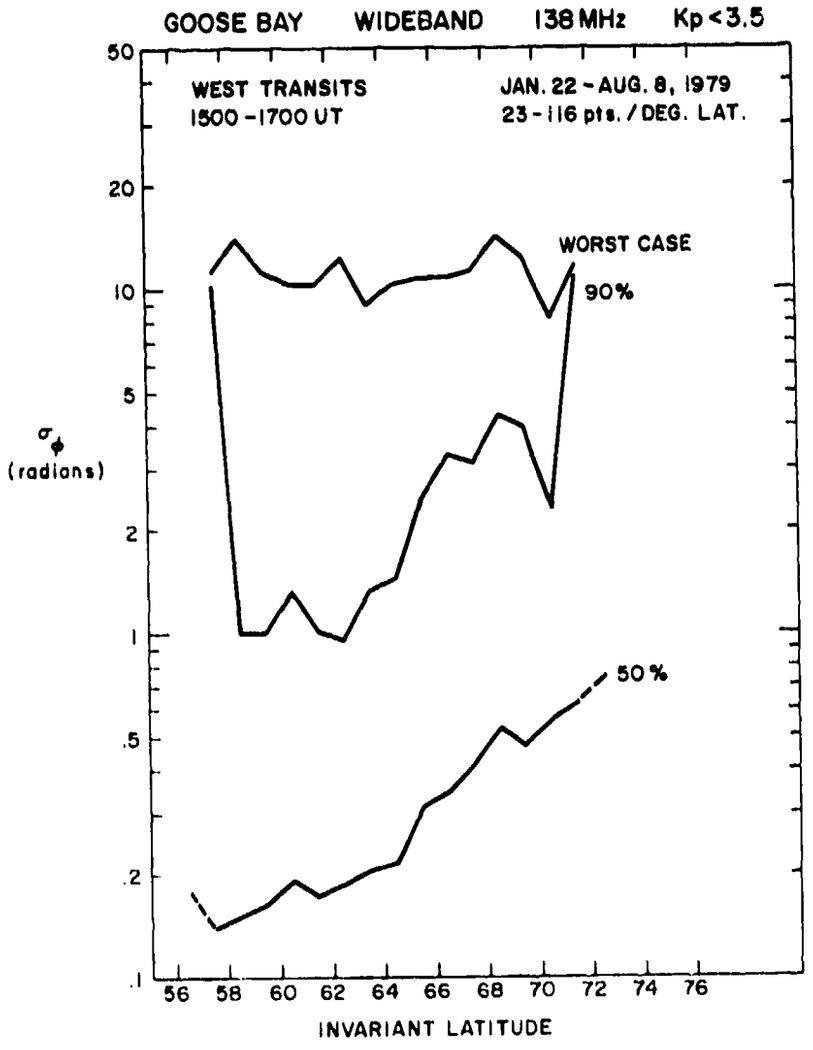

Figure 30a. Phase Scintillation Index σ_ϕ vs. Invariant Latitude for Daytime Transits West of Goose Bay Under Quiet Magnetic Conditions

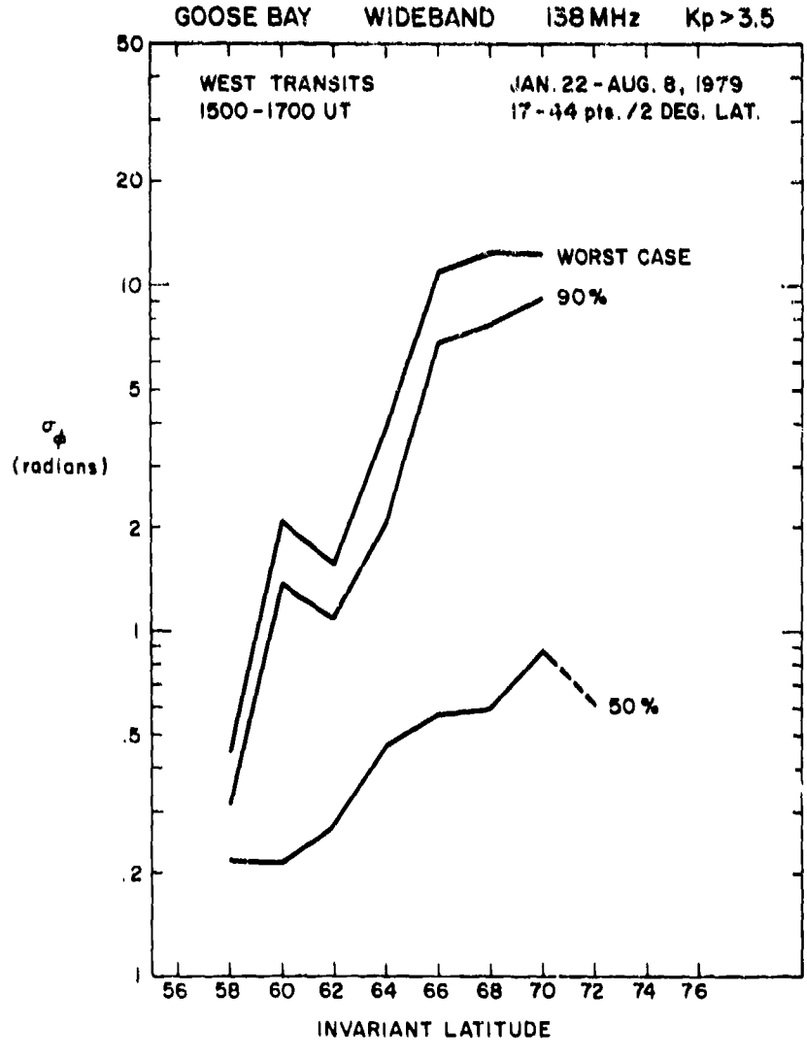

Figure 30b. Phase Scintillation Index σ_ϕ vs. Invariant Latitude for Daytime Transits West of Goose Bay Under Disturbed Magnetic Conditions

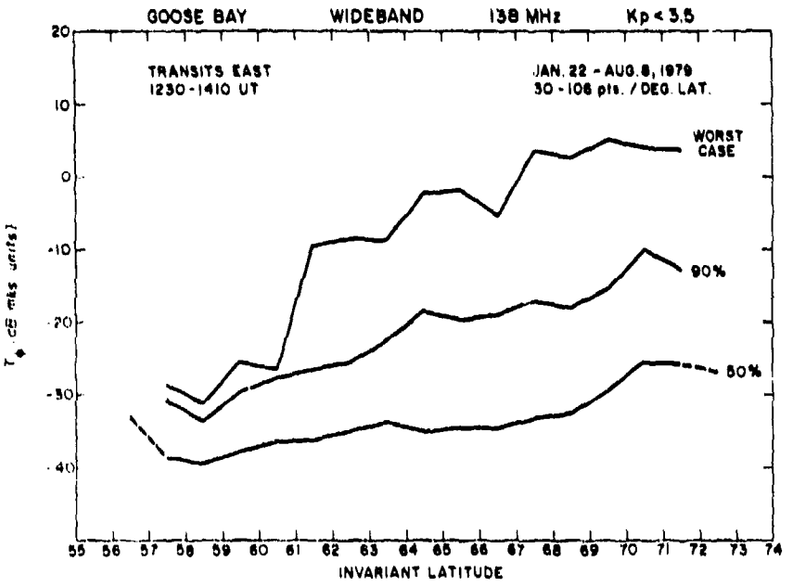

Figure 31a. Spectral Strength T_ϕ of Phase at 1 Hz vs. Invariant Latitude for Daytime Transits East of Goose Bay Under Quiet Magnetic Conditions

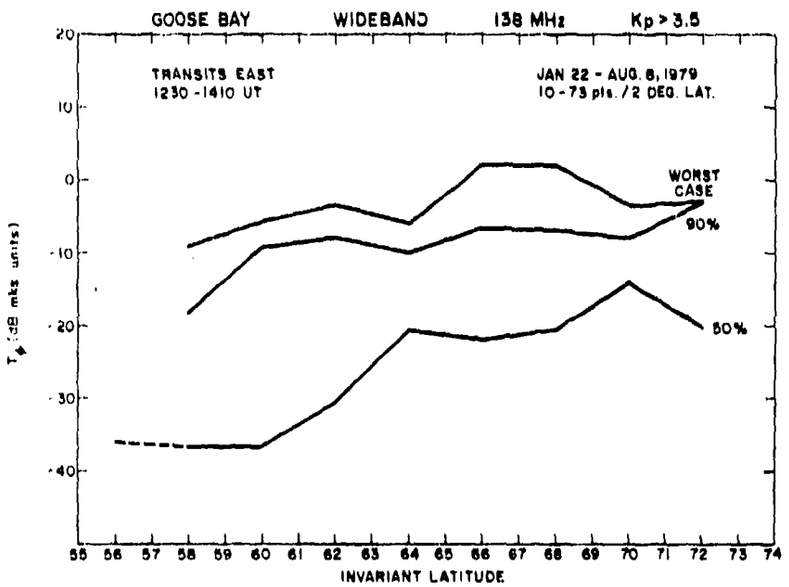

Figure 31b. Spectral Strength T_ϕ of Phase at 1 Hz vs. Invariant Latitude for Daytime Transits East of Goose Bay Under Disturbed Magnetic Conditions

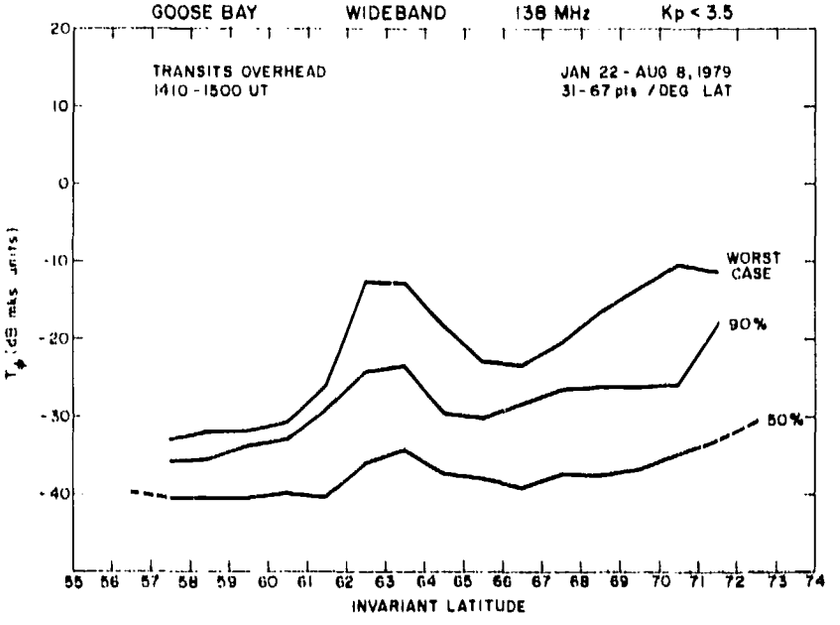

Figure 32a. Spectral Strength T_ϕ of Phase at 1 Hz vs. Invariant Latitude for Daytime Transits Overhead of Goose Bay Under Quiet Magnetic Conditions

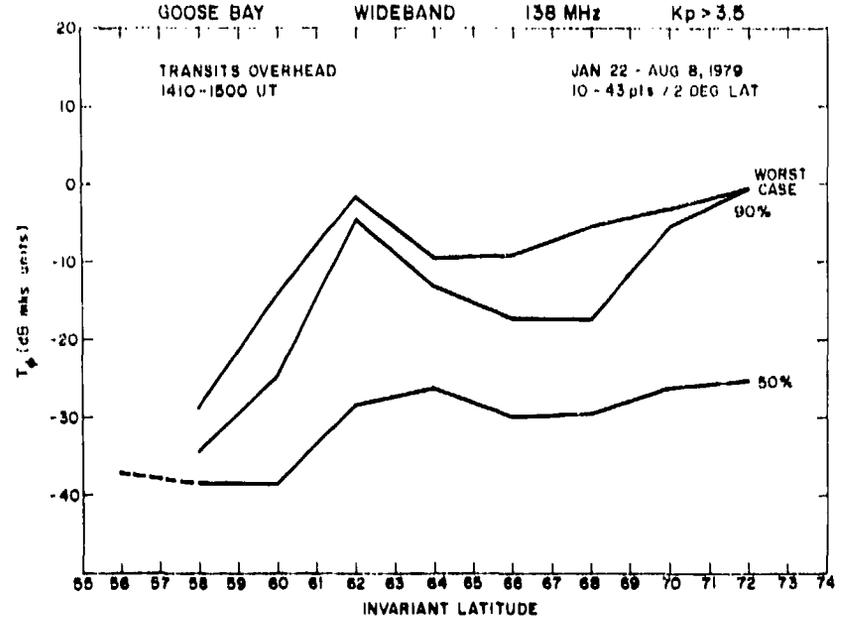

Figure 32b. Spectral Strength T_ϕ of Phase at 1 Hz vs. Invariant Latitude for Daytime Transits Overhead of Goose Bay Under Disturbed Magnetic Conditions

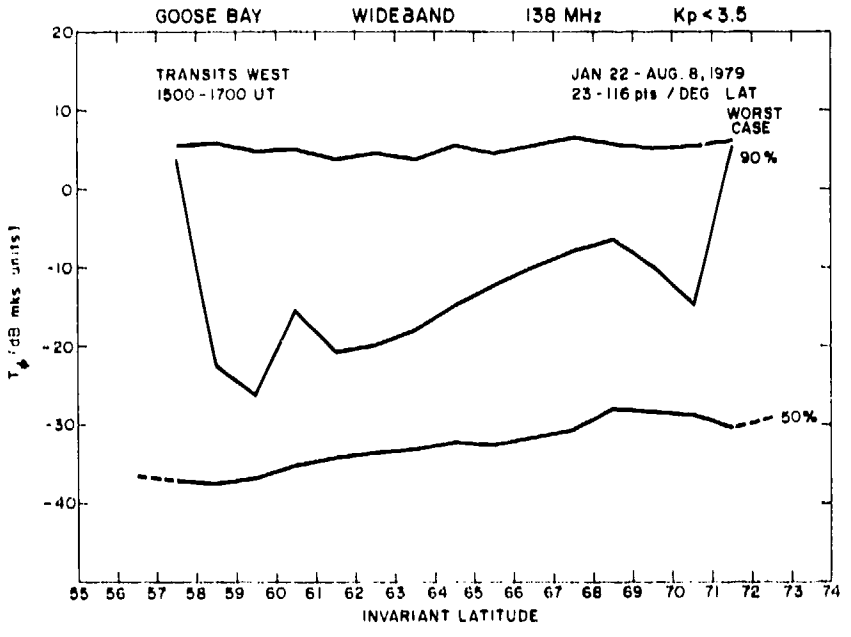

Figure 33a. Spectral Strength T_ϕ of Phase at 1 Hz vs. Invariant Latitude for Daytime Transits West of Goose Bay Unde . Quiet Magnetic Conditions

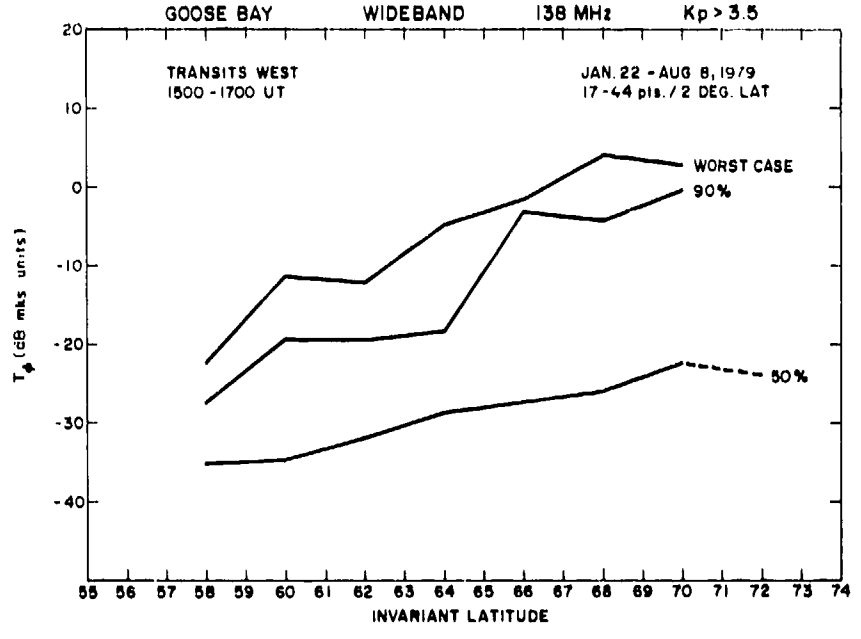

Figure 33b. Spectral Strength T_ϕ of Phase at 1 Hz vs. Invariant Latitude for Daytime Transits West of Goose Bay Under Disturbed Magnetic Conditions

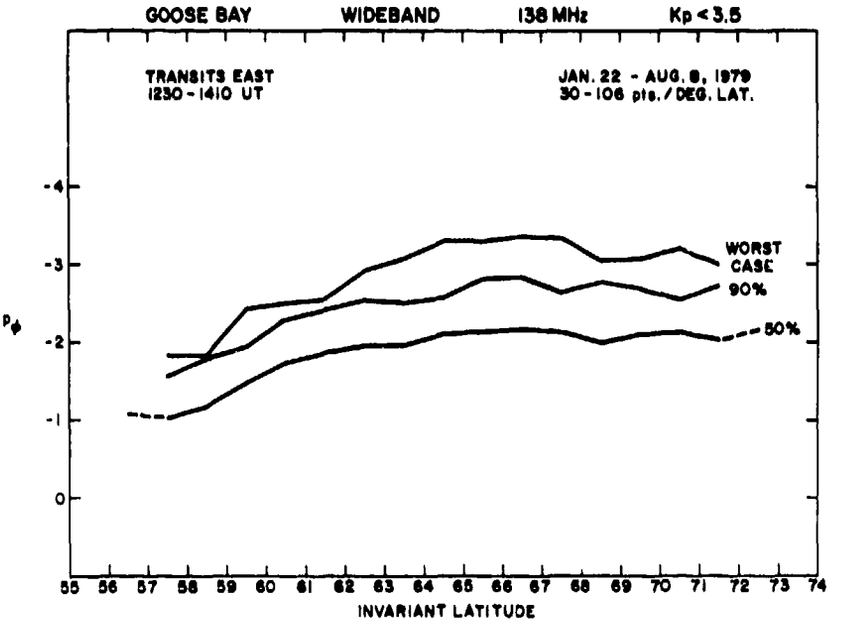

Figure 34a. Phase Spectral Index p_ϕ vs. Invariant Latitude for Daytime Transits East of Goose Bay Under Quiet Magnetic Conditions

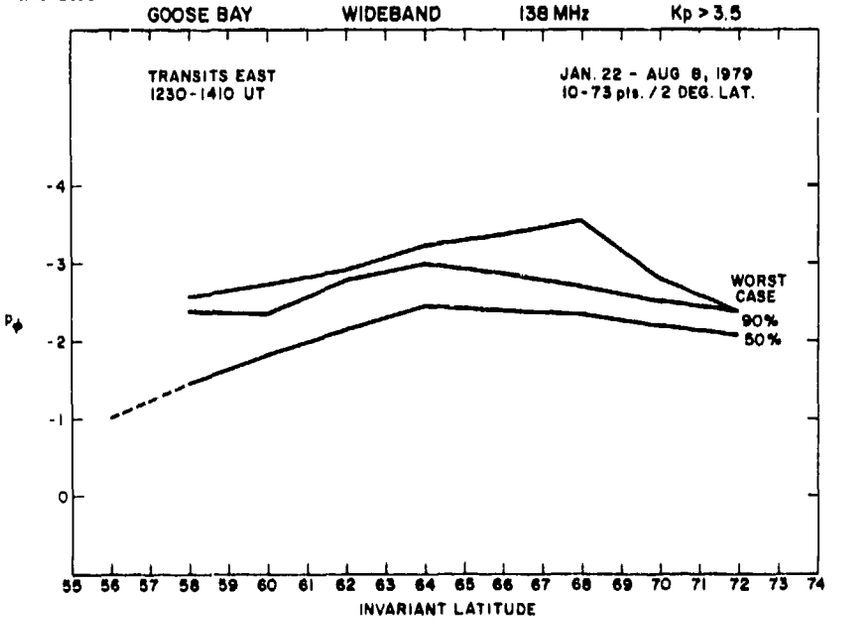

Figure 34b. Phase Spectral Index p_ϕ vs. Invariant Latitude for Daytime Transits East of Goose Bay Under Disturbed Magnetic Conditions

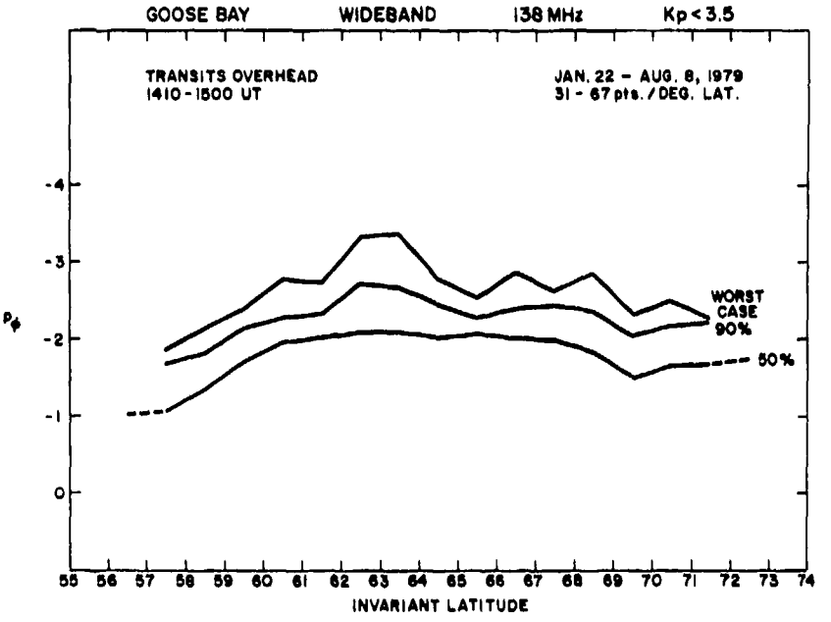

Figure 35a. Phase Spectral Index p_ϕ vs. Invariant Latitude for Daytime Transits Overhead of Goose Bay Under Quiet Magnetic Conditions

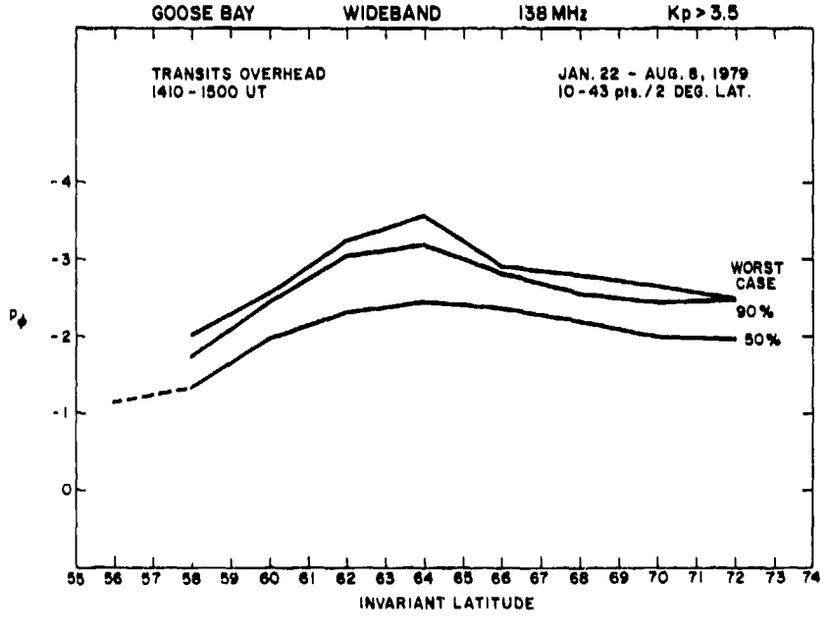

Figure 35b. Phase Spectral Index p_ϕ vs. Invariant Latitude for Daytime Transits Overhead of Goose Bay Under Disturbed Magnetic Conditions

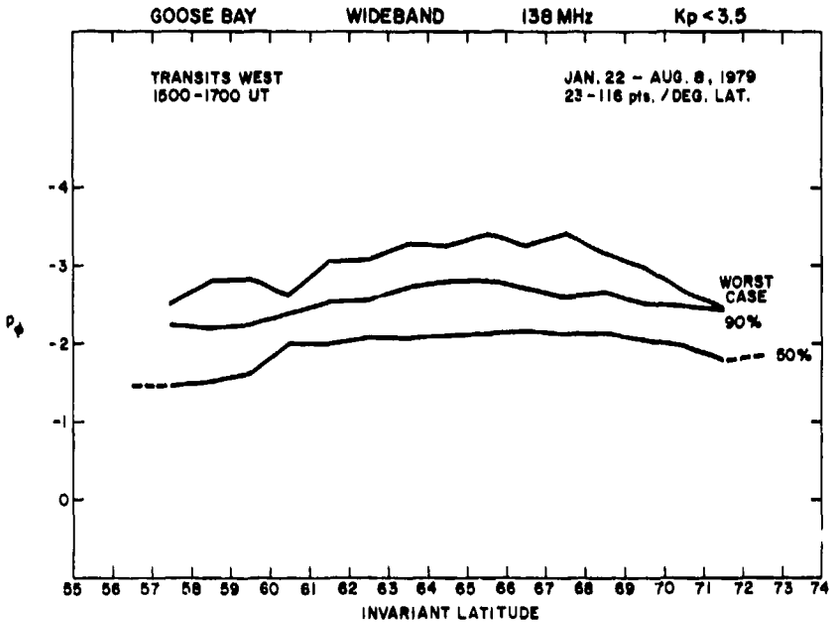

Figure 36a. Phase Spectral Index p_ϕ vs. Invariant Latitude for Daytime Transits West of Goose Bay Under Quiet Magnetic Conditions

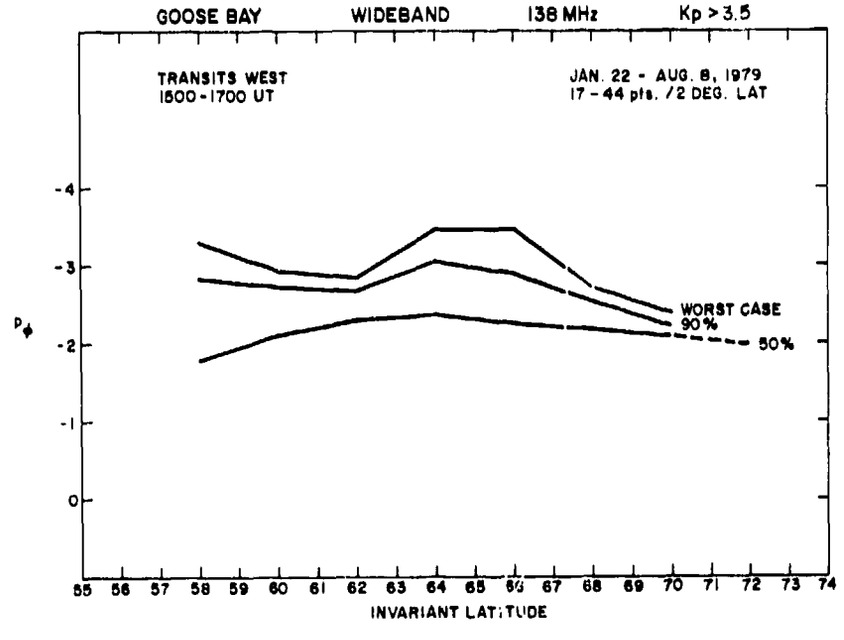

Figure 36b. Phase Spectral Index p_ϕ vs. Invariant Latitude for Daytime Transits West of Goose Bay Under Disturbed Magnetic Conditions

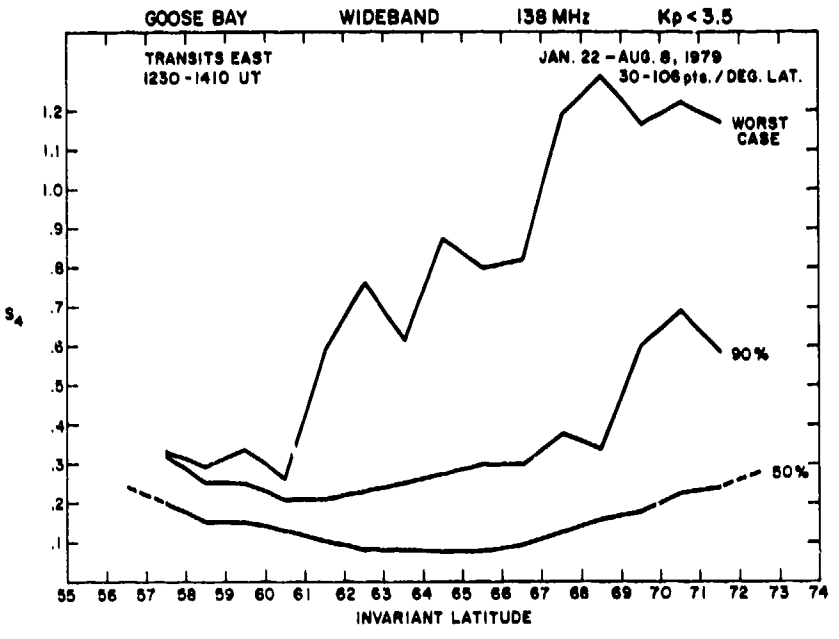

Figure 37a. Intensity Scintillation Index S_4 vs. Invariant Latitude for Daytime Transits East of Goose Bay Under Quiet Magnetic Conditions

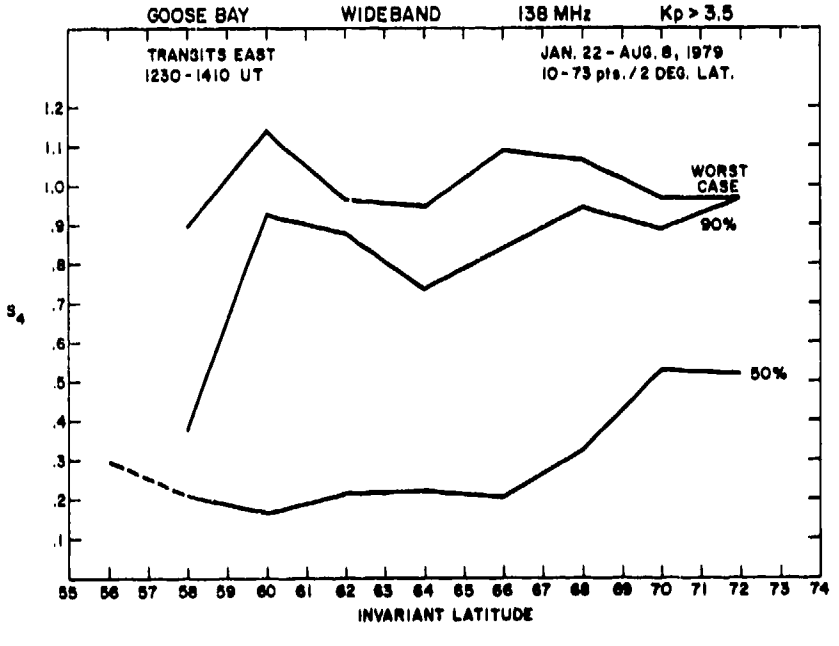

Figure 37b. Intensity Scintillation Index S_4 vs. Invariant Latitude for Daytime Transits East of Goose Bay Under Disturbed Magnetic Conditions

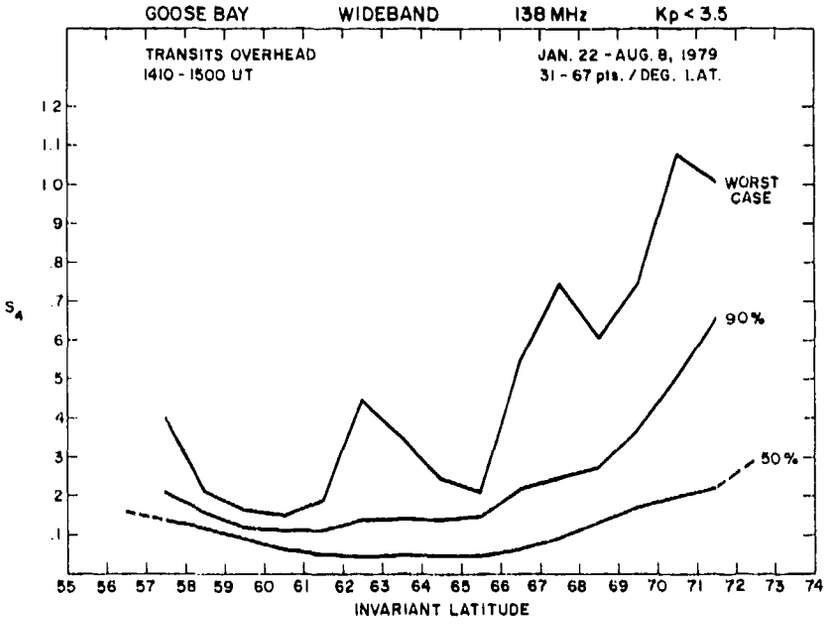

Figure 38a. Intensity Scintillation Index S_4 vs. Invariant Latitude for Daytime Transits Overhead of Goose Bay Under Quiet Magnetic Conditions

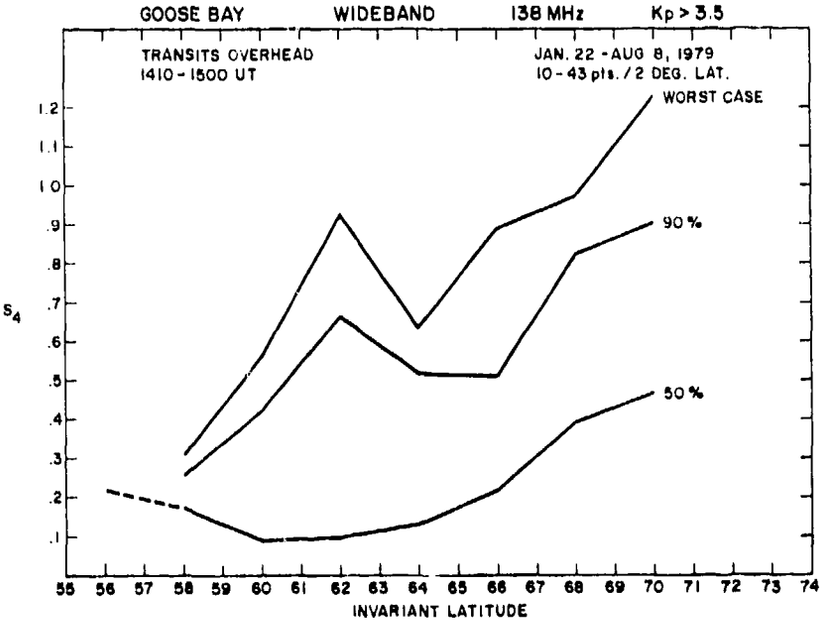

Figure 38b. Intensity Scintillation Index S_4 vs. Invariant Latitude for Daytime Transits Overhead of Goose Bay Under Disturbed Magnetic Conditions

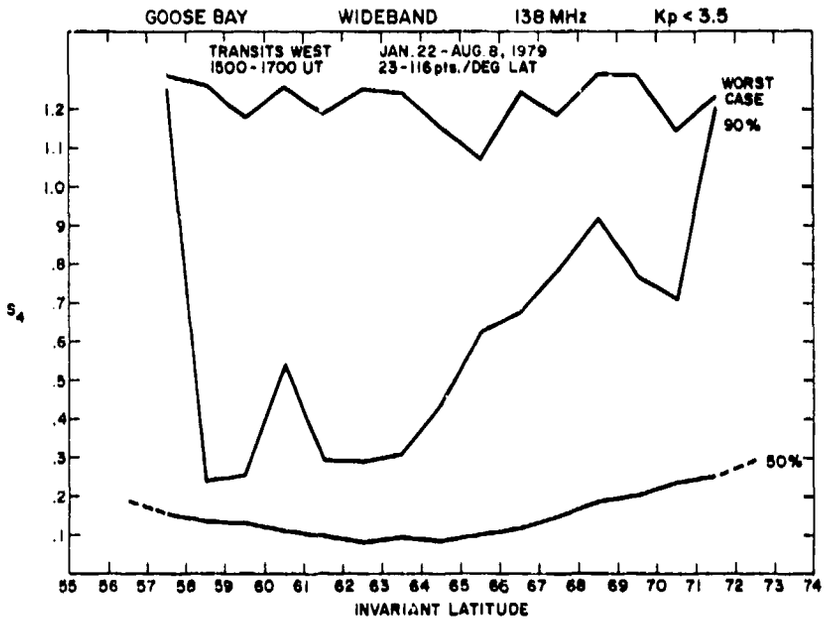

Figure 39a. Intensity Scintillation Index S_4 vs. Invariant Latitude for Daytime Transits West of Goose Bay Under Quiet Magnetic Conditions

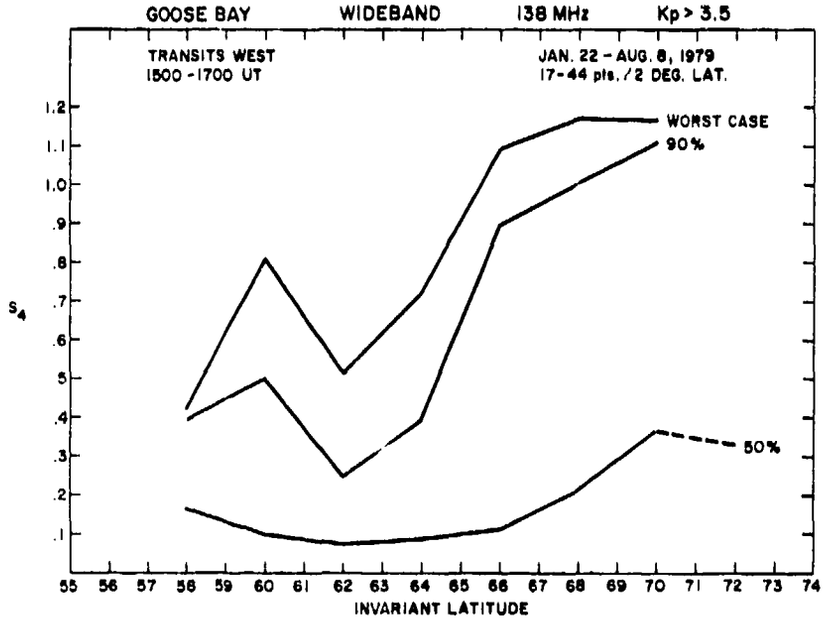

Figure 39b. Intensity Scintillation Index S_4 vs. Invariant Latitude for Daytime Transits West of Goose Bay Under Disturbed Magnetic Conditions

4.5 Nighttime Phase Statistics at Anchorage

The Anchorage data covers only the period 24 January through 3 April 1979, while the Goose Bay data also covered the following summer period until early August, 1979, when the Wideband satellite failure stopped observations. We will point out the salient features of this small data base and compare it with the Goose Bay results using the same format as used for the Goose Bay data display. In Sections 5 and 6 we will present magnetic activity and seasonal variations of the phase and amplitude scintillations obtained at these two widely-separated auroral stations.

The nighttime phase scintillation data in the 3 corridors is shown in Figures 40a, 40b, 41a, 41b, 42a, and 42b for quiet and disturbed times. The position of the geometrical enhancement for individual cases is between 60-61°Λ rather than between 63-64°Λ as with Goose Bay. This results from the different invariant latitude locations of the two stations as given in Table 1. However the median values at Anchorage often show enhancements at somewhat higher latitudes. Rino and Owen (1980)[30] also found that the median position of the geometrical enhancement for Fort Yukon based on a small data set was poleward of the theoretically predicted position for sheetlike irregularities. The geometrical enhancement seems to be most marked in the overhead and western corridors but not in the eastern corridor. We believe that the latter may be due to a lack of alignment with a particular L-shell over a large altitude region. The same situation prevailed in the western corridor for Goose Bay where the smearing took place over a larger range of magnetic azimuths. Thus, the behavior of the geometrical enhancement in the off-overhead corridors is different in the two longitude sectors and seems to be connected with the location of the magnetic pole with respect to the observing stations (magnetic pole to the west of Goose Bay and east of Anchorage), which produces the different magnetic azimuth dependence with altitude of the ray paths in the eastern and western corridors. That is to say that the declination of the magnetic field changes fastest with altitude in longitude sectors which are closest to that of the magnetic pole. Fremouw and Lansinger (1981),[29] on the other hand, postulated that the sheetlike anisotropy is local time dependent attaining its most sheetlike form at 0200 LT wher the western corridor passes are observed in the Alaskan sector.

This set of Anchorage phase scintillation curves is very similar to the σ_ϕ set for Goose Bay in most other respects. It is interesting to note, however, that the low-latitude enhancement observed at Goose Bay in Figures 10a, 10b, and 11a is missing from their counterparts (Figures 40a, 40b, and 41a) even though Rino and Matthews (1980)[9] observed such low-latitude enhancements at Poker Flat.

30. Rino, C. L. and Owen, J. (1980) The structure of localized nighttime auroral zone scintillation enhancements, J. Geophys. Res. 85:2941.

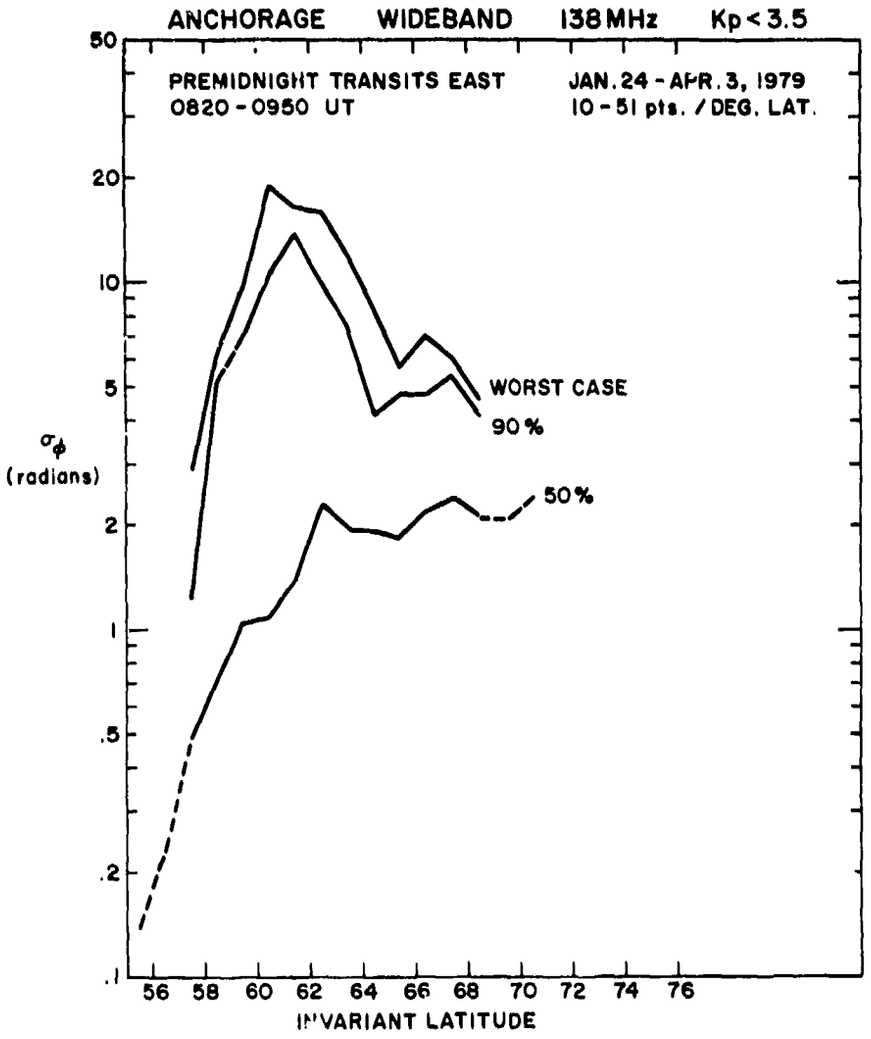

Figure 40a. Phase Scintillation Index σ_ϕ vs. Invariant Latitude for Nighttime Transits East of Anchorage Under Quiet Magnetic Conditions

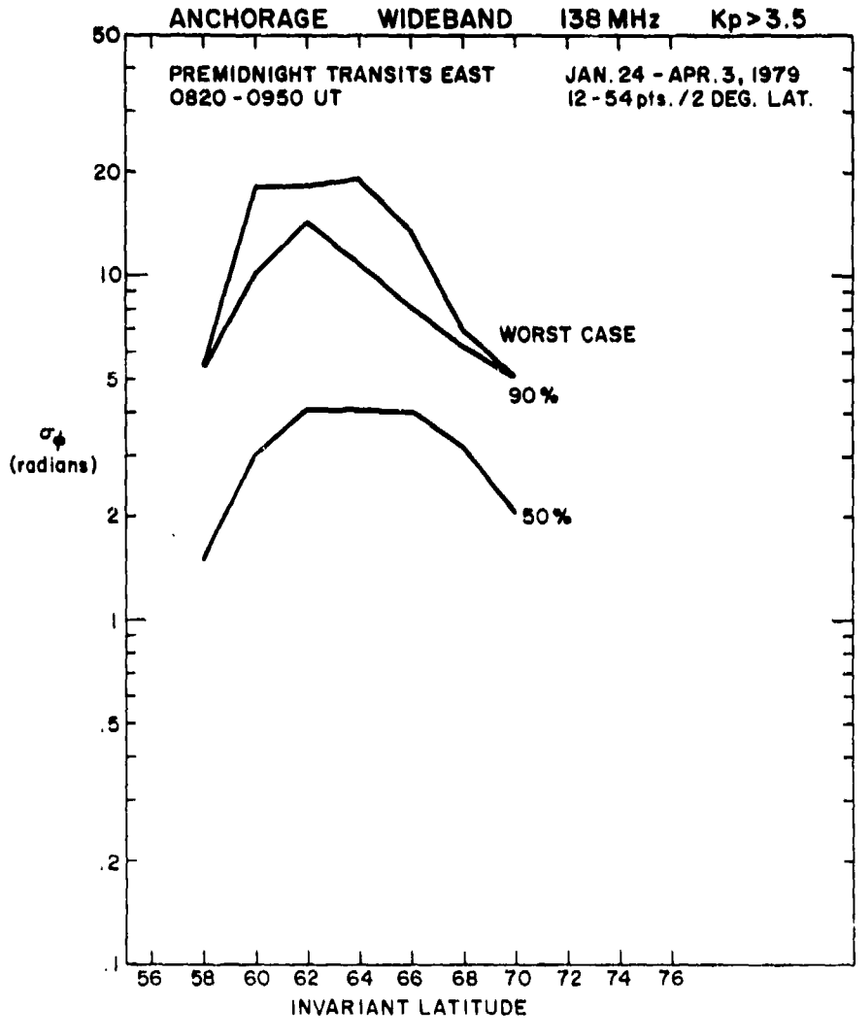

Figure 40b. Phase Scintillation Index σ_ϕ vs. Invariant Latitude for Nighttime Transits East of Anchorage Under Disturbed Magnetic Conditions

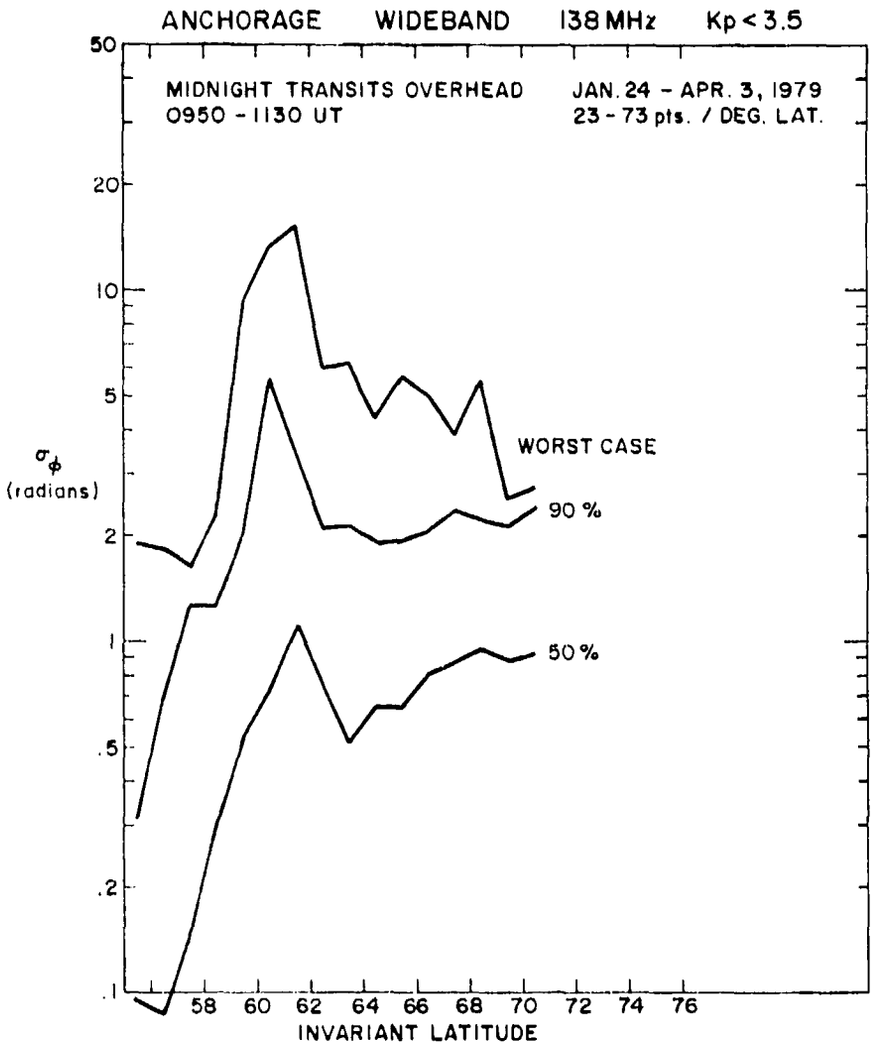

Figure 41a. Phase Scintillation Index σ_ϕ vs. Invariant Latitude for Nighttime Transits Overhead of Anchorage Under Quiet Magnetic Conditions

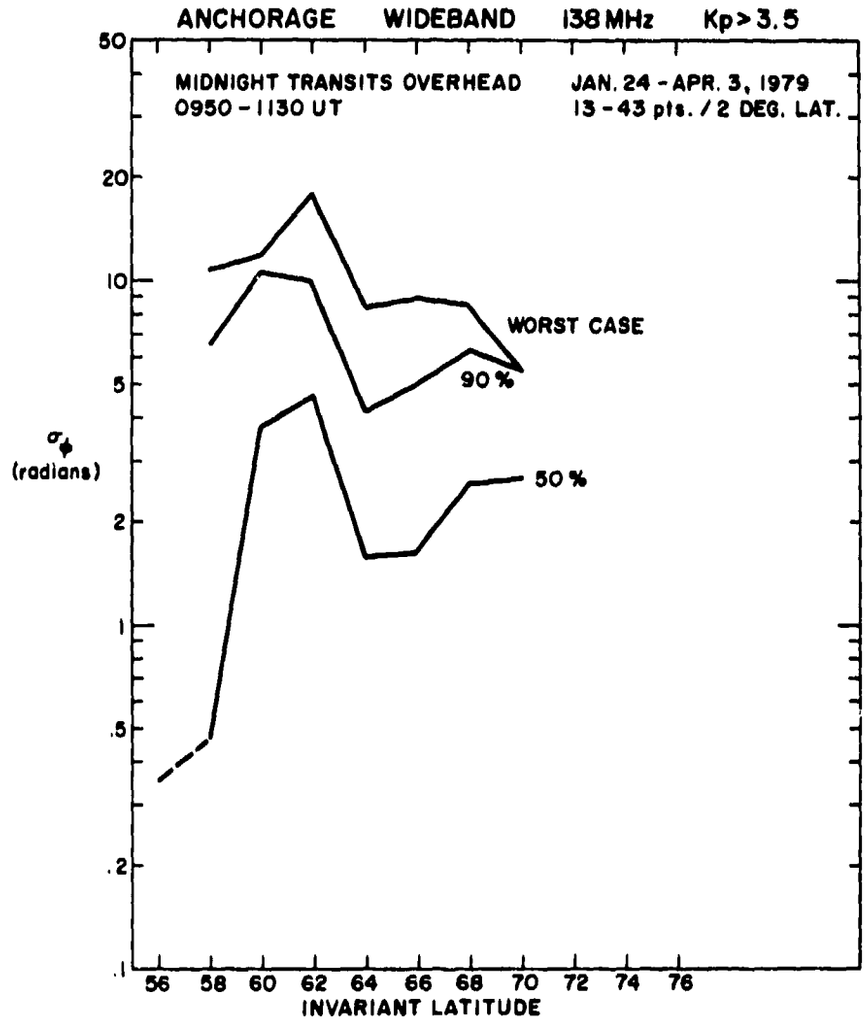

Figure 41b. Phase Scintillation Index σ_ϕ vs. Invariant Latitude for Nighttime Transits Overhead of Anchorage Under Disturbed Magnetic Conditions

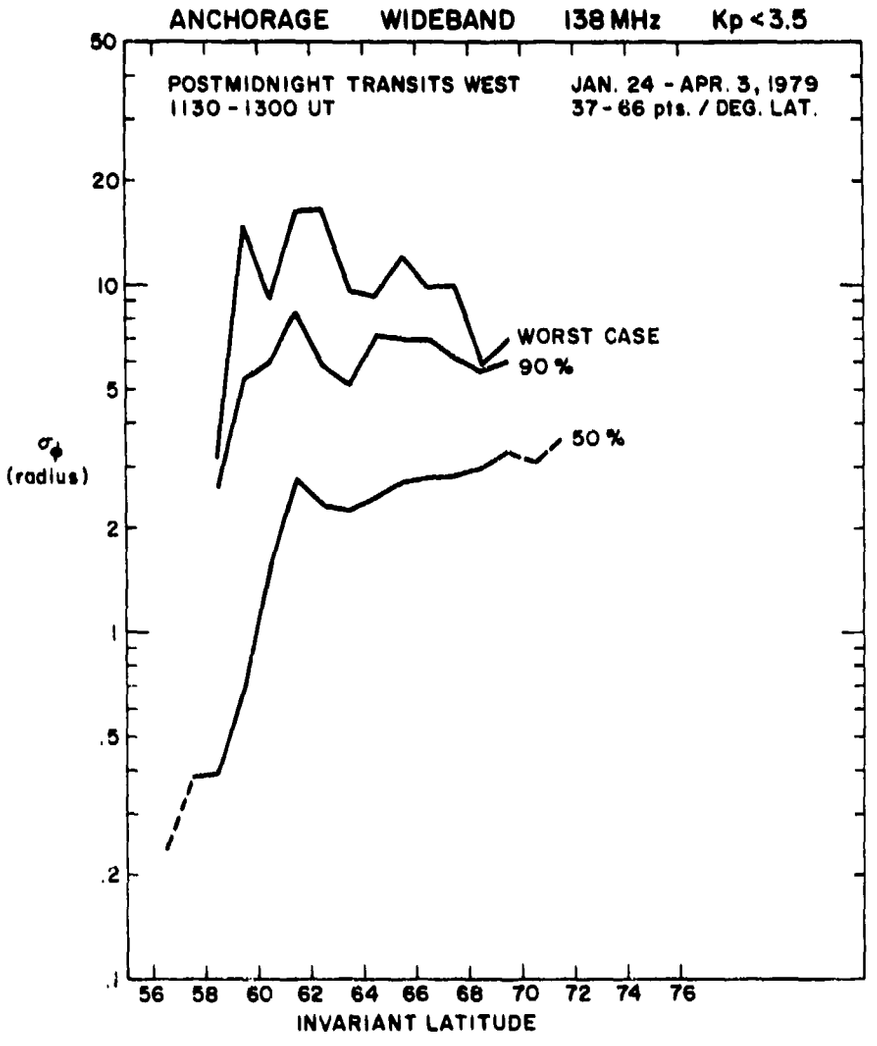

Figure 42a. Phase Scintillation Index σ_ϕ vs. Invariant Latitude for Nighttime Transits West of Anchorage Under Quiet Magnetic Conditions

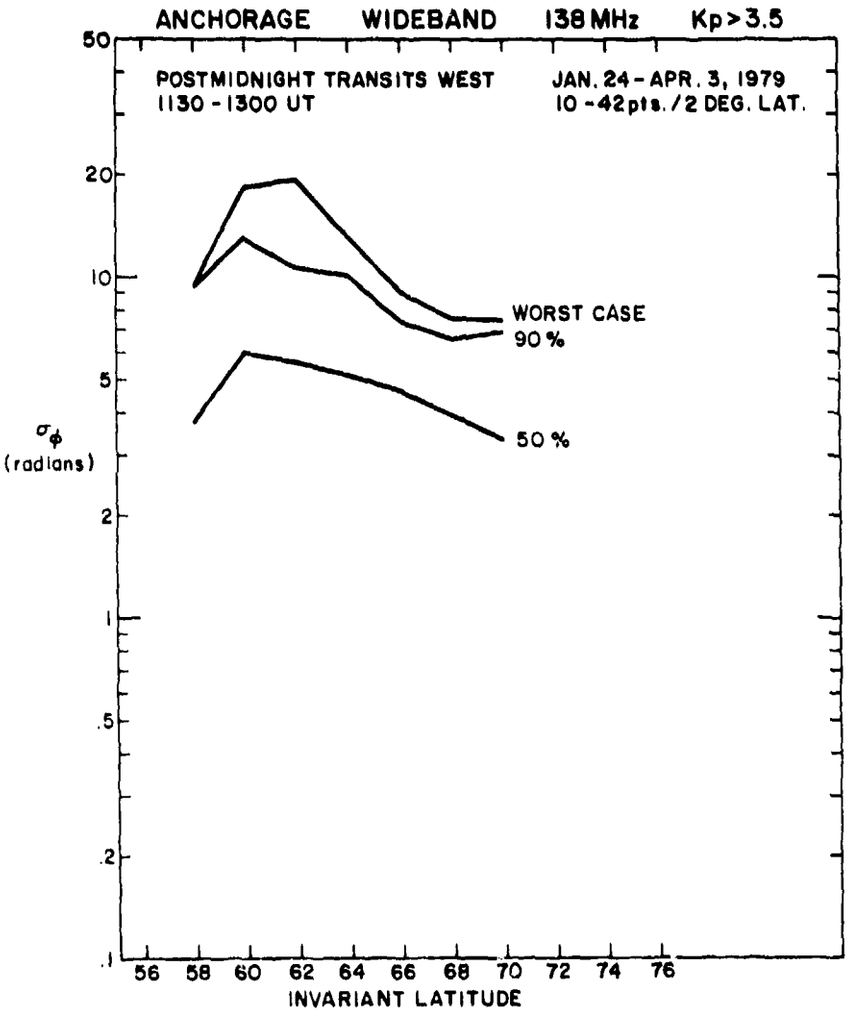

Figure 42b. Phase Scintillation Index σ_ϕ vs. Invariant Latitude for Nighttime Transits West of Anchorage Under Disturbed Magnetic Conditions

We shall discuss this point further in Section 6. The T_ϕ behavior (Figures 43a, 43b, 44a, 44b, 45a, and 45b) follows the σ_ϕ behavior quite predictably. The p_ϕ curves (Figures 46a, 46b, 47a, 47b, 48a, 48b) show median values of 2.1-2.4 and no increase in p_ϕ in the geometrical enhancement region. These are in agreement with Goose Bay results.

4.6 Nighttime Intensity Statistics at Anchorage

The S_4 index is plotted as a function of invariant latitude in the three groups for the Anchorage station in Figures 49a, 49b, 50a, 50b, 51a, and 51b. Two factors are immediately apparent from Figure 50a: 1) the lack of a geometrical enhancement in the median for the overhead quiet data and 2) the absence of an amplitude scintillation increase at the low-latitude end of the coverage. Both these factors are contrary to the nighttime observations at Goose Bay. The lack of the geometrical enhancement is probably due to the low level of irregularities expected at $\sim 60^\circ\Lambda$ under quiet conditions. Indeed a geometrical enhancement is observed during disturbed times (Figure 50b). The lack of enhanced scintillations both in phase and amplitude at the low-latitude end could be a seasonal effect and will be discussed further in Section 6.

The T_I and p_I curves (Figures 52a, 52b, 53a, 53b, 54a, and 54b and 55a, 55b, 56a, 56b, 57a, and 57b, respectively) behave very similarly to their counterparts in the Goose Bay sector.

4.7 Daytime Phase Statistics at Anchorage

Unfortunately, the latitude coverage for the Anchorage daytime phase scintillation data shown in Figures 58a, 58b, 59a, 59b, 60a, and 60b is limited, particularly for the east and west corridors. What is surprising, however, is that the magnitude of σ_ϕ is much larger compared to the daytime σ_ϕ observed at Goose Bay. This will become more apparent when we present the seasonal comparisons in Section 6. As with the daytime overhead Goose Bay data (Figure 29a) a geometrical enhancement is clearly apparent in Figure 59a. In the western corridor, also, a geometrical enhancement is observed as with nighttime data. Investigation of individual pass behavior shows that a fairly prominent geometrical enhancement is observed in almost half the daytime passes observed in the western corridor. Thus, at least, during this high sunspot period it may not be quite correct to assume that daytime irregularities are always rodlike in nature as has been done by Fremouw and Lansinger (1981).[29] This is again similar to the situation at Goose Bay where two corridors also showed daytime enhancements as pointed out in Section 4.5. This finding needs further careful investigation.

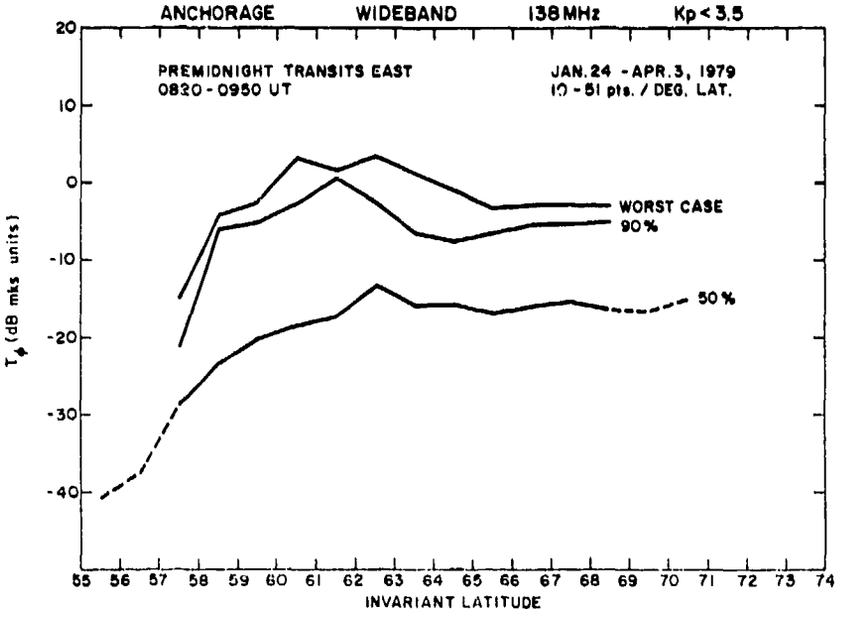

Figure 43a. Spectral Strength T_ϕ of Phase at 1 Hz vs. Invariant Latitude for Nighttime Transits East of Anchorage Under Quiet Magnetic Conditions

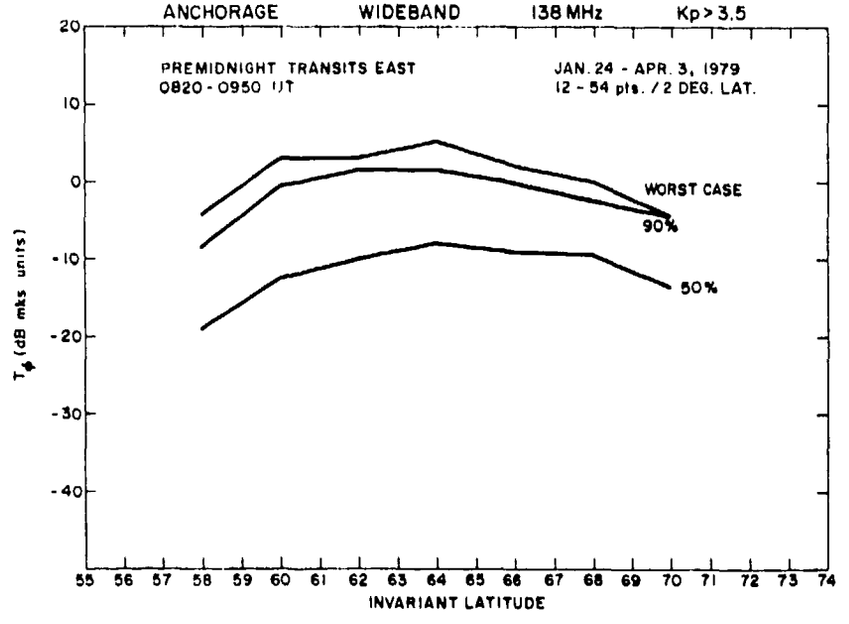

Figure 43b. Spectral Strength T_ϕ of Phase at 1 Hz vs. Invariant Latitude for Nighttime Transits East of Anchorage Under Disturbed Magnetic Conditions

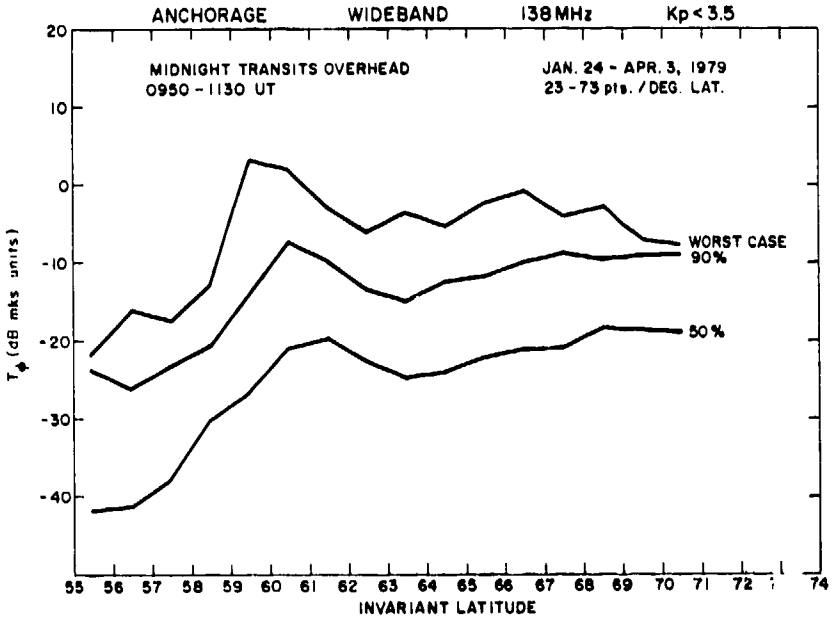

Figure 44a. Spectral Strength T_ϕ of Phase at 1 Hz vs. Invariant Latitude for Nighttime Transits Overhead of Anchorage Under Quiet Magnetic Conditions

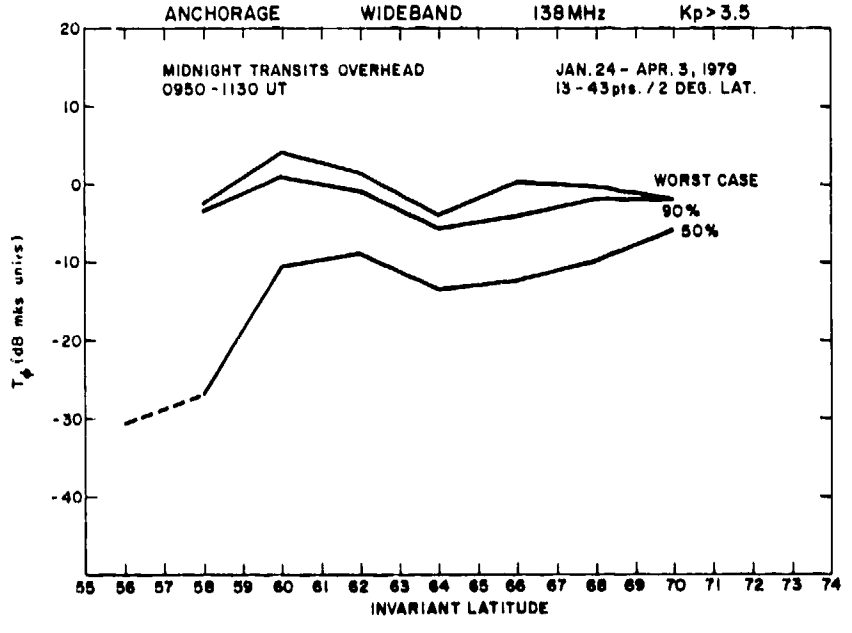

Figure 44b. Spectral Strength T_ϕ of Phase at 1 Hz vs. Invariant Latitude for Nighttime Transits Overhead of Anchorage Under Disturbed Magnetic Conditions

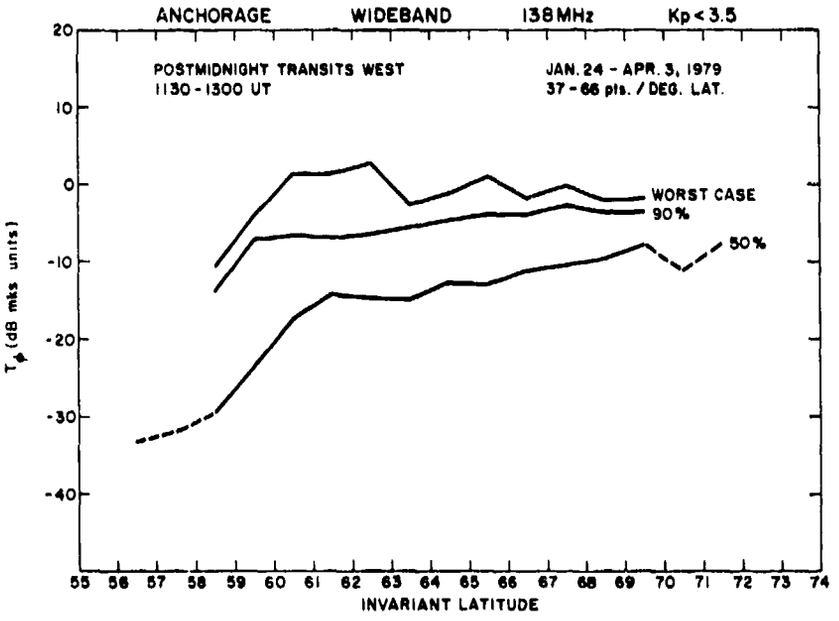

Figure 45a. Spectral Strength T_ϕ of Phase at 1 Hz vs. Invariant Latitude for Nighttime Transits West of Anchorage Under Quiet Magnetic Conditions

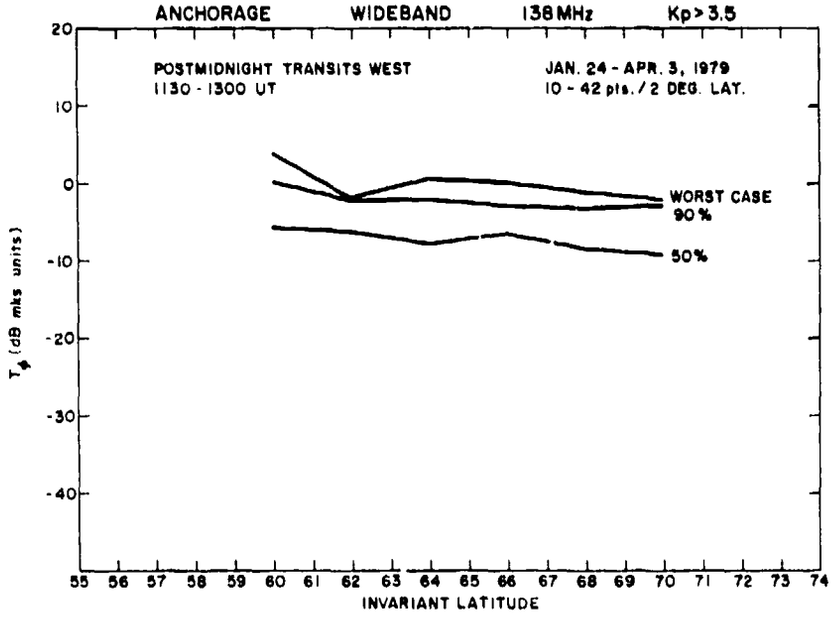

Figure 45b. Spectral Strength T_ϕ of Phase at 1 Hz vs. Invariant Latitude for Nighttime Transits West of Anchorage Under Disturbed Magnetic Conditions

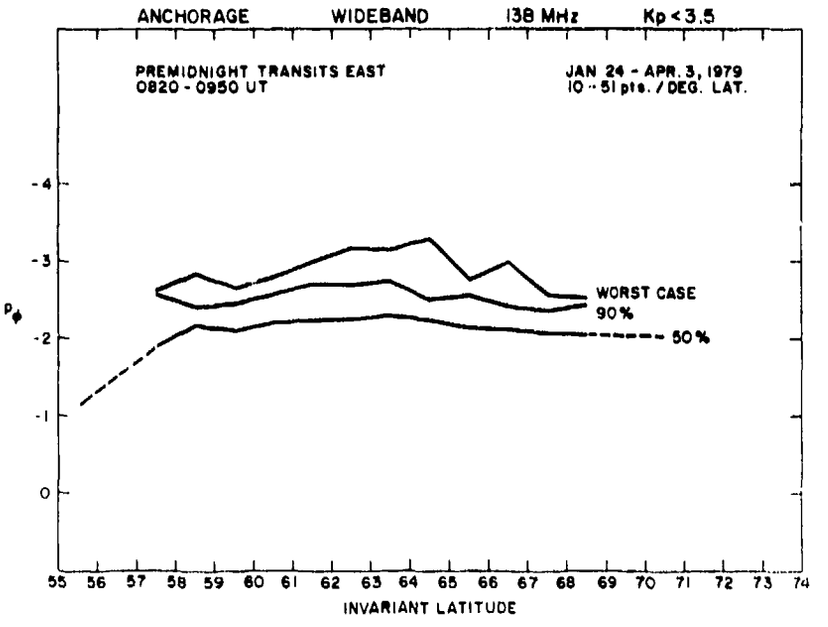

Figure 46a. Phase Spectral Index p_ϕ vs. Invariant Latitude for Nighttime Transits East of Anchorage Under Quiet Magnetic Conditions

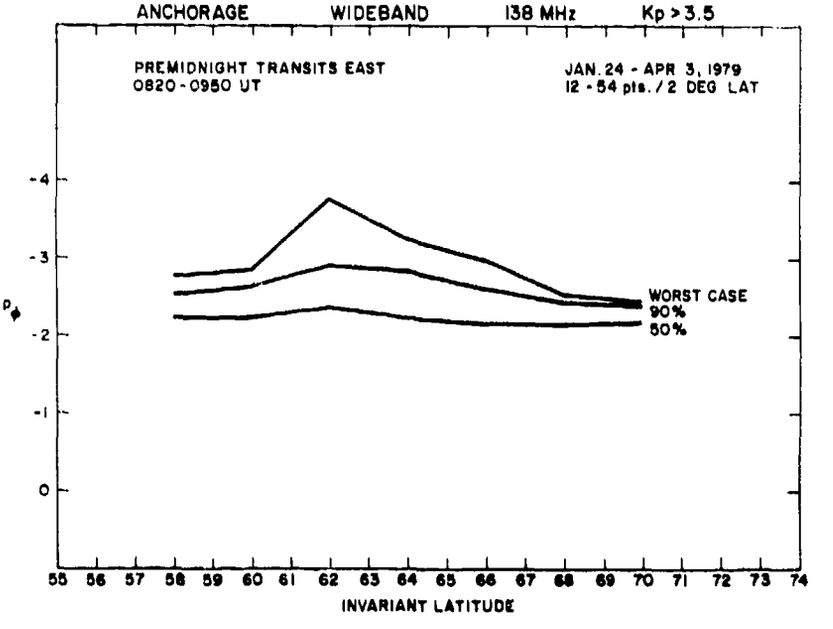

Figure 46b. Phase Spectral Index p_ϕ vs. Invariant Latitude for Nighttime Transits East of Anchorage Under Disturbed Magnetic Conditions

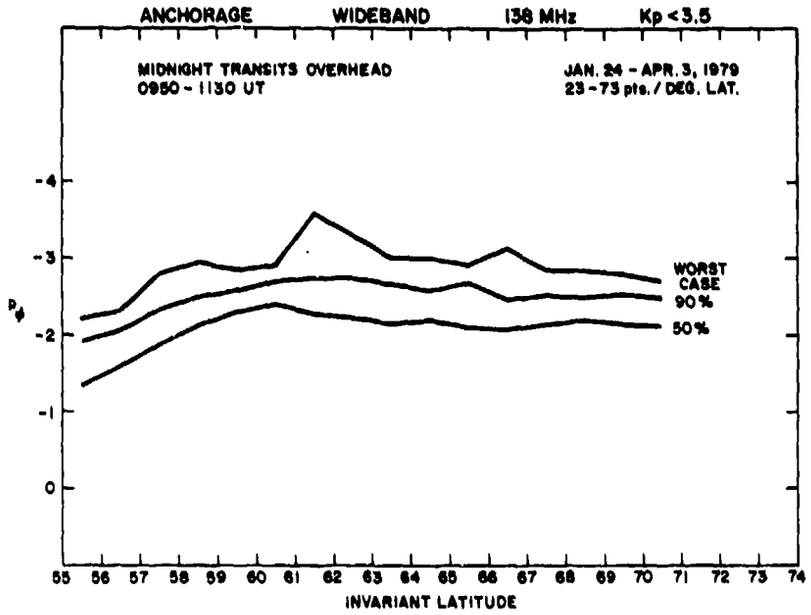

Figure 47a. Phase Spectral Index p_ϕ vs. Invariant Latitude for Nighttime Transits Overhead of Anchorage Under Quiet Magnetic Conditions

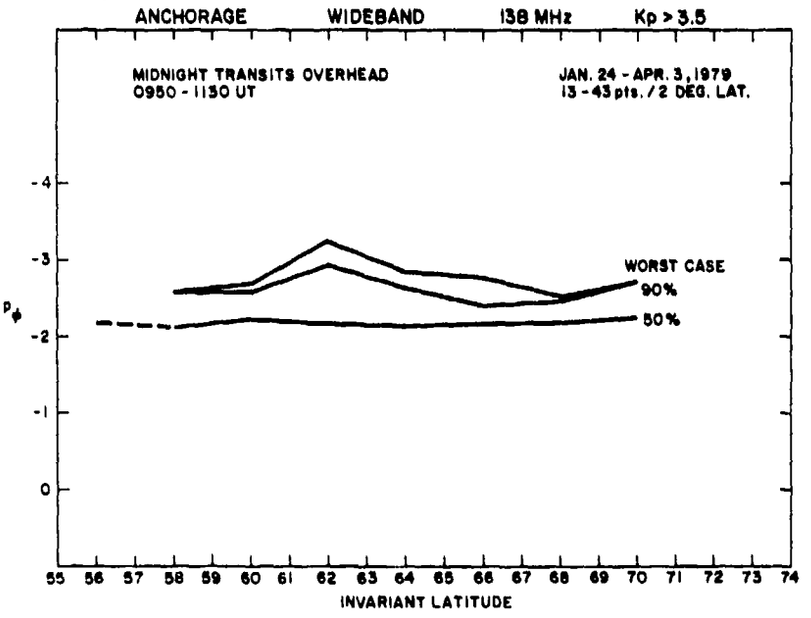

Figure 47b. Phase Spectral Index p_ϕ vs. Invariant Latitude for Nighttime Transits Overhead of Anchorage Under Disturbed Magnetic Conditions

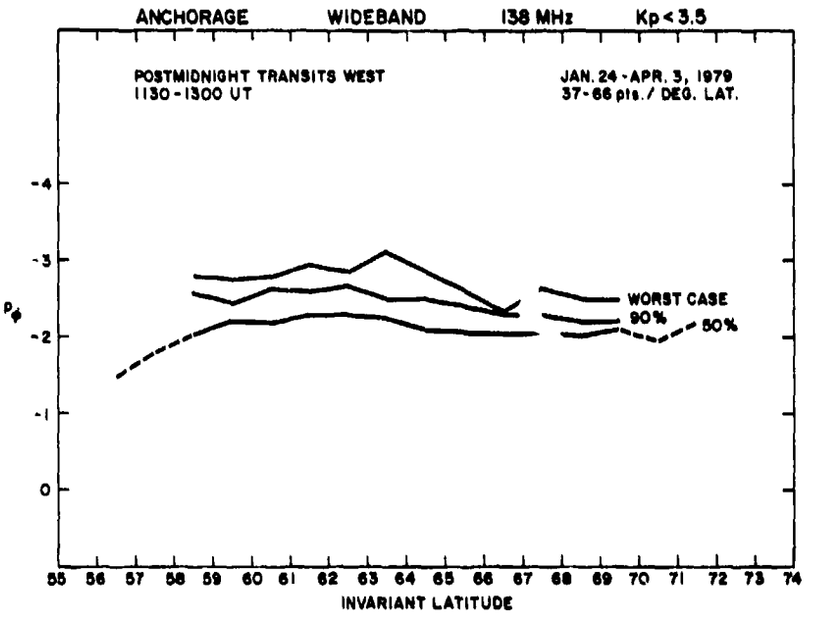

Figure 48a. Phase Spectral Index p_ϕ vs. Invariant Latitude for Nighttime Transits West of Anchorage Under Quiet Magnetic Conditions

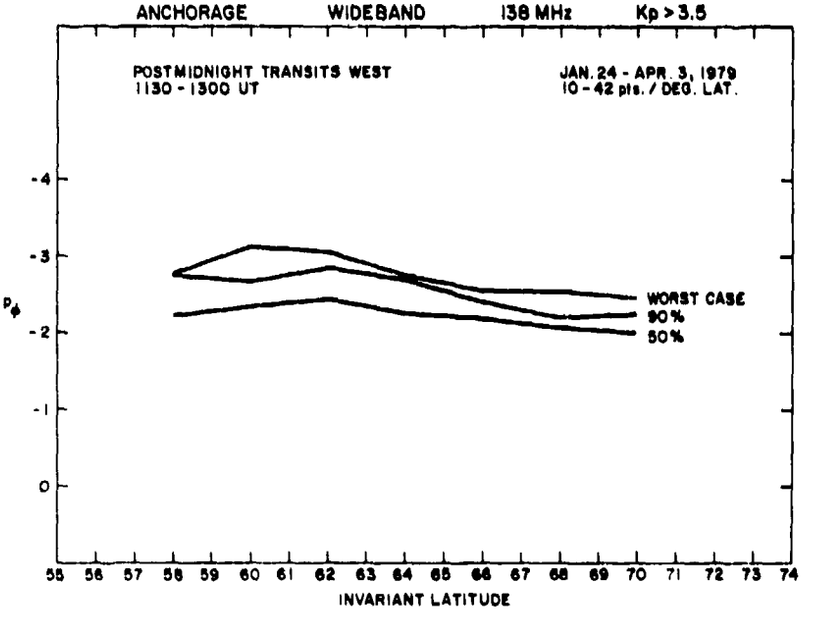

Figure 48b. Phase Spectral Index p_ϕ vs. Invariant Latitude for Nighttime Transits West of Anchorage Under Disturbed Magnetic Conditions

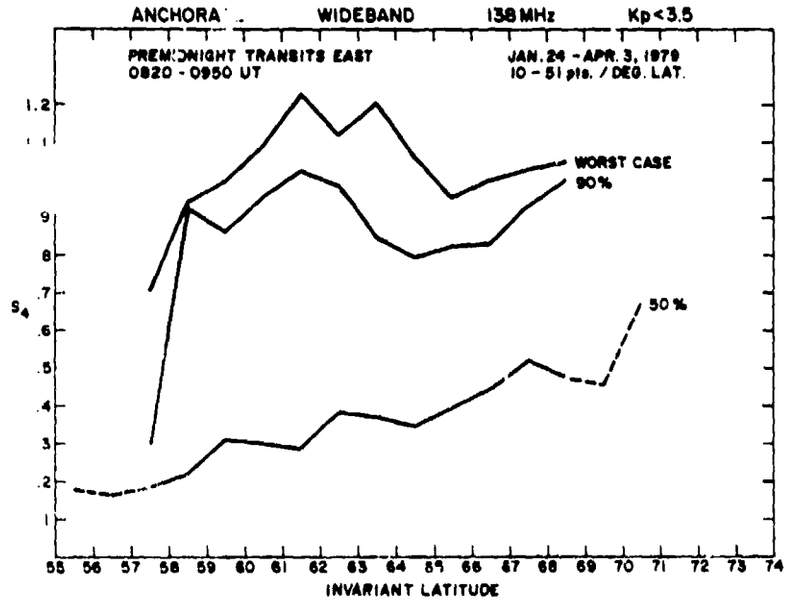

Figure 49a. Intensity Scintillation Index S_4 vs. Invariant Latitude for Nighttime Transits East of Anchorage Under Quiet Magnetic Conditions

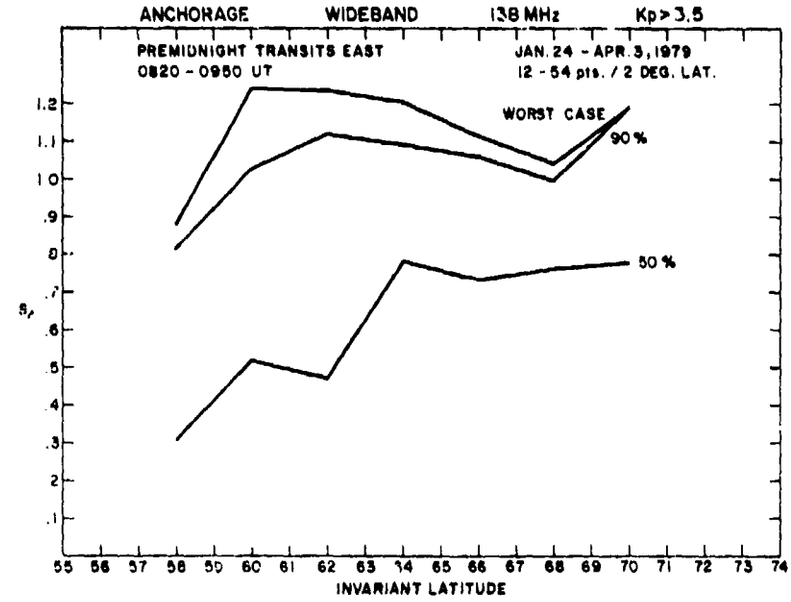

Figure 49b. Intensity Scintillation Index S_4 vs. Invariant Latitude for Nighttime Transits East of Anchorage Under Disturbed Magnetic Conditions

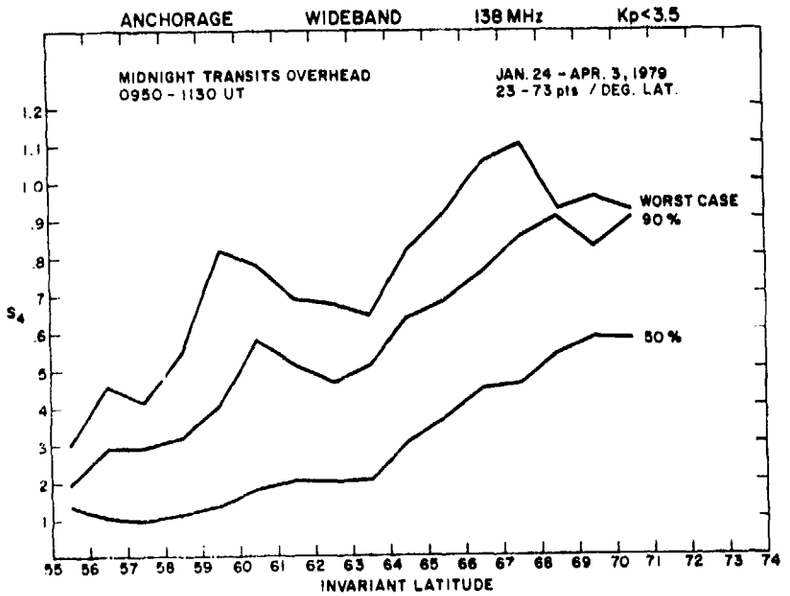

Figure 50a. Intensity Scintillation Index S_4 vs. Invariant Latitude for Nighttime Transits Overhead of Anchorage Under Quiet Magnetic Conditions

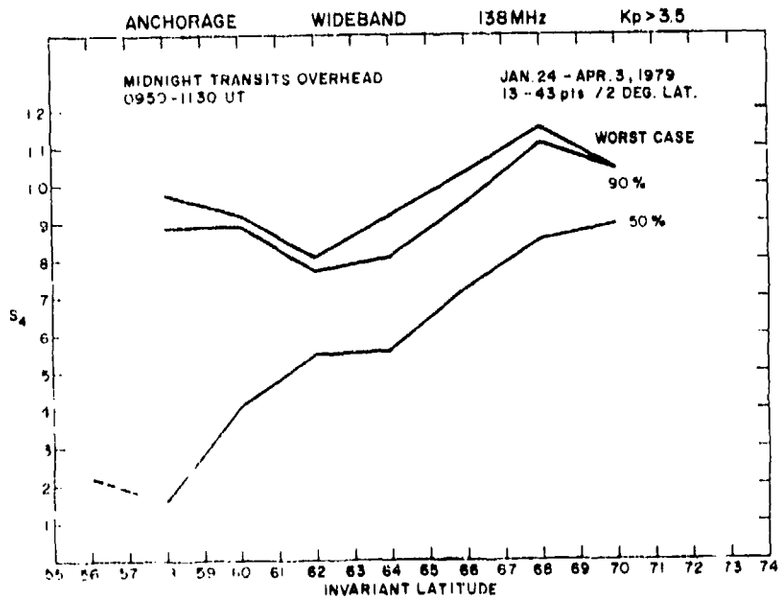

Figure 50b. Intensity Scintillation Index S_4 vs. Invariant Latitude for Nighttime Transits Overhead of Anchorage Under Disturbed Magnetic Conditions

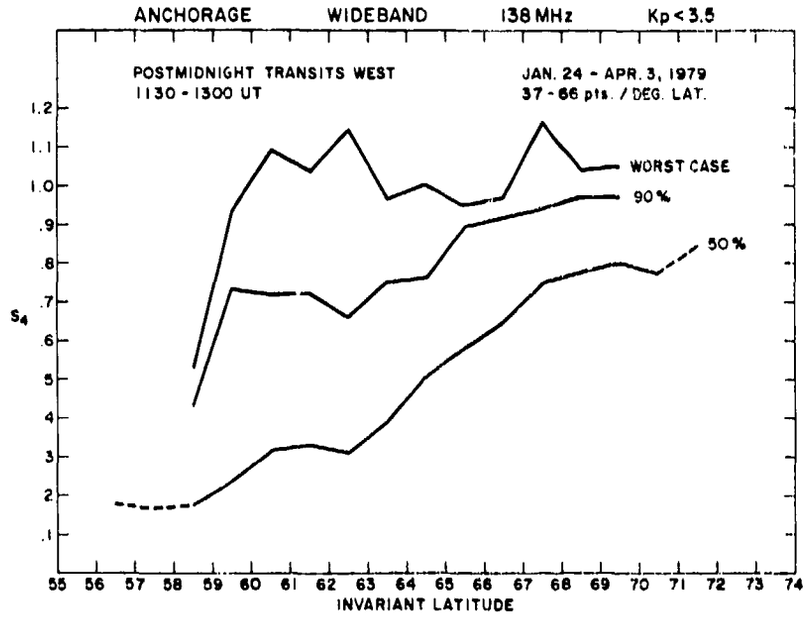

Figure 51a. Intensity Scintillation Index S_4 vs. Invariant Latitude for Nighttime Transits West of Anchorage Under Quiet Magnetic Conditions

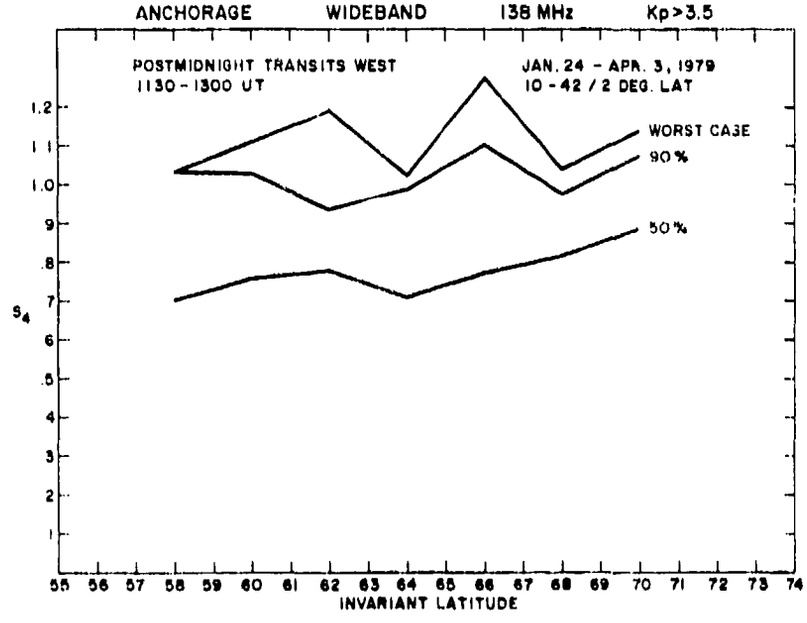

Figure 51b. Intensity Scintillation Index S_4 vs. Invariant Latitude for Nighttime Transits West of Anchorage Under Disturbed Magnetic Conditions

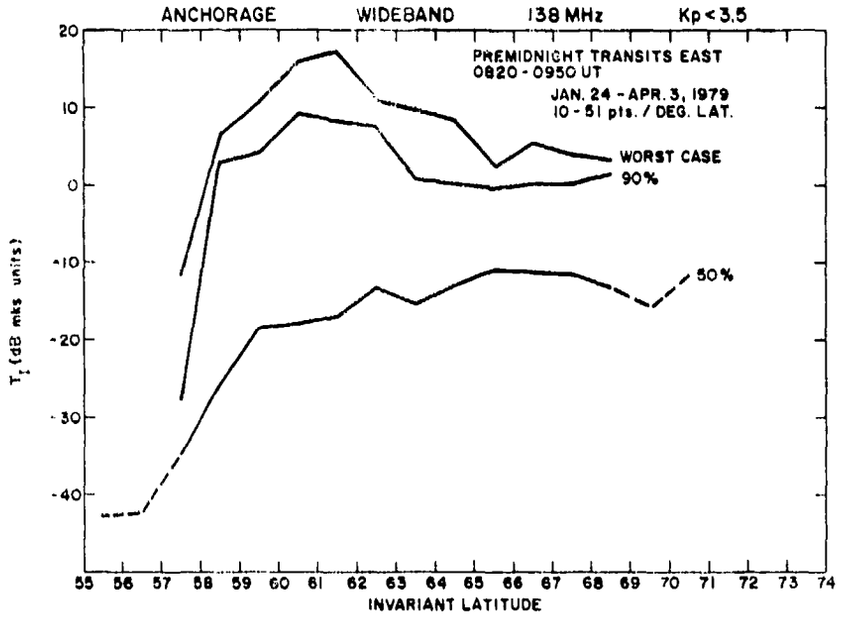

Figure 52a. Spectral Strength T_I of Intensity at 1 Hz vs. Invariant Latitude for Nighttime Transits East of Anchorage Under Quiet Magnetic Conditions

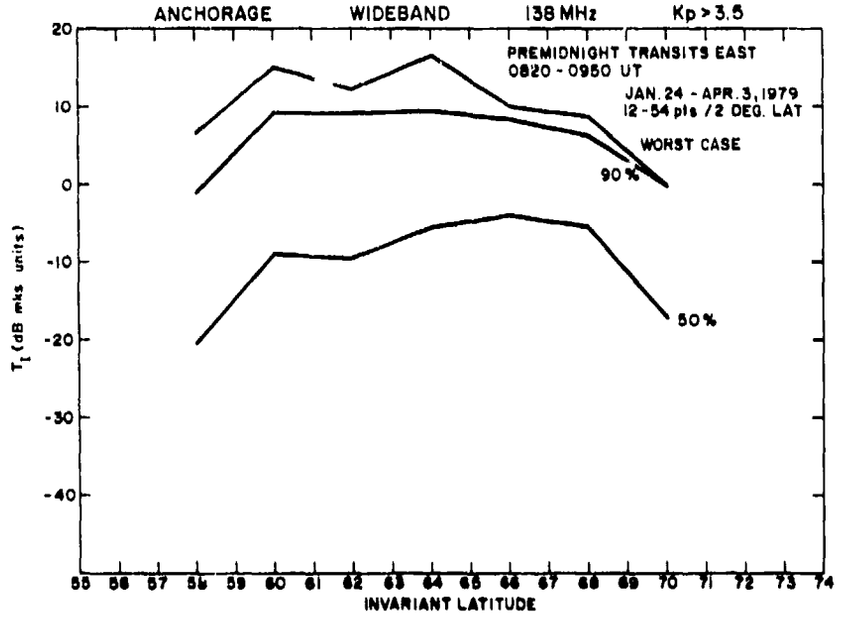

Figure 52b. Spectral Strength T_I of Intensity at 1 Hz vs. Invariant Latitude for Nighttime Transits East of Anchorage Under Disturbed Magnetic Conditions

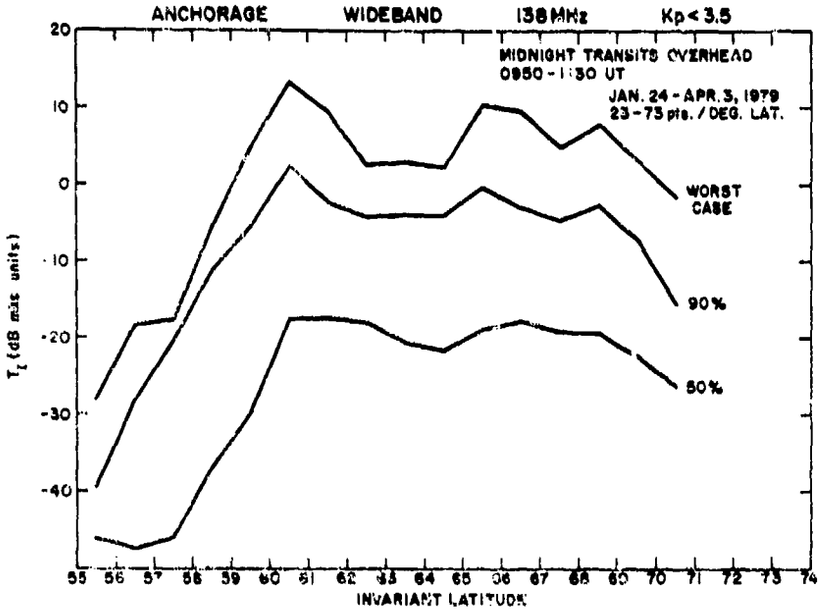

Figure 53a. Spectral Strength T_I of Intensity at 1 Hz vs. Invariant Latitude for Nighttime Transits Overhead of Anchorage Under Quiet Magnetic Conditions

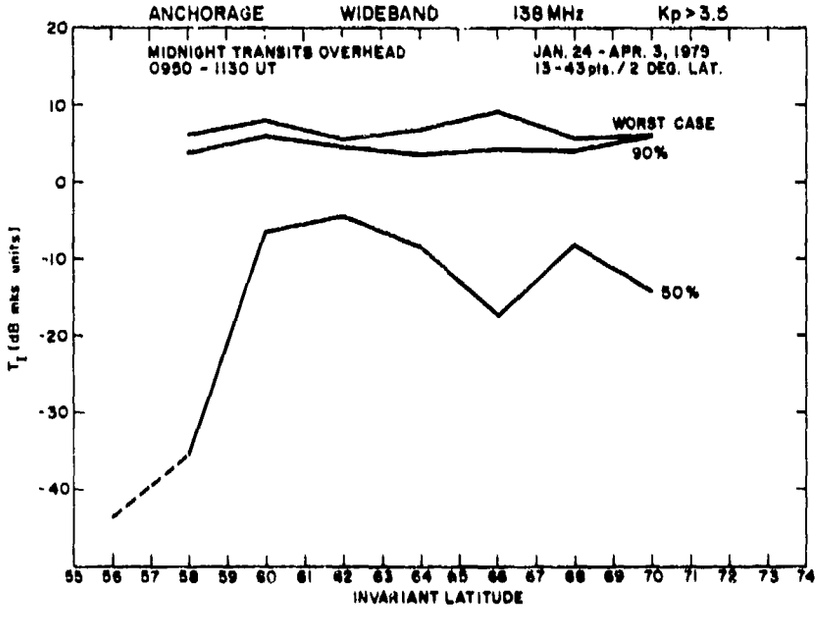

Figure 53b. Spectral Strength T_I of Intensity at 1 Hz vs. Invariant Latitude for Nighttime Transits Overhead of Anchorage Under Disturbed Magnetic Conditions

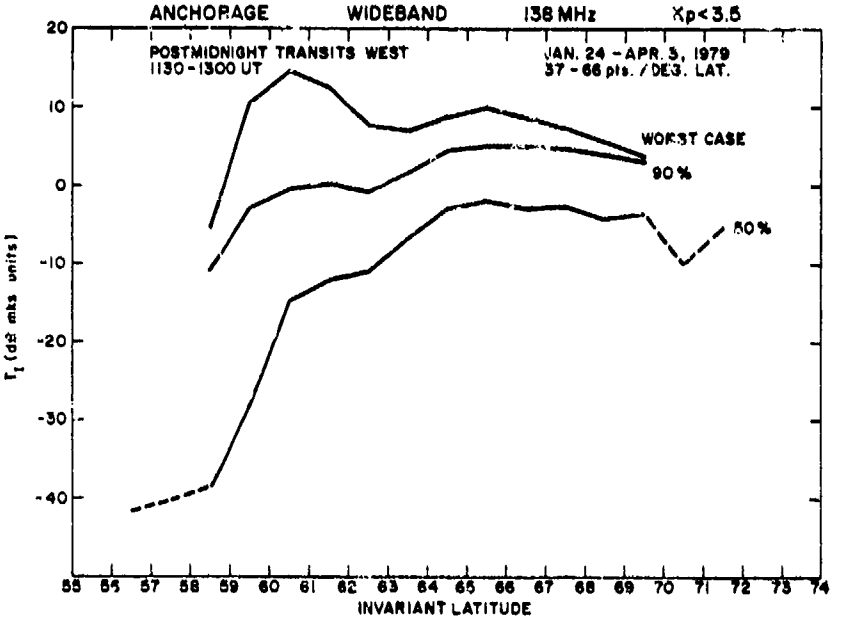

Figure 54a. Spectral Strength T_I of Intensity at 1 Hz vs. Invariant Latitude for Nighttime Transits West of Anchorage Under Quiet Magnetic Conditions

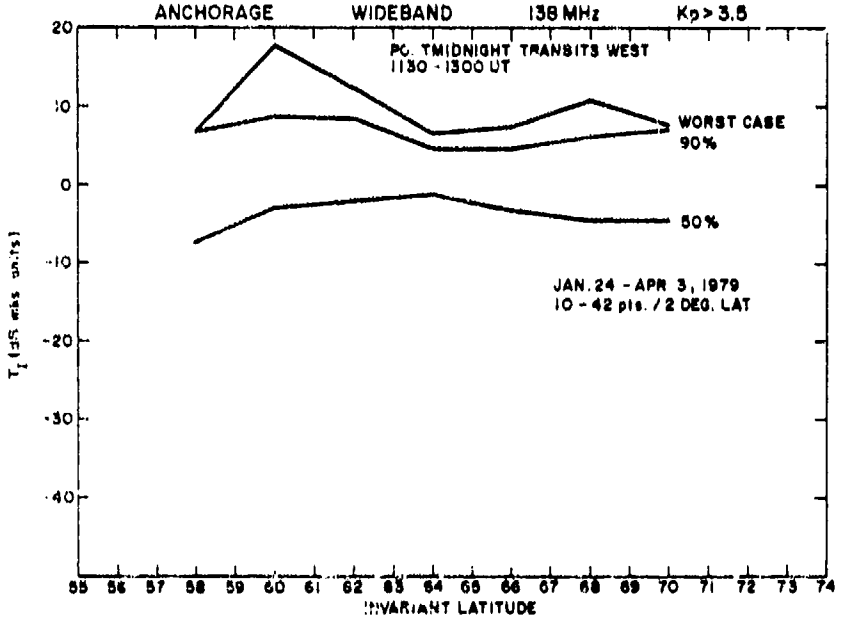

Figure 54b. Spectral Strength T_I of Intensity at 1 Hz vs. Invariant Latitude for Nighttime Transits West of Anchorage Under Disturbed Magnetic Conditions

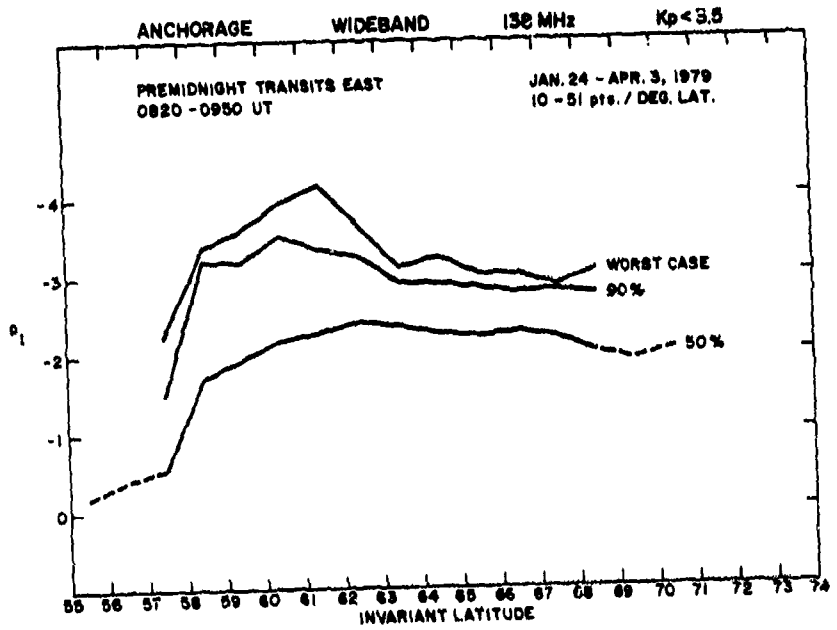

Figure 55a. Intensity Spectral Index p_I vs. Invariant Latitude for Nighttime Transits East of Anchorage Under Quiet Magnetic Conditions

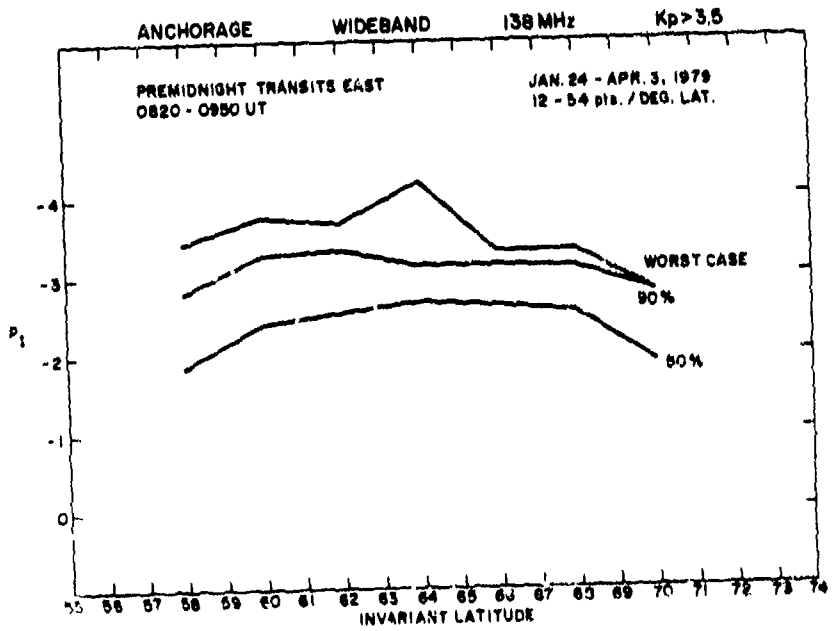

Figure 55b. Intensity Spectral Index p_I vs. Invariant Latitude for Nighttime Transits East of Anchorage Under Disturbed Magnetic Conditions

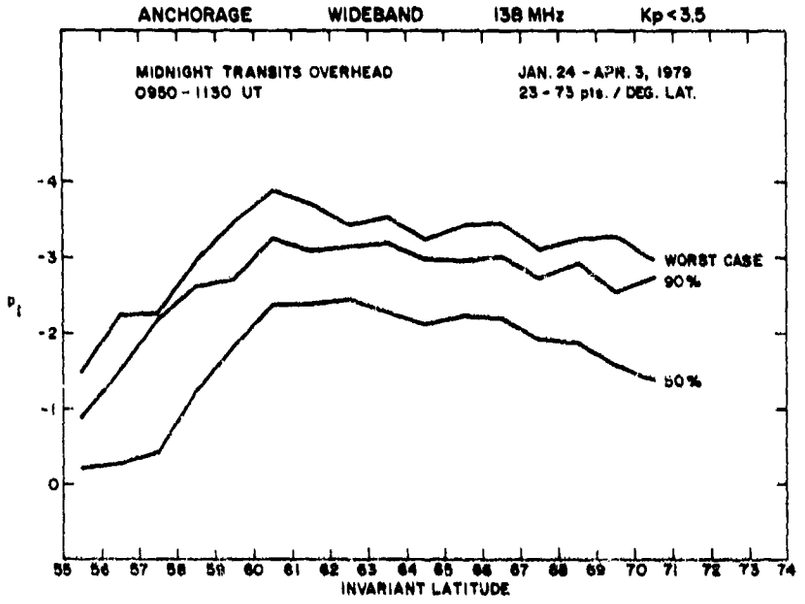

Figure 56a. Intensity Spectral Index p_I vs. Invariant Latitude for Nighttime Transits Overhead of Anchorage Under Quiet Magnetic Conditions

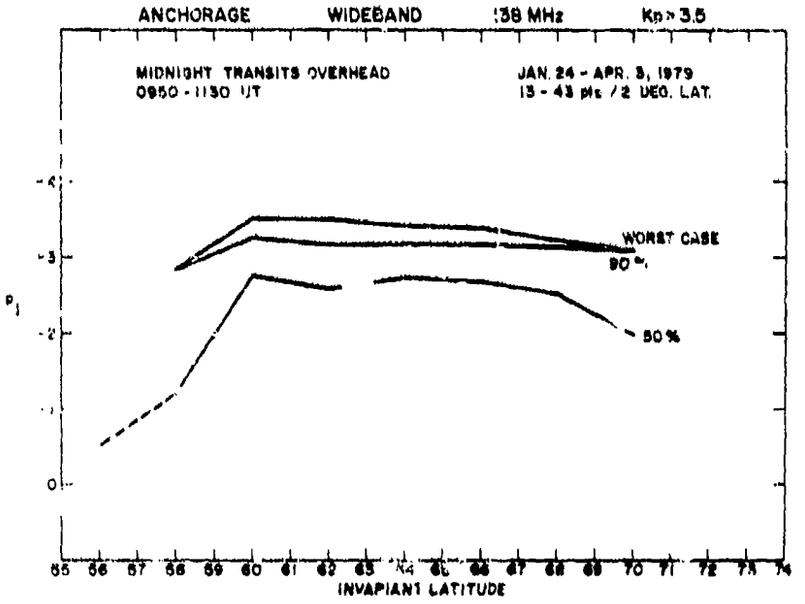

Figure 56b. Intensity Spectral Index p_I vs. Invariant Latitude for Nighttime Transits Overhead of Anchorage Under Disturbed Magnetic Conditions

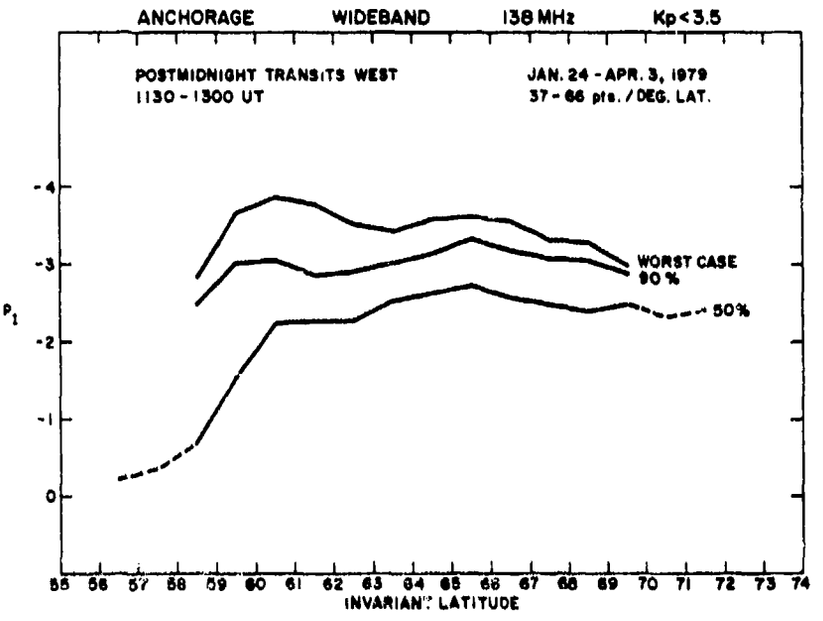

Figure 57a. Intensity Spectral Index p_I vs. Invariant Latitude for Nighttime Transits West of Anchorage Under Quiet Magnetic Conditions

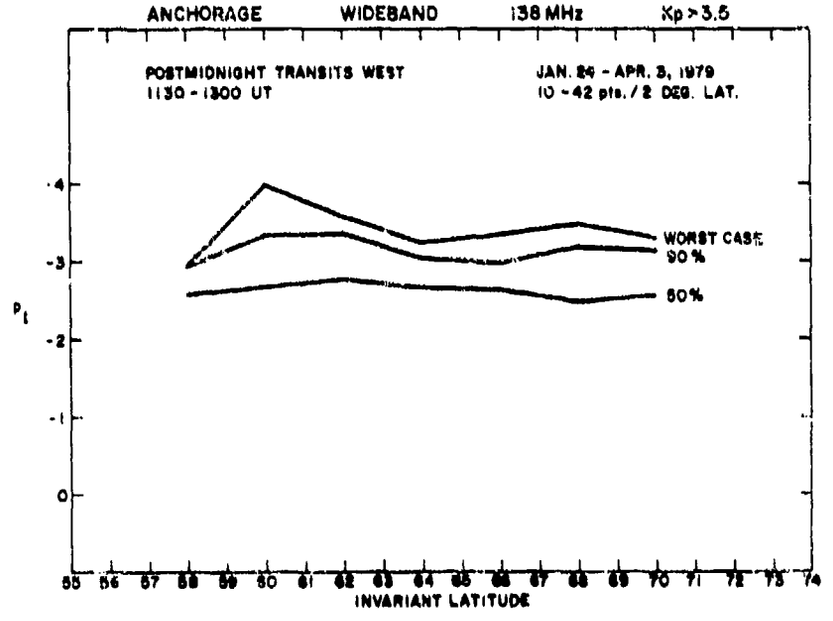

Figure 57b. Intensity Spectral Index p_I vs. Invariant Latitude for Nighttime Transits West of Anchorage Under Disturbed Magnetic Conditions

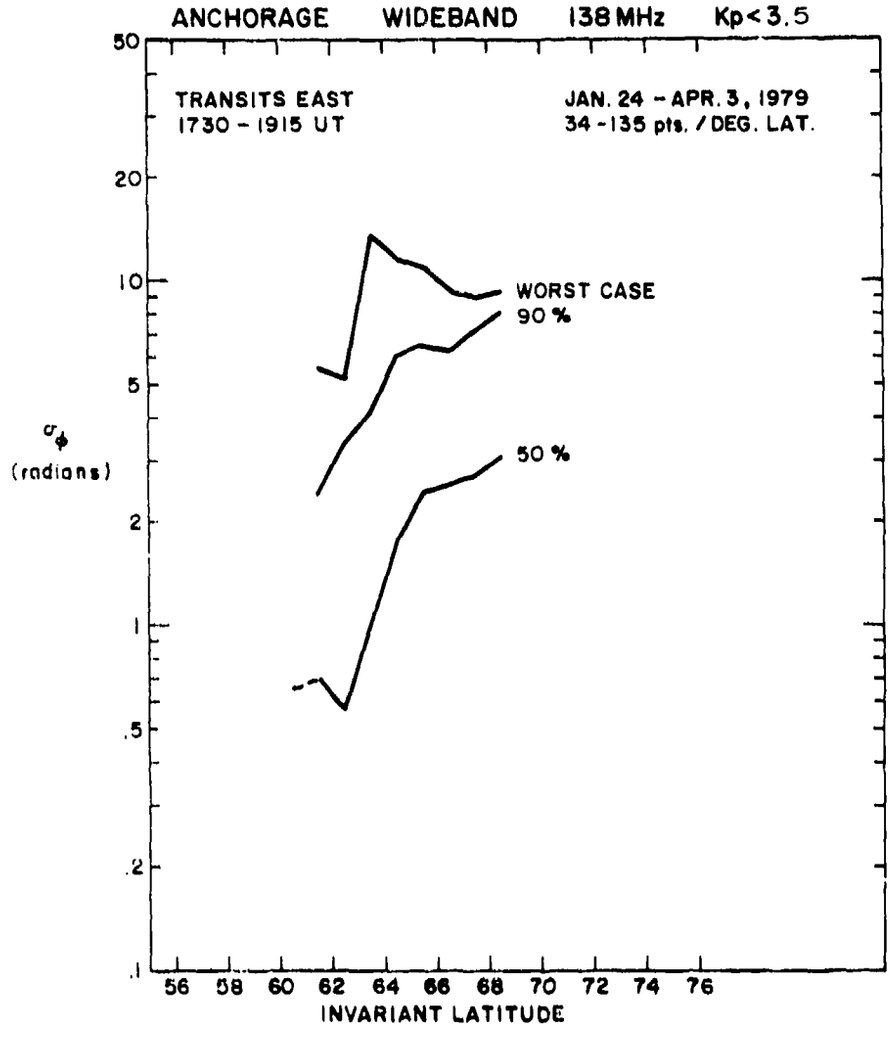

Figure 58a. Phase Scintillation Index σ_ϕ vs. Invariant Latitude for Daytime Transits East of Anchorage Under Quiet Magnetic Conditions

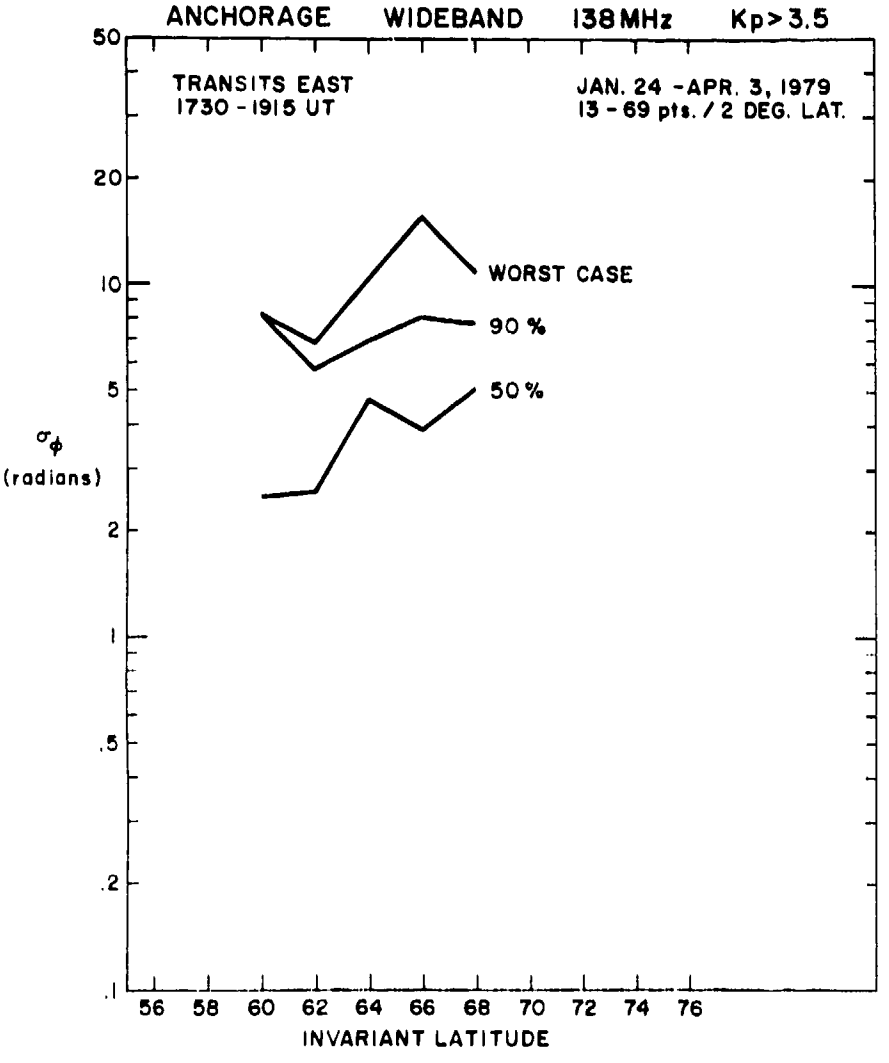

Figure 58b. Phase Scintillation Index σ_ϕ vs. Invariant Latitude for Daytime Transits East of Anchorage Under Disturbed Magnetic Conditions

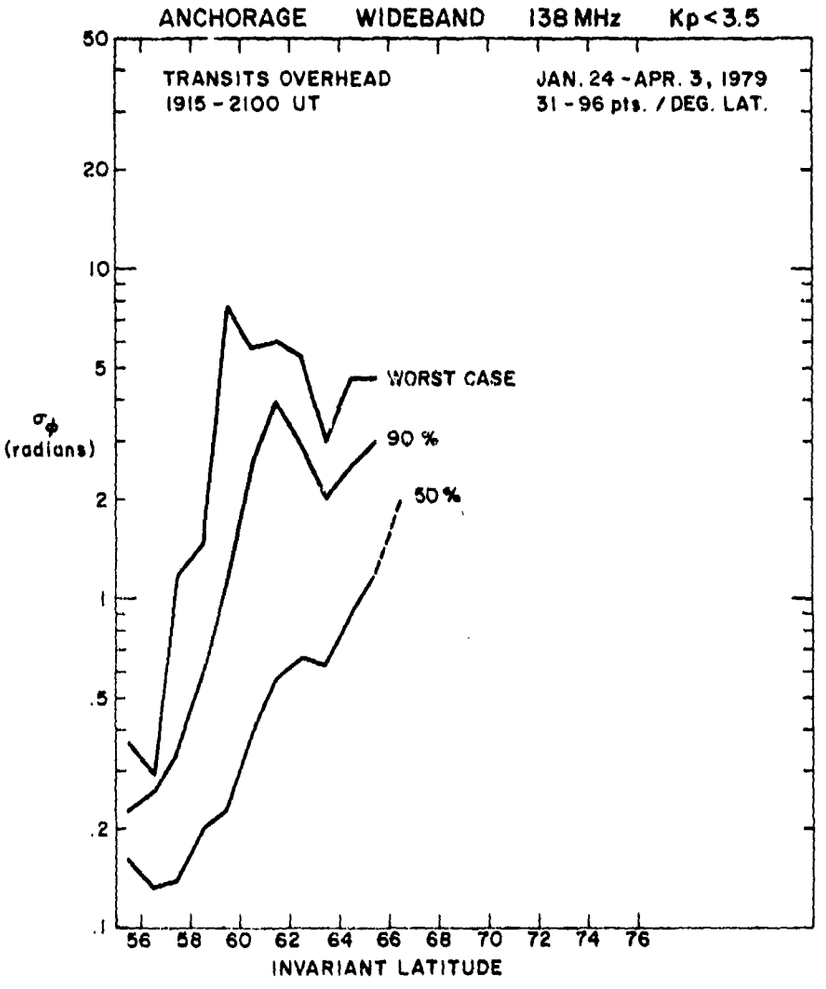

Figure 59a. Phase Scintillation Index σ_ϕ vs. Invariant Latitude for Daytime Transits Overhead of Anchorage Under Quiet Magnetic Conditions

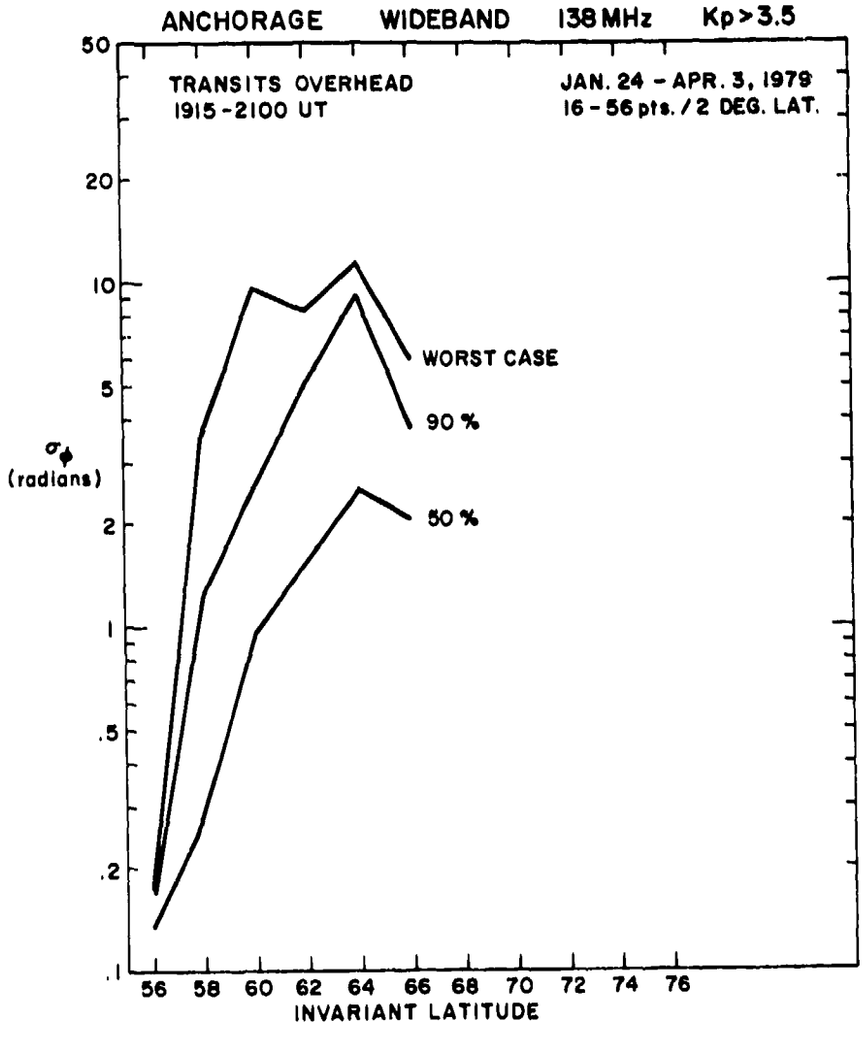

Figure 59b. Phase Scintillation Index σ_ϕ vs. Invariant Latitude for Daytime Transits Overhead of Anchorage Under Disturbed Magnetic Conditions

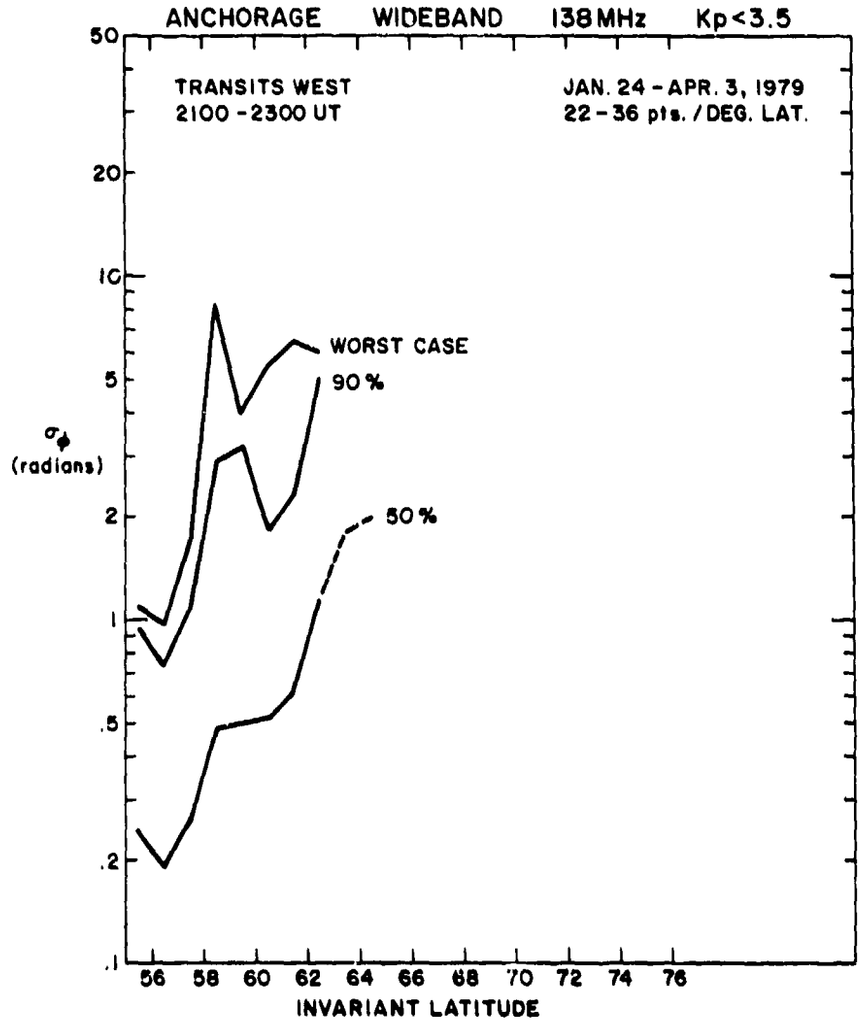

Figure 60a. Phase Scintillation Index σ_ϕ vs. Invariant Latitude for Daytime Transits West of Anchorage Under Quiet Magnetic Conditions

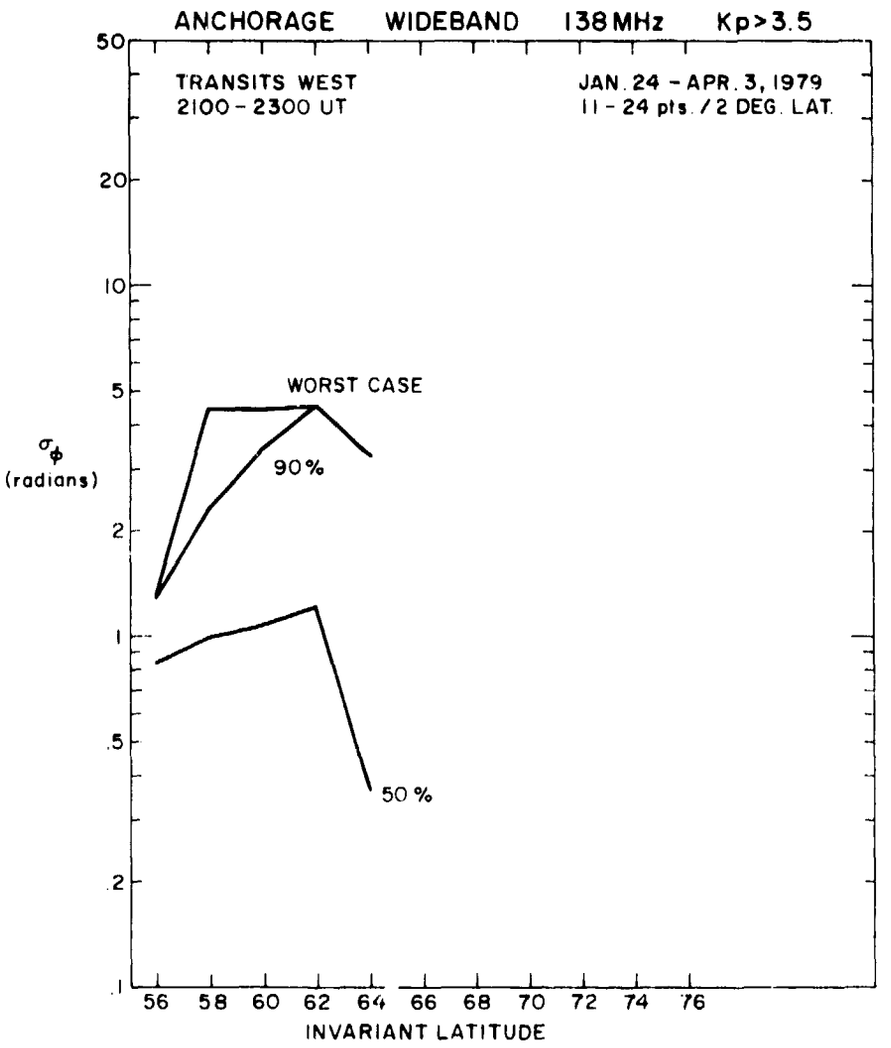

Figure 60b. Phase Scintillation Index σ_ϕ vs. Invariant Latitude for Daytime Transits West of Anchorage Under Disturbed Magnetic Conditions

The T_ϕ curves (Figures 61a, 61b, 62a, 62b, 63a, and 63b) behave similarly to the σ_ϕ set with again the same two corridors (Figures 62a and 63a) showing geometrical enhancements. The magnitude of T_ϕ, however, is much larger than that observed at Goose Bay. For instance, in the Goose Bay overhead daytime T_ϕ plot (Figure 32a) the magnitude of median T_ϕ at 65°Λ is approximately -40 dB whereas, at Anchorage at the same position (Figure 62a) it is a little below -20 dB. (The 65°Λ position was chosen because it is outside the geometrical enhancement region of the two stations.) This is a very large difference in phase spectral density at the two stations.

The p_ϕ values, shown in Figures 64a, 64b, 65a, 65b, 66a, and 66b are in their median values slightly higher than their Goose Bay counterparts. For instance, comparing Figure 35a with Figure 65a we find that p_ϕ varies between 2.0 and 2.1 in the latitude interval 61-67°Λ at Goose Bay whereas, at Anchorage p_ϕ is 2.2 between 60-65°Λ. This slight elevation of p_ϕ can probably be explained by invoking better signal-to-noise ratios associated with the higher phase scintillations in the Anchorage sector.

4.8 Daytime Intensity Statistics at Anchorage

As is to be expected from the phase statistics, the amplitude statistics at Anchorage shown in Figures 67a, 67b, 68a, 68b, 69a, and 69b show a much higher level of S_4 index as well as magnetic storm increase in S_4 when contrasted with similar curves in the Goose Bay sector. This is an unexpected result emanating from this comparative study and reasons for such behavior are unclear at this time.

5. MAGNETIC ACTIVITY VARIATION OF SCINTILLATIONS

In Section 4 the scintillation data at the two stations were lumped into two wide ranges of magnetic activity. To study the effect of magnetic activity over smaller ranges we constructed three subgroups of the data: the lowest range being Kp = 0-2⁻, an intermediate range with Kp = 2-5⁻, and the high activity group with Kp ≥ 5. To obtain some statistical validity of the median scintillation values, particularly in the highest activity range, we put together the three different time sectors for nighttime and daytime passes and considered 2° latitude bins. Magnetic activity seems to affect the nighttime auroral oval region at latitudes <68° as may be observed from Figures 70 and 71 which show the median σ_ϕ and S_4 as a function of latitude for Goose Bay. It is somewhat surprising that about 68°Λ there seems to be little effect of magnetic storms in increasing either of these parameters significantly.

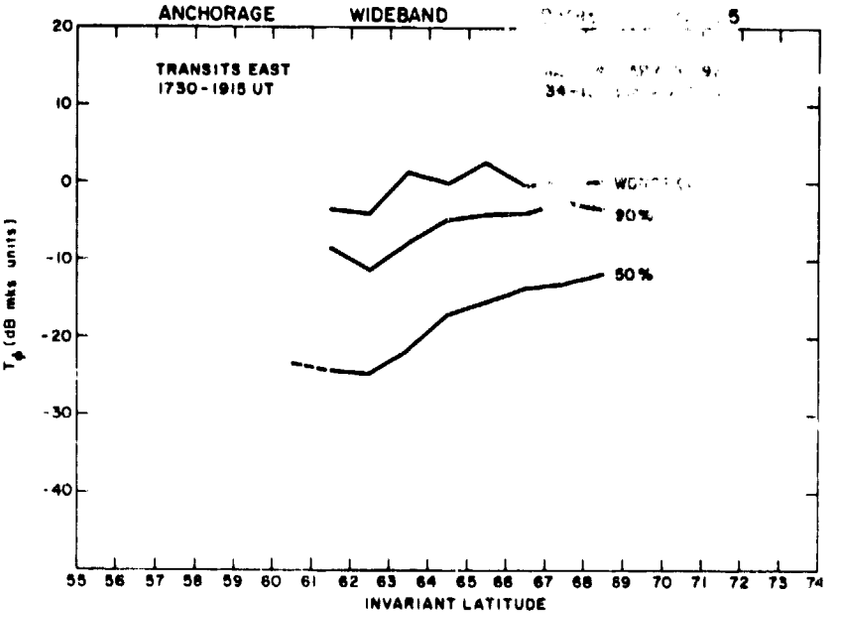

Figure 61a. Spectral Strength T_ϕ of Phase at 1 Hz vs. Invariant Latitude for Daytime Transits East of Anchorage Under Quiet Magnetic Conditions

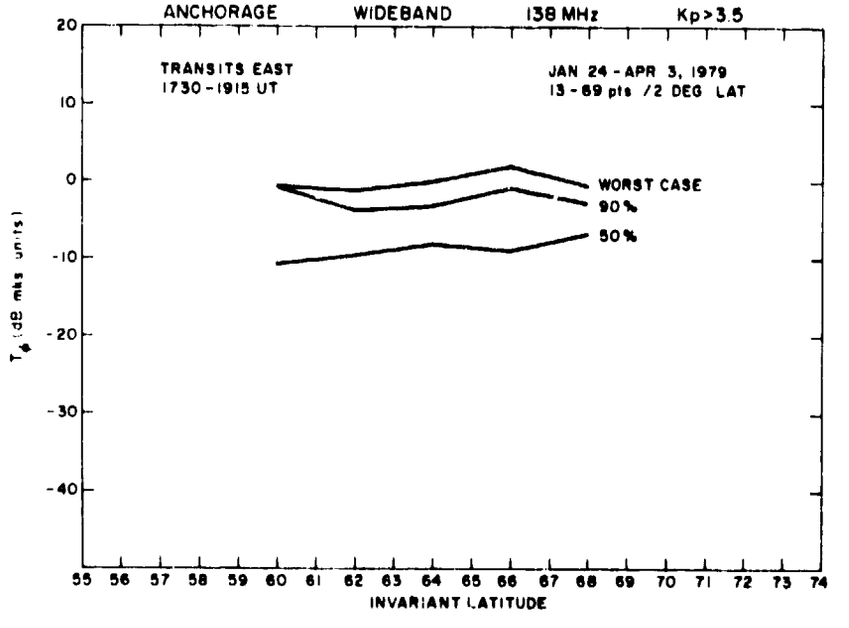

Figure 61b. Spectral Strength T_ϕ of Phase at 1 Hz vs. Invariant Latitude for Daytime Transits East of Anchorage Under Disturbed Magnetic Conditions

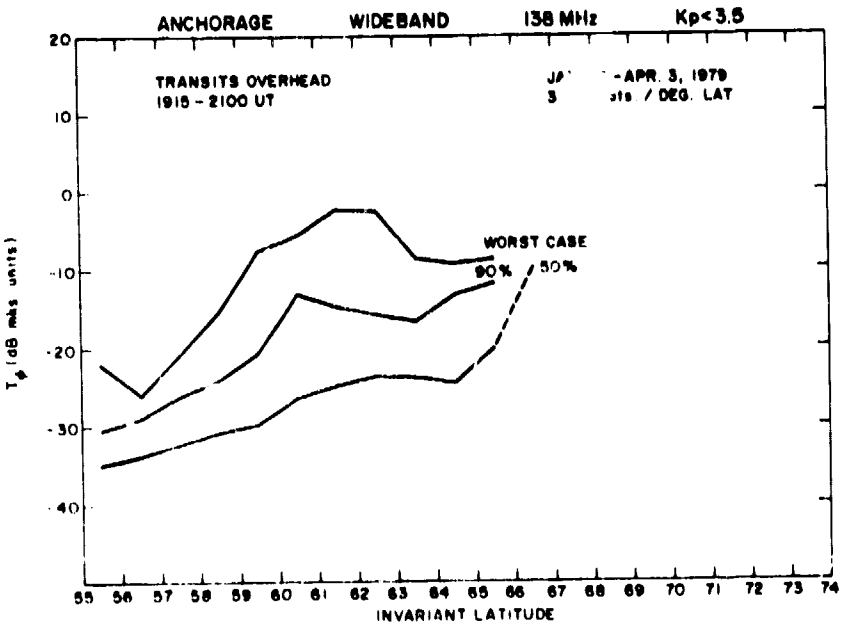

Figure 62a. Spectral Strength T_ϕ of Phase at 1 Hz vs. Invariant Latitude for Daytime Transits Overhead of Anchorage Under Quiet Magnetic Conditions

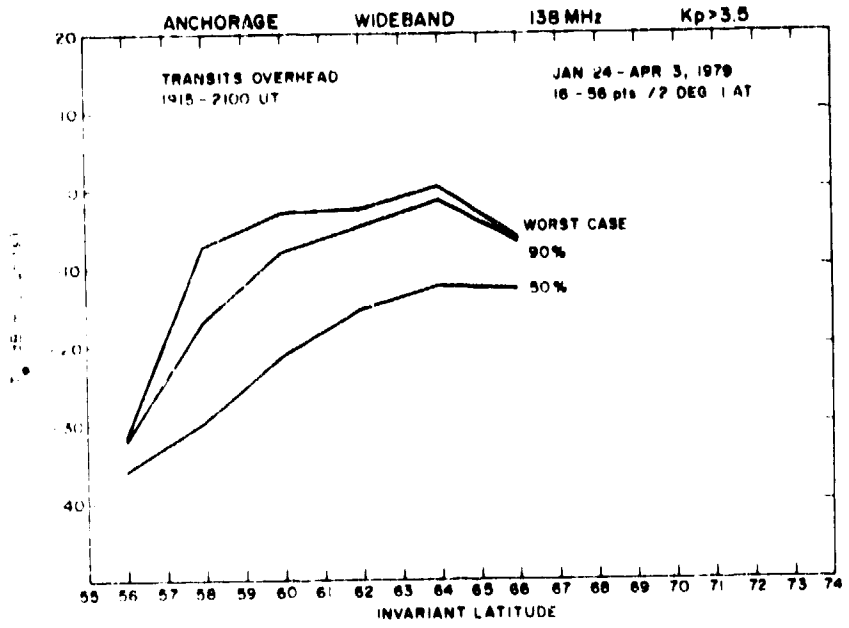

Figure 62b. Spectral Strength T_ϕ of Phase at 1 Hz vs. Invariant Latitude for Daytime Transits Overhead of Anchorage Under Disturbed Magnetic Conditions

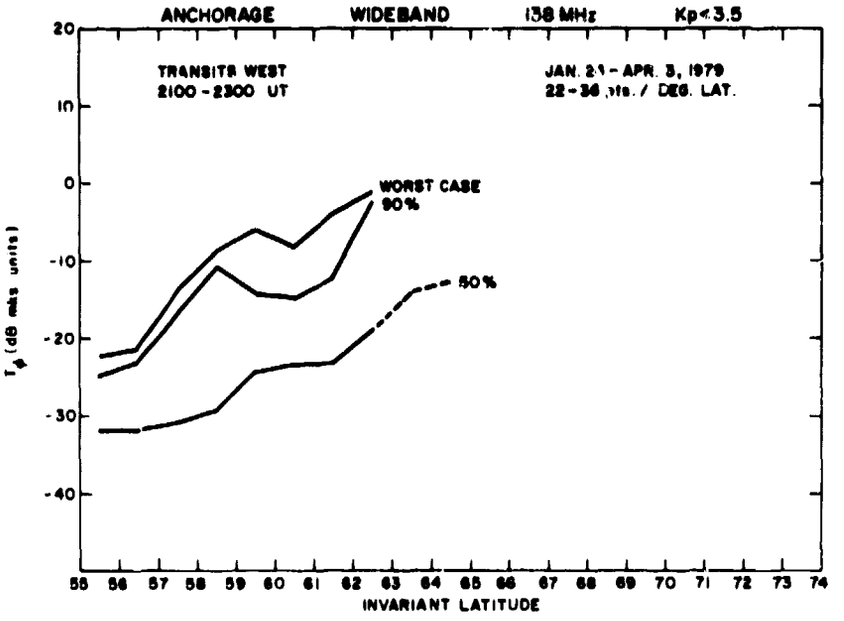

Figure 63a. Spectral Strength T_ϕ of Phase at 1 Hz vs. Invariant Latitude for Daytime Transits West of Anchorage Under Quiet Magnetic Conditions

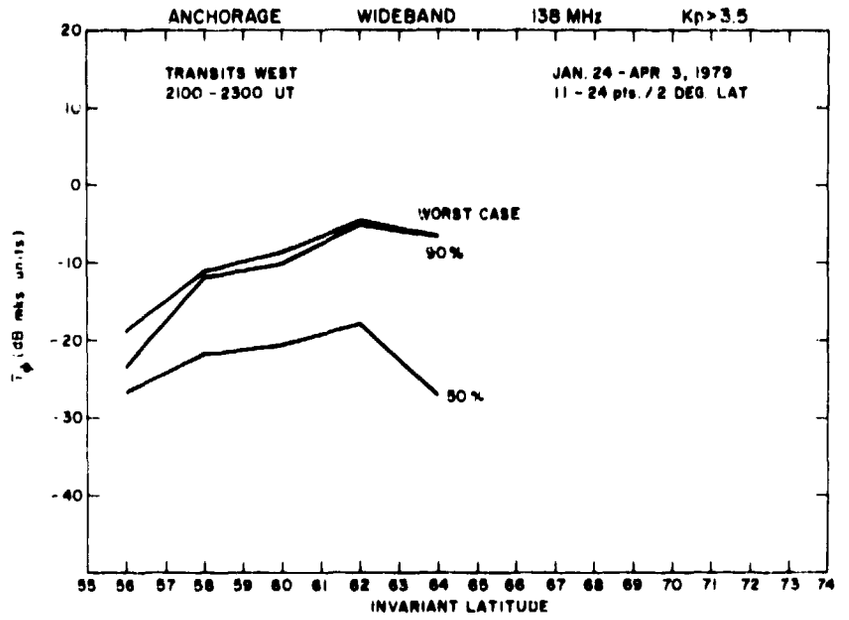

Figure 63b. Spectral Strength T_ϕ of Phase at 1 Hz vs. Invariant Latitude for Daytime Transits West of Anchorage Under Disturbed Magnetic Conditions

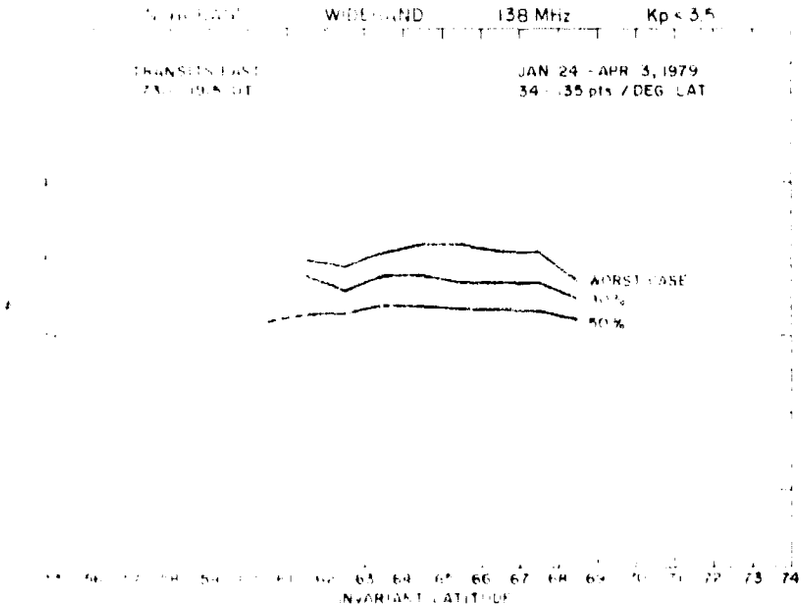

[illegible] Invariant Latitude for [illegible] Under Quiet Magnetic Conditions

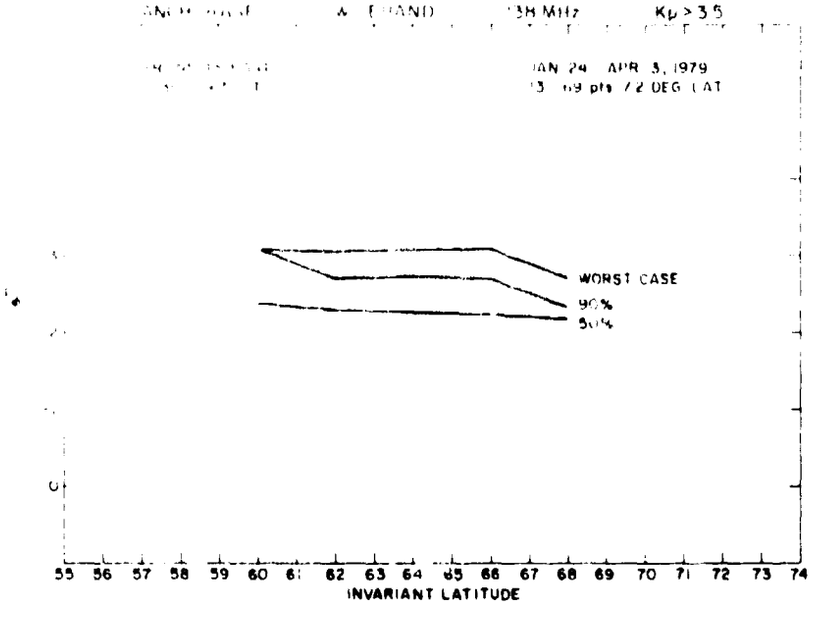

Figure 64b. Phase Spectral Index p_ϕ vs. Invariant Latitude for Daytime Transits East of Anchorage Under Disturbed Magnetic Conditions

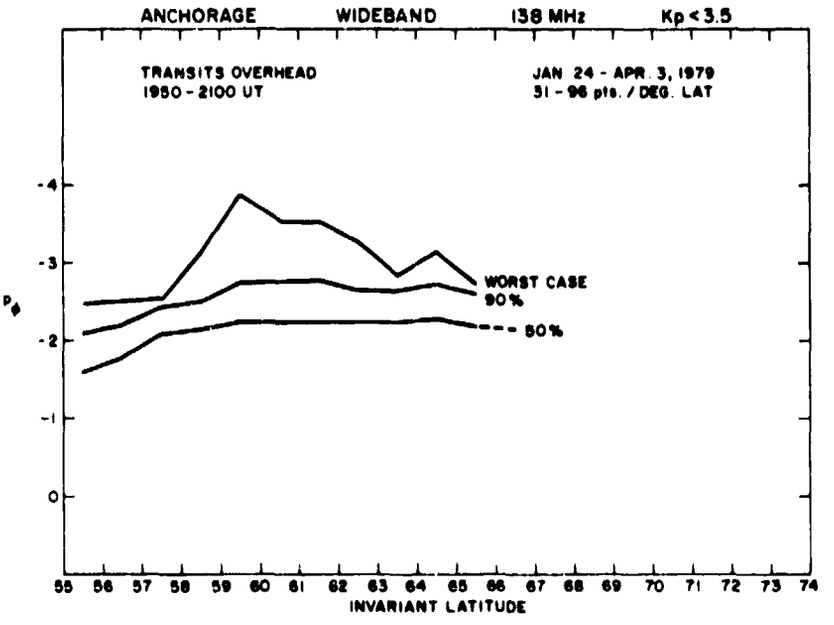

Figure 65a. Phase Spectral Index p_ϕ vs. Invariant Latitude for Daytime Transits Overhead of Anchorage Under Quiet Magnetic Conditions

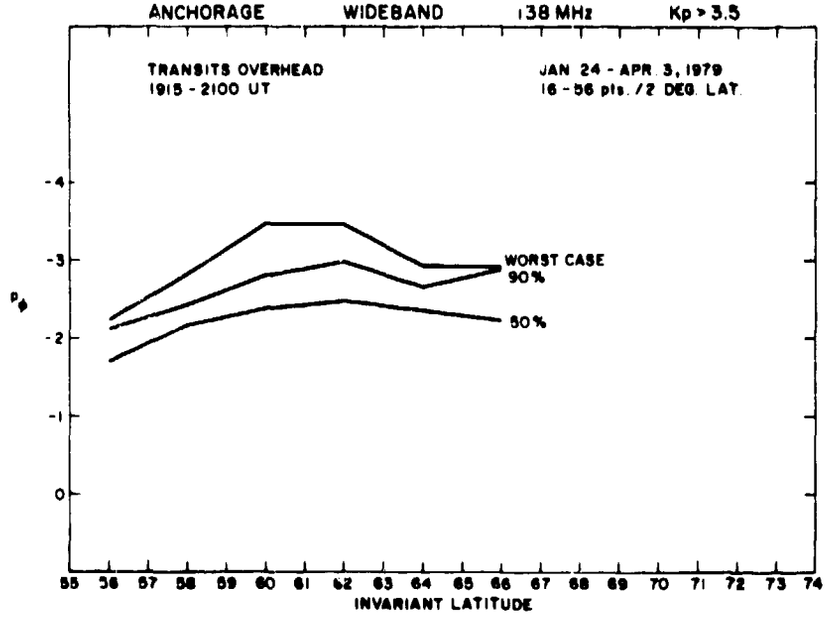

Figure 65b. Phase Spectral Index p_ϕ vs. Invariant Latitude for Daytime Transits Overhead of Anchorage Under Disturbed Magnetic Conditions

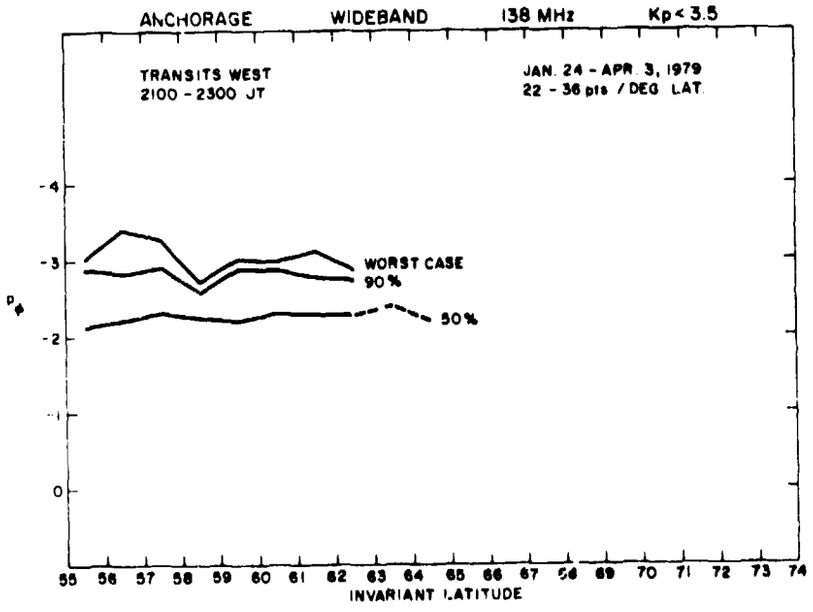

Figure 66a. Phase Spectral Index p_ϕ vs. Invariant Latitude for Daytime Transits West of Anchorage Under Quiet Magnetic Conditions

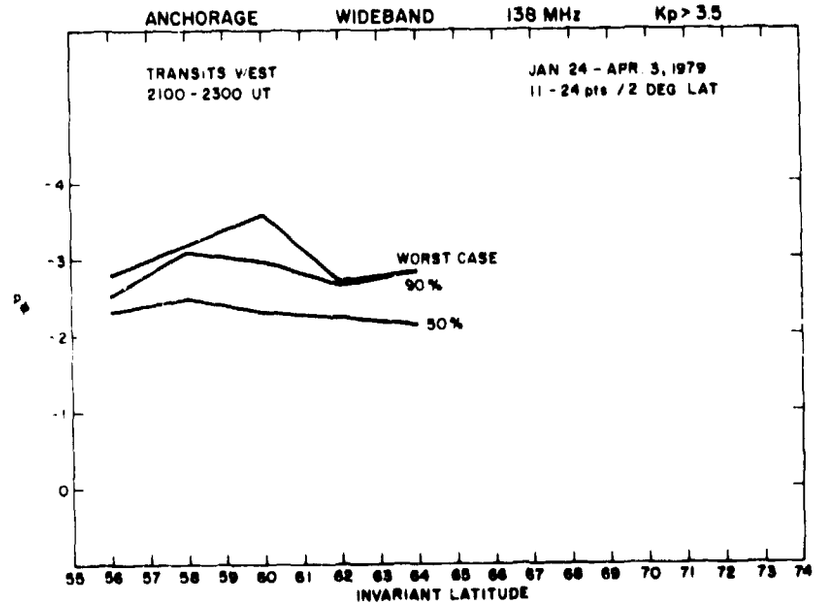

Figure 66b. Phase Spectral Index p_ϕ vs. Invariant Latitude for Daytime Transits West of Anchorage Under Disturbed Magnetic Conditions

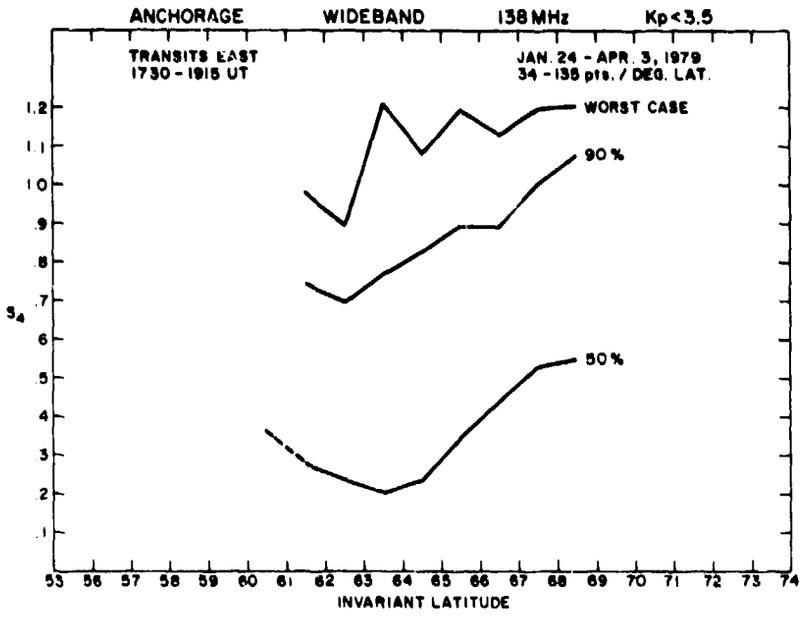

Figure 67a. Intensity Scintillation Index S_4 vs. Invariant Latitude for Daytime Transits East of Anchorage Under Quiet Magnetic Conditions

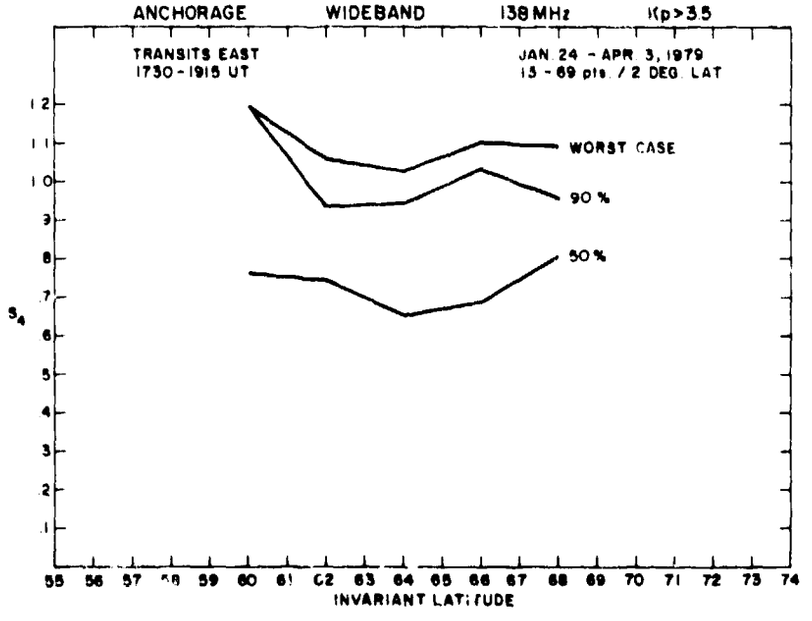

Figure 67b. Intensity Scintillation Index S_4 vs. Invariant Latitude for Daytime Transits East of Anchorage Under Disturbed Magnetic Conditions

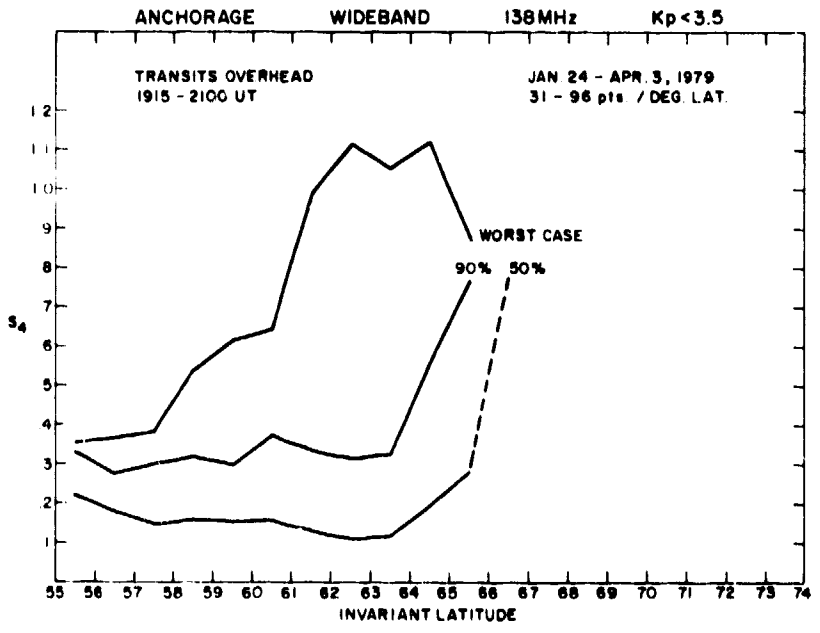

Figure 68a. Intensity Scintillation Index S_4 vs. Invariant Latitude for Daytime Transits Overhead of Anchorage Under Quiet Magnetic Conditions

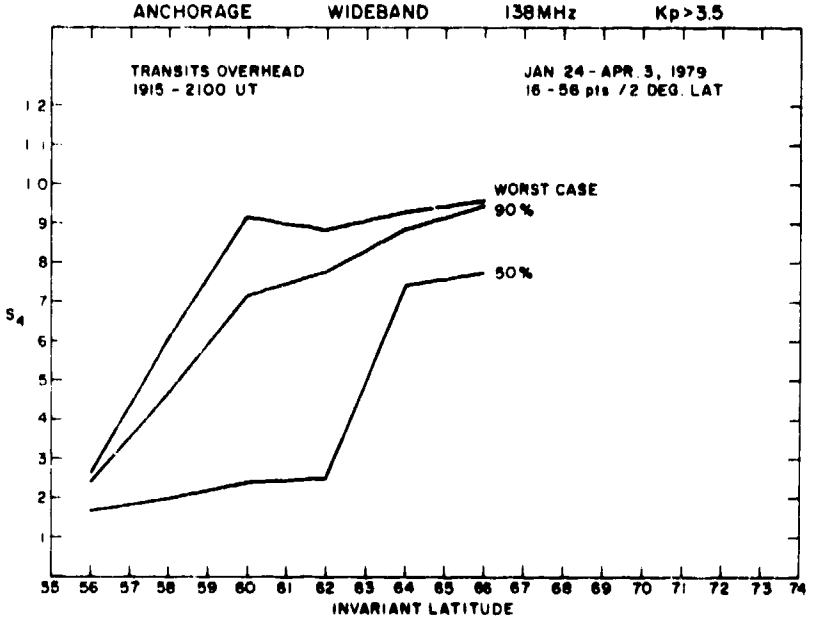

Figure 68b. Intensity Scintillation Index S_4 vs. Invariant Latitude for Daytime Transits Overhead of Anchorage Under Disturbed Magnetic Conditions

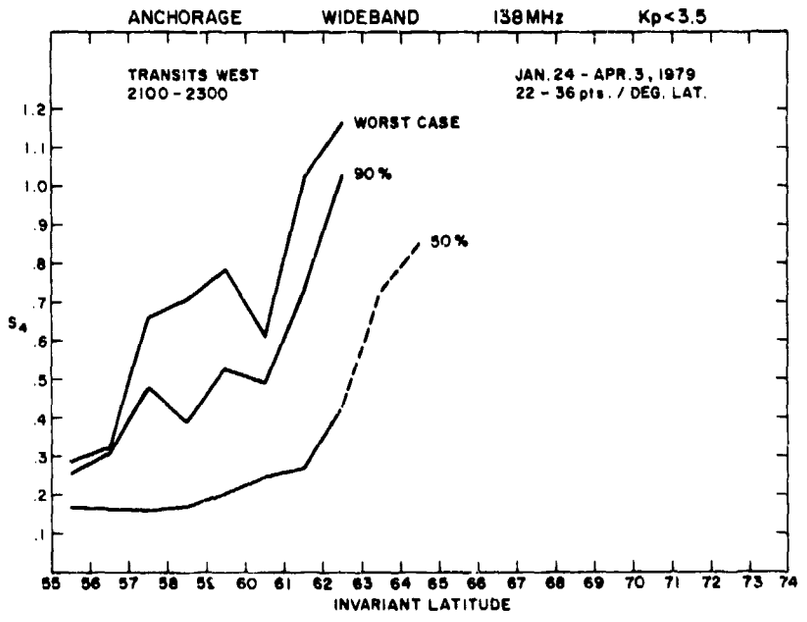

Figure 69a. Intensity Scintillation Index S_4 vs. Invariant Latitude for Daytime Transits West of Anchorage Under Quiet Magnetic Conditions

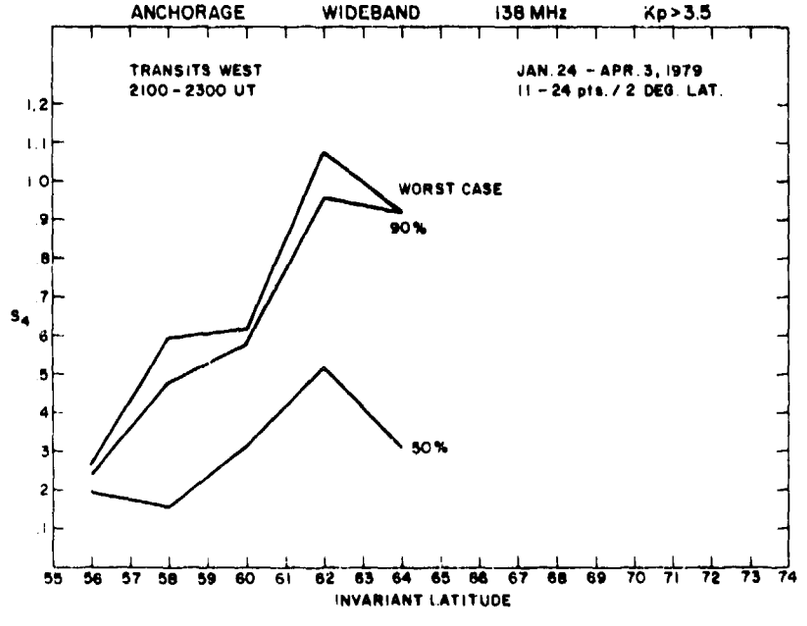

Figure 69b. Intensity Scintillation Index S_4 vs. Invariant Latitude for Daytime Transits West of Anchorage Under Disturbed Magnetic Conditions

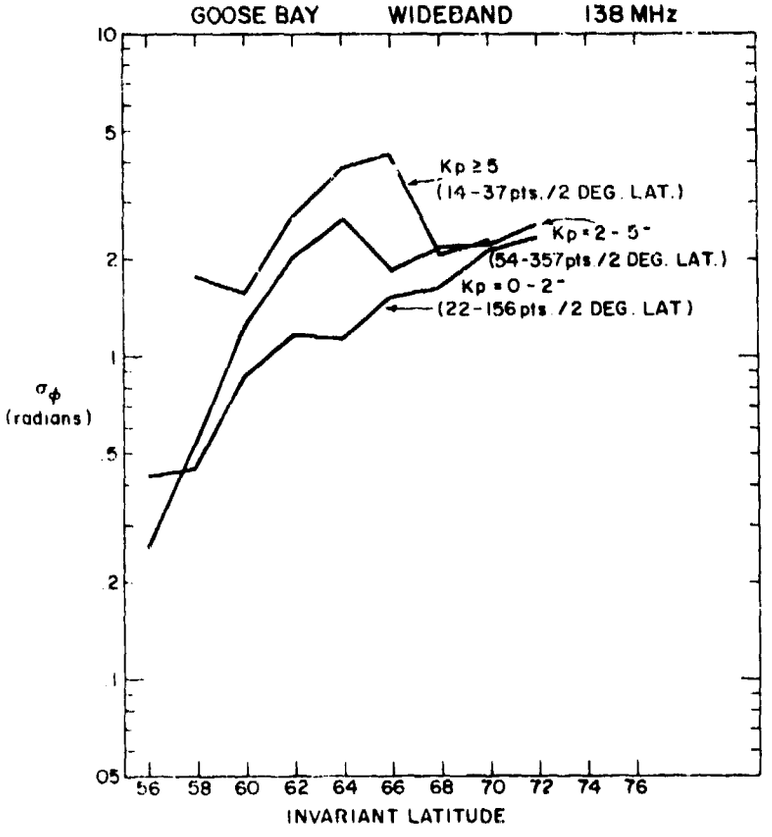

Figure 70. Median Nighttime Latitudinal Distribution in Goose Bay Region of Phase Scintillation Index σ_ϕ as a Function of Magnetic Index Kp

The situation is quite different for daytime Goose Bay σ_ϕ and S_4 data shown in Figures 72 and 73 where the effect of high magnetic activity (Kp ≥ 5) is to greatly increase both σ_ϕ and S_4 throughout the latitude range covered (58°-$72^\circ\Lambda$). In fact, the effect of magnetic activity dramatically increases the median level of scintillation indices above about $66^\circ\Lambda$. However, particularly for the S_4 index there is little Kp control of scintillations in the low and intermediate range.

In the Alaskan sector scintillations at night seem to be more sensitively controlled by magnetic activity particularly at the high-latitude end as shown by the Anchorage data in Figures 74 and 75. The Goose Bay nighttime S_4 data generally show a larger median level than similar Anchorage data. For instance, if the scintillation boundary is arbitrarily defined by $S_4 = 0.3$ (peak-to-peak fluctuations of 6 dB) then the low-Kp boundary at Goose Bay is $59^\circ\Lambda$ (from Figure 71)

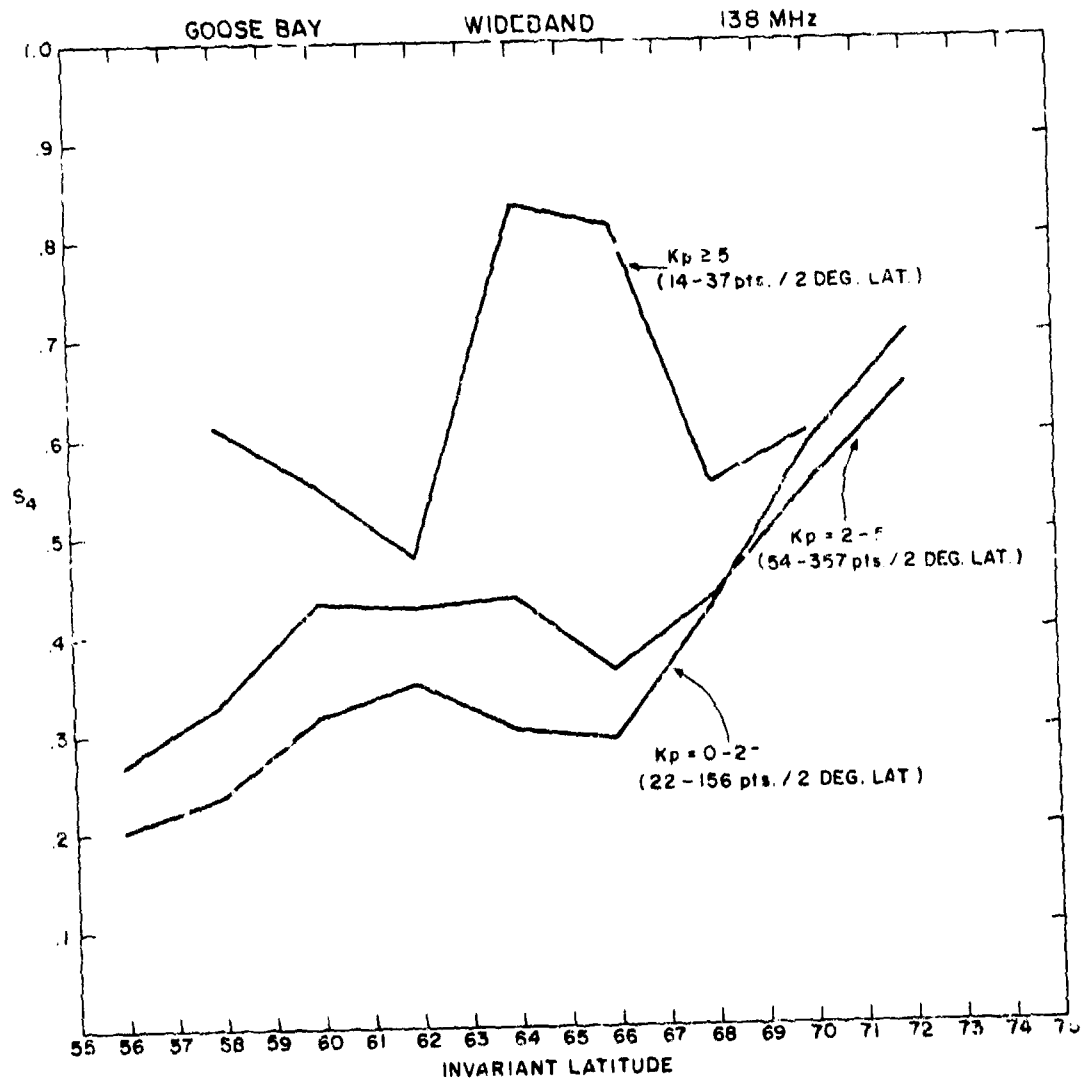

Figure 71. Median Nighttime Latitudinal Distribution in the Goose Bay Region of Amplitude Scintillation Index S_4 as a Function of Magnetic Index Kp

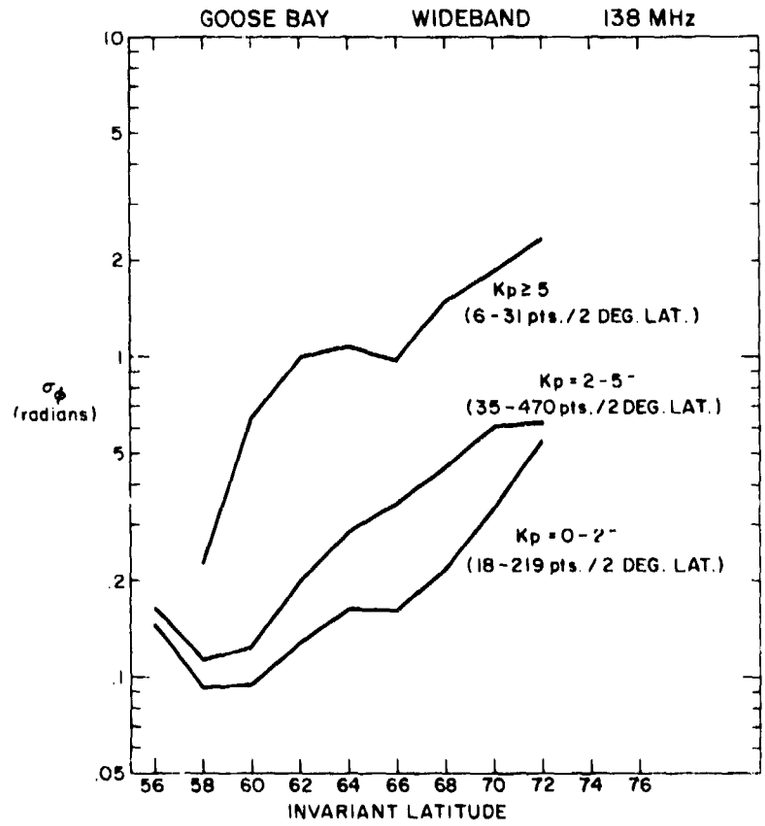

Figure 72. Median Daytime Latitudinal Distribution in Goose Bay Region of Phase Scintillation Index σ_ϕ as a Function of Magnetic Index Kp

whereas, Anchorage data puts it at 64°Λ. The intermediate Kp is at 57°Λ at Goose Bay and 59°Λ at Anchorage, while for high activity Goose Bay is always poleward of the boundary, whereas Anchorage shows that the boundary is between 58° and 59°Λ. A similar comparison of the phase scintillation boundary is difficult because the prominent geometrical enhancement occurs at two different positions at the two stations.

The daytime magnetic activity variations of σ_ϕ and S_4 at Anchorage are shown in Figures 76 and 77. Both parameters seem to be quite sensitively controlled by the Kp index. The daytime S_4 comparison between Goose Bay and Anchorage points out dramatic differences. If we again use the concept of the scintillation boundary defined by S_4 = 0.3 at the two stations, then we find from Figures 73 and 77 that the entire latitude range of 56°-71°Λ in the Goose Bay sector is

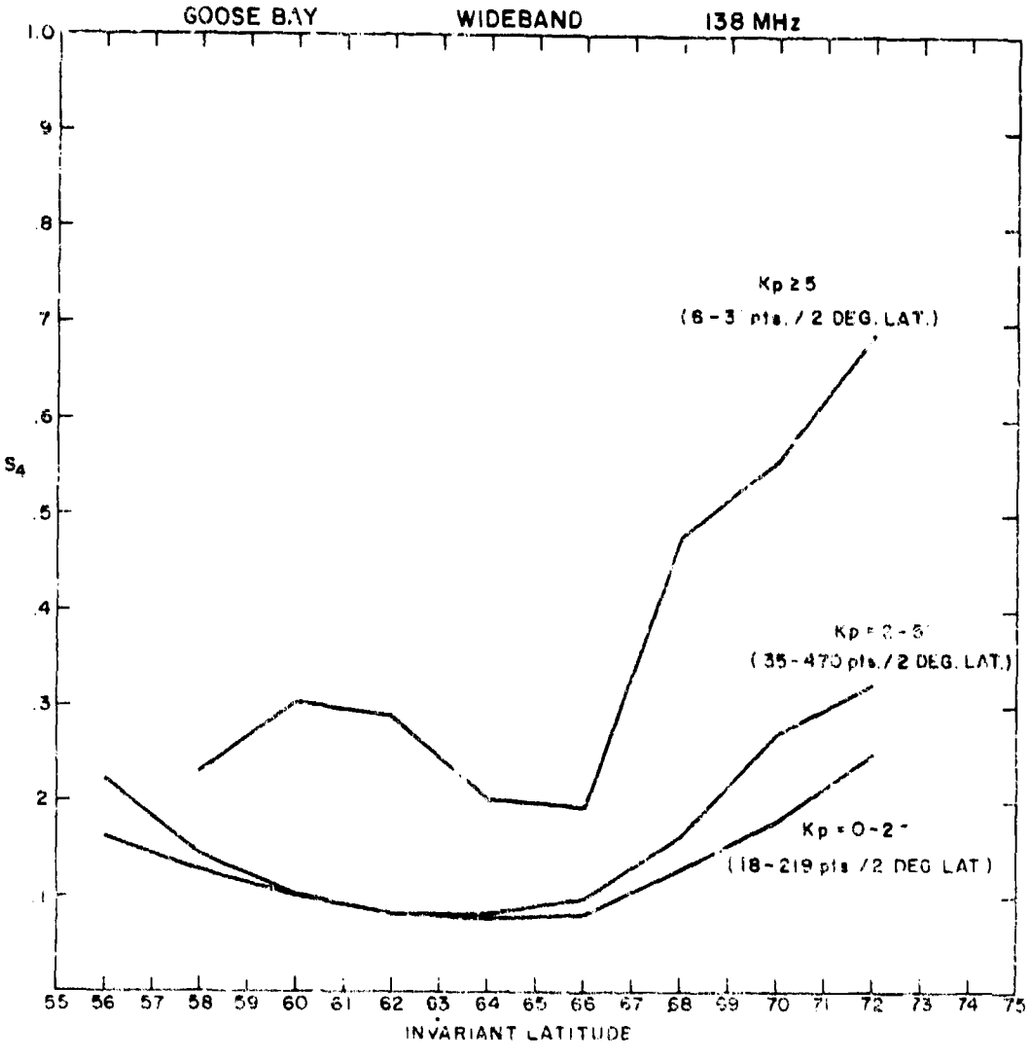

Figure 73. Median Daytime Latitudinal Distribution in Goose Bay Region of Amplitude Scintillation Index S_4 as a Function of Magnetic Index Kp

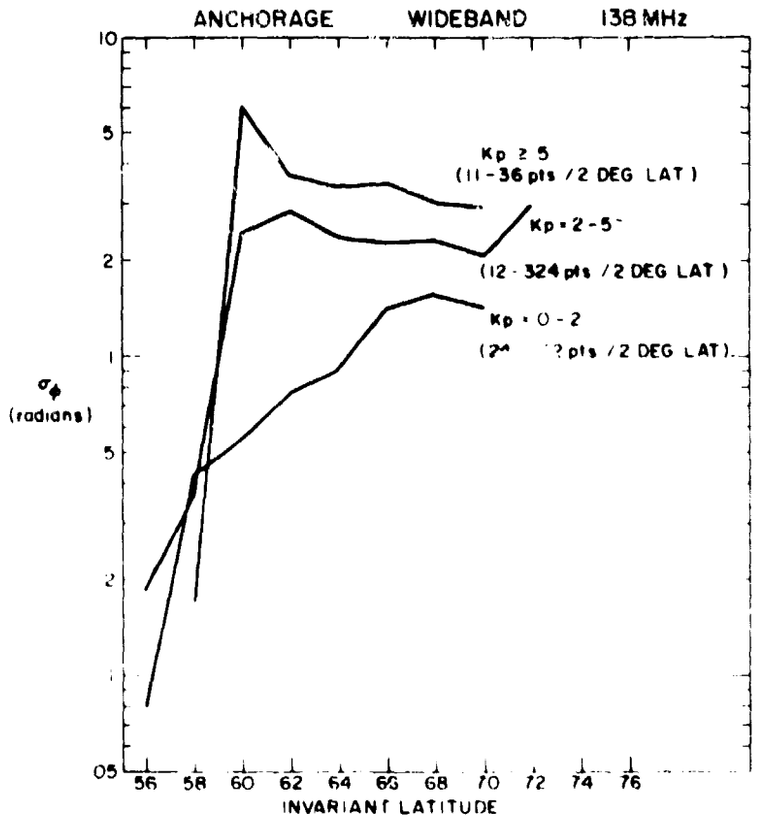

Figure 74. Median Nighttime Latitudinal Distribution in Anchorage Region of Phase Scintillation Index σ_ϕ as a Function of Magnetic Index Kp

equatorward of the boundary for low and intermediate Kp values. Very different is the behavior at Anchorage where the low-Kp boundary is observed at $66^{O}\Lambda$ and the intermediate Kp boundary is at $63^{O}\Lambda$. The high Kp boundary shows a double humped behavior at Goose Bay with the boundary crossings at $61^{O}\Lambda$ and $67^{O}\Lambda$, while the boundary at Anchorage is observed at only $58^{O}\Lambda$, the S_4 rising steeply with latitude in a monotonic way. This much-increased daytime scintillation level at Anchorage is opposite to the generally reduced level observed at night in this sector. The nighttime and daytime boundaries at the two stations are shown in tabular form in Table 2. Further daytime-nighttime comparisons in the two sectors observed during the same season will be presented in the next section.

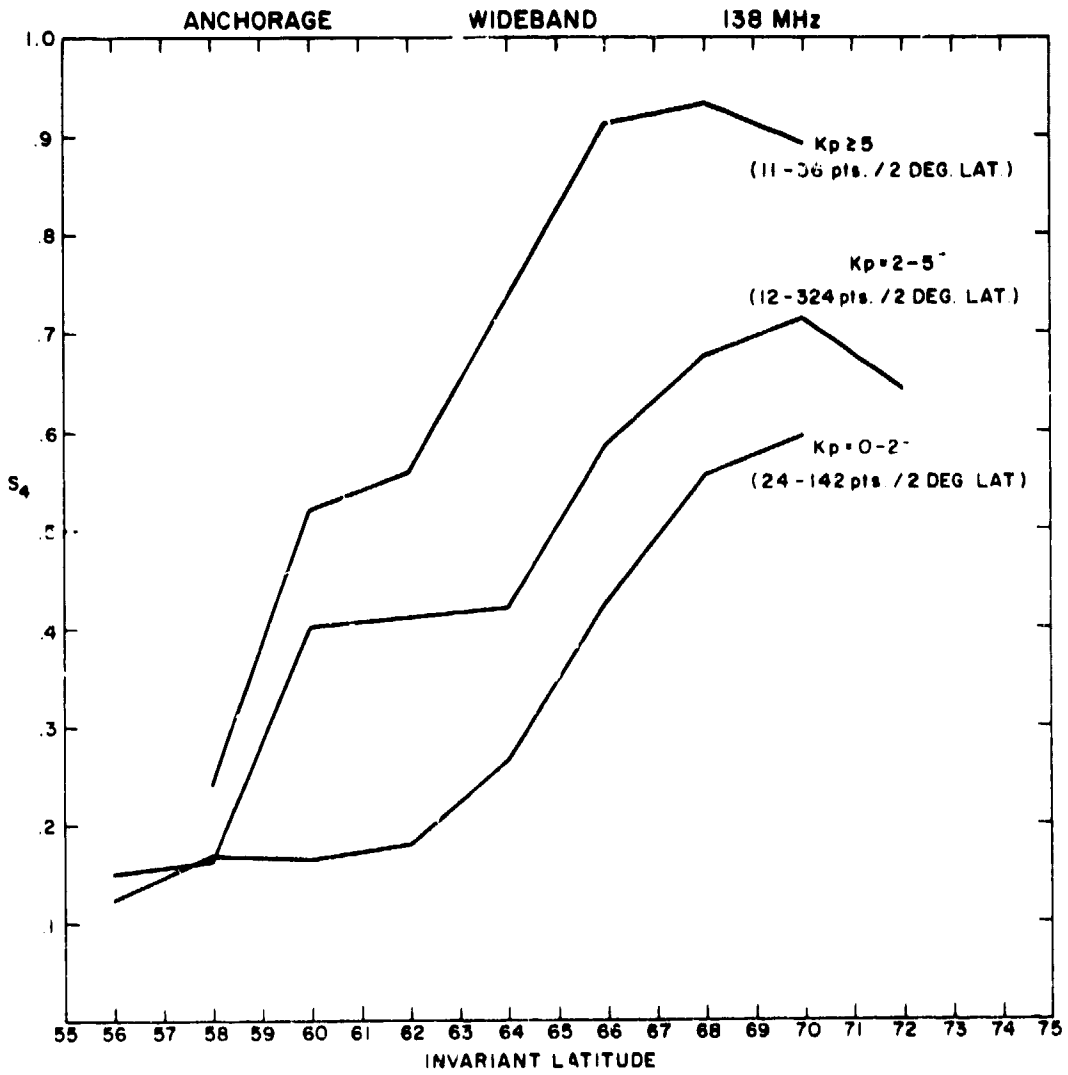

Figure 75. Median Nighttime Latitudinal Distribution in Anchorage Region of Amplitude Scintillation Index S_4 as a Function of Magnetic Index Kp

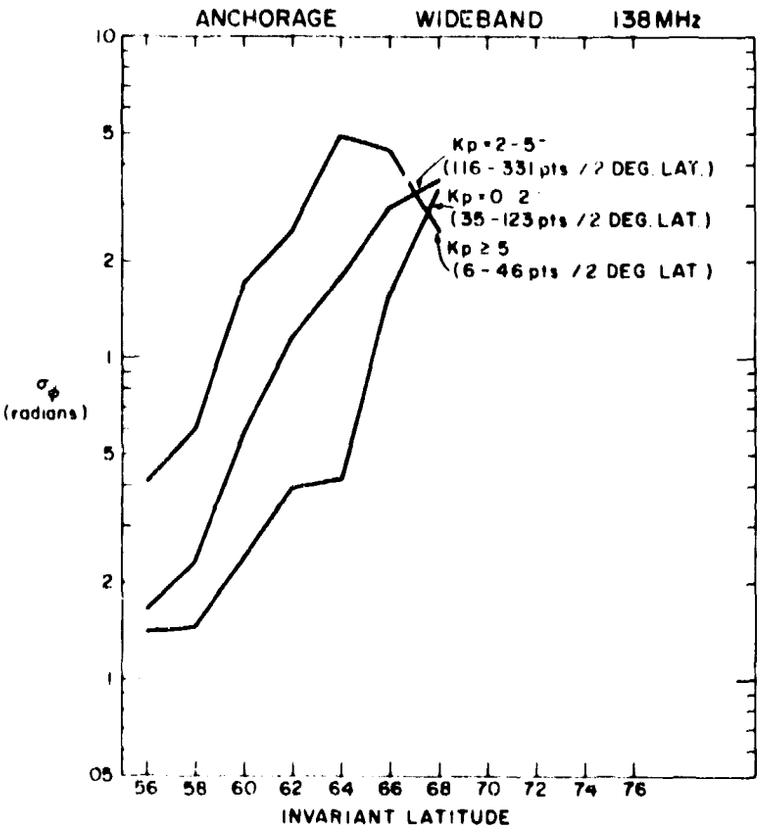

Figure 76. Median Daytime Latitudinal Distribution in Anchorage Region of Phase Scintillation Index σ_ϕ as a Function of Magnetic Index Kp

Table 2. S_4 Boundary

	Goose Bay		Anchorage	
	Night	Day	Night	Day
Low Kp (0-2⁻)	$59^{O}\Lambda$	$>71^{O}\Lambda$	$64^{O}\Lambda$	$66^{O}\Lambda$
Inter Kp (2-5⁻)	$57^{O}\Lambda$	$>71^{O}\Lambda$	$59^{O}\Lambda$	$63^{O}\Lambda$
High Kp (≥5)	$<56^{O}\Lambda$	$61^{O} + 67^{O}\Lambda$ (double)	$58\text{-}59^{O}\Lambda$	$58^{O}\Lambda$

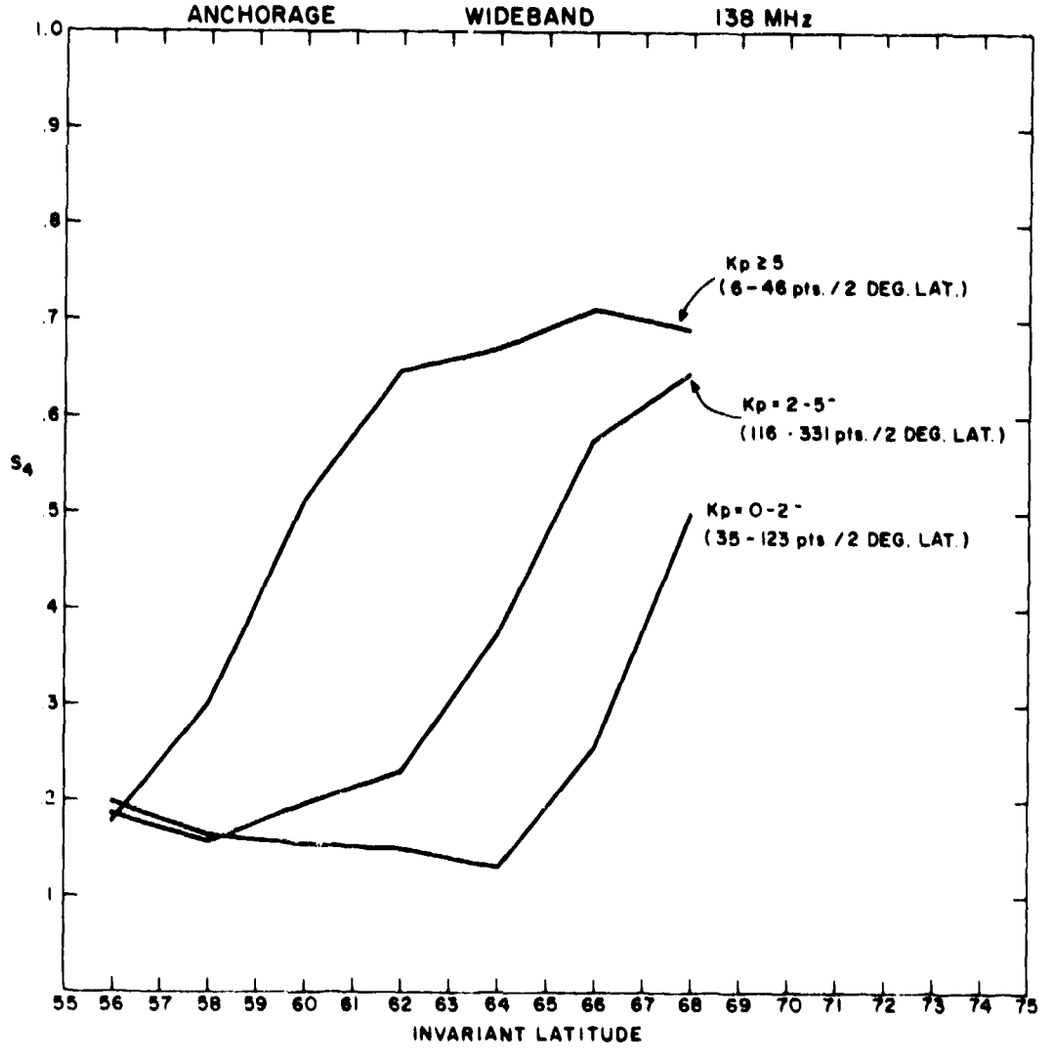

Figure 77. Median Daytime Latitudinal Distribution in Anchorage Region of Amplitude Scintillation Index S_4 as a Function of Magnetic Index Kp

6. LIMITED SEASONAL SCINTILLATION COMPARISONS AT GOOSE BAY AND ANCHORAGE

It was pointed out earlier that Wideband data at Goose Bay exists from late January, 1979, through August of the same year when the satellite ceased transmitting. However, at Anchorage the data starts at the same time but ends in April, 1979. As far as seasonal comparisons are concerned only the vernal equinox behavior can be compared in the two sectors of the auroral oval. For Goose Bay it is possible to study the vernal equinox and summer behavior of scintillations. While the equinox comparison at the two stations may be of interest given the conflicting long-term behavior in the two sectors (Figures 1 and 2), the vernal equinox and summer pattern at Goose Bay during high sunspot conditions may turn out to be very similar as was observed in 1968-69 for Narssarssuaq observations. It is unfortunate that a full year's Wideband observations are not available from Goose Bay.

To make the comparison in the two sectors meaningful we have plotted, in Figures 78 and 79, the nighttime and daytime phase scintillation data observed during the vernal equinox (22 January through 30 April 1979) at the two stations under quiet magnetic conditions (Kp < 3.5), while Figures 80 and 81 show the same data during magnetically disturbed conditions. As with the magnetic activity study presented in Section 5, we have put together data from all three corridors and show only median values of phase scintillation in Figures 78 through 81 and in all other diagrams to be presented in this section. The difference in phase scintillation behavior is quite large in the two sectors, the relative nighttime and daytime behavior being quite different. The median level of nighttime phase scintillation is much higher at Goose Bay, while the opposite is the situation during the daytime. To quantize the differences in terms of an arbitrary phase scintillation boundary set at 1 rad, we find that the nighttime boundary is at $58^{o}\Lambda$ for Goose Bay and $60^{o}\Lambda$ for Anchorage. Obviously these numbers are somewhat affected by the geometrical enhancement. The daytime differences, where such geometrical factor has little or no effect at the 1 rad level, are vivid with the boundary being at $70^{o}\Lambda$ for Goose Bay, while it is only $64^{o}\Lambda$ for Anchorage. Indeed poleward of $65^{o}\Lambda$, the daytime phase scintillation exceeds the nighttime level in the Alaskan sector. This particular behavior is also observed at Anchorage during magnetically disturbed times (Figure 81), while nighttime phase scintillation always exceeds the daytime level at Goose Bay (Figure 80).

The four corresponding diagrams for the amplitude scintillation are shown in Figures 82 through 85. Using the amplitude scintillation boundary concept with the boundary defined at $S_4 = 0.3$, as in Section 5, we find the nighttime and daytime Goose Bay sector boundaries for quiet magnetic conditions (Figure 82) to be at

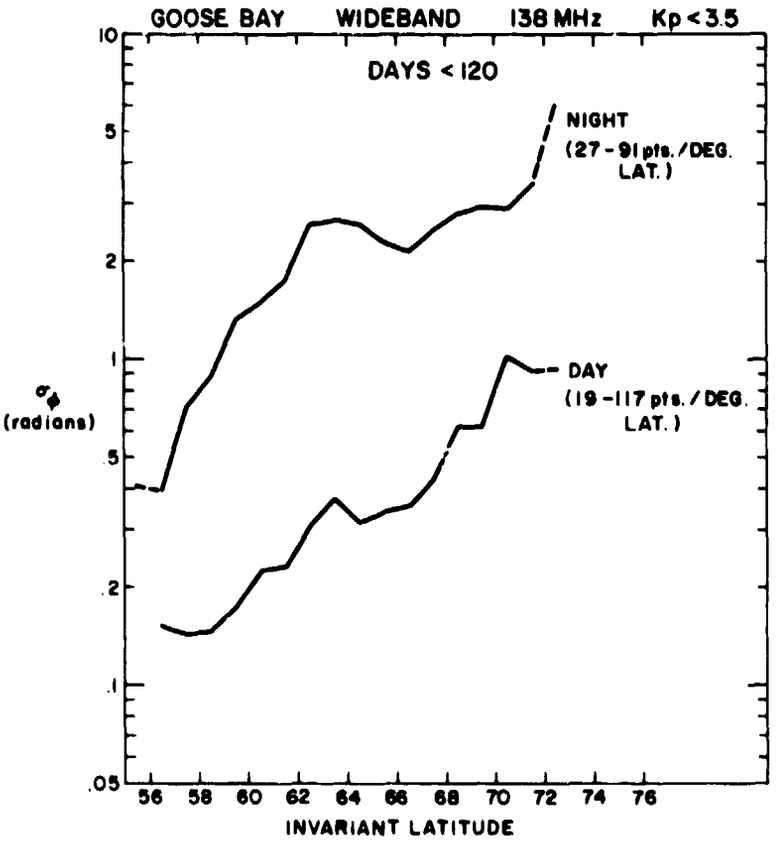

Figure 78. Phase Scintillation Index σ_ϕ Observed During the Vernal Equinox (22 January through 30 April 1979) at Goose Bay as a Function of Invariant Latitude Under Quiet Magnetic Conditions (Kp < 3.5) Separated into Night and Daytime Periods

57° and 70°Λ, respectively. These compare well with those defined in terms of the phase scintillation boundary of 1 rad. The corresponding numbers in the Anchorage sector are given by 63° and 65°Λ. There is a discrepancy between the nighttime phase and amplitude boundary at Anchorage primarily because the nighttime phase boundary is somewhat artificially lowered by the geometrical enhancement near 60°Λ. The amplitude scintillation during night and day become sensibly of the same magnitude polewards of 66°Λ for quiet times (Figure 83) and polewards of 63°Λ for disturbed times (Figure 85) but, the daytime values do not actually exceed the nighttime values as was the case with phase scintillations (Figures 79 and 81). The Goose Bay amplitude scintillation behavior follows that of the phase as may be observed by comparing Figures 78 and 80 with

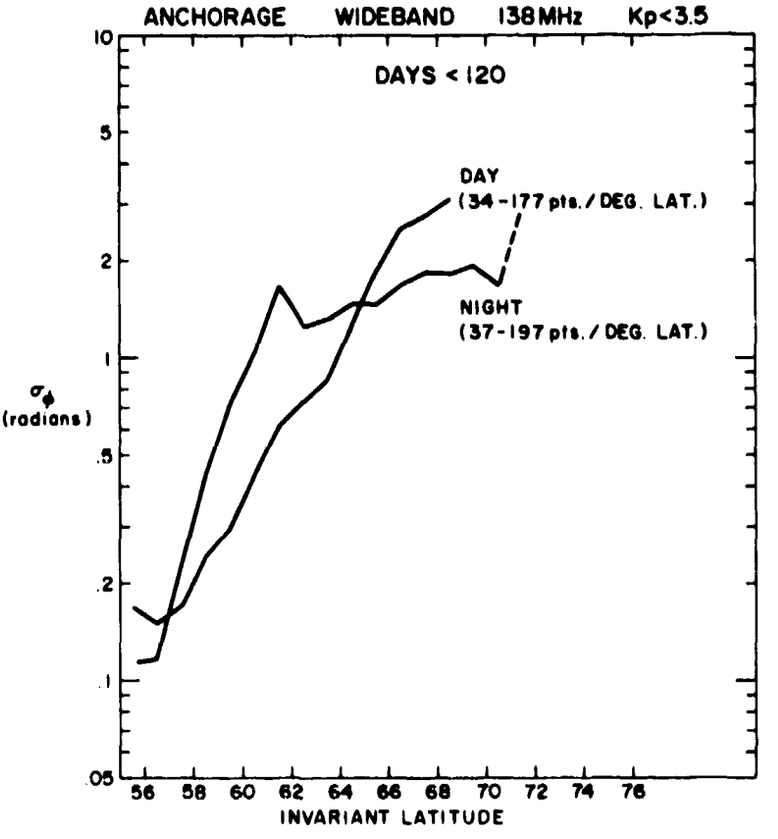

Figure 79. Phase Scintillation Index σ_ϕ Observed During the Vernal Equinox (22 January through 30 April 1979) at Anchorage as a Function of Invariant Latitude Under Quiet Magnetic Conditions (Kp < 3.5) Separated into Night and Daytime Periods

Figures 82 and 84, respectively. The various boundaries are summarized in Table 3.

The differences in the day-night scintillation behavior at the two stations are probably the most significant results to emanate from this comparative study. The reasons for such differences seems quite unclear at the present time. Unfortunately, Wideband data from Poker Flat for the same time period is not available. The data would have helped in determining whether a consistent pattern is observed at Anchorage and Poker Flat, two stations almost on the same longitude but 5° apart in latitude.

It is very encouraging to note from published amplitude scintillation data from Poker Flat (Rino and Matthews, 1980)[9] that the daytime 50 percent exceedance level of S_4 exceeds the nighttime S_4 levels poleward of approximately 67°

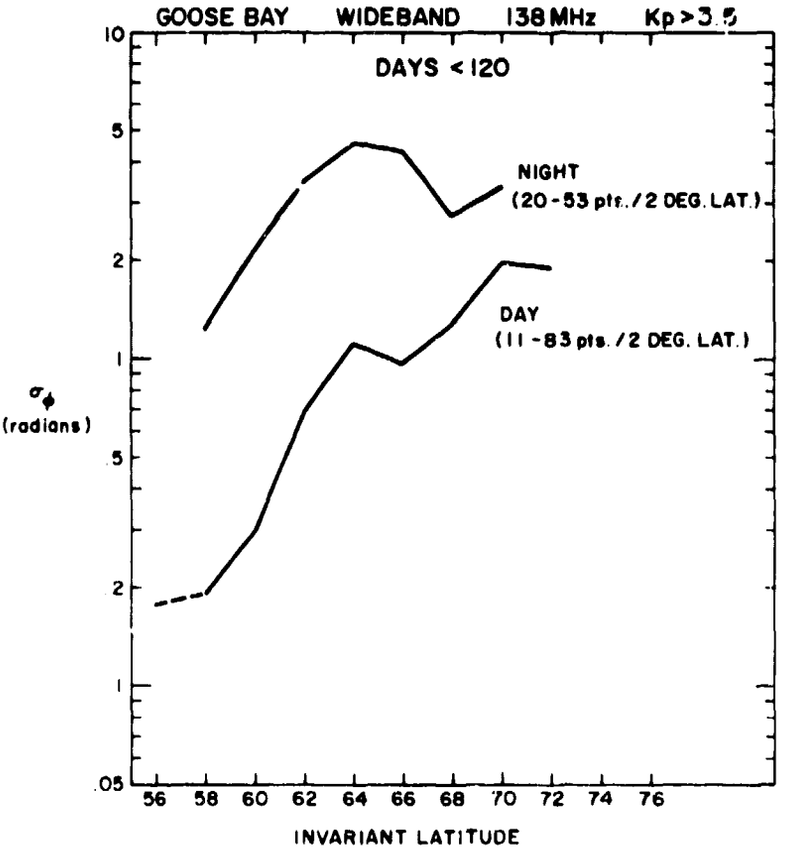

Figure 80. Phase Scintillation Index σ_ϕ Observed During the Vernal Equinox (22 January through 30 April 1979) at Goose Bay as a Function of Invariant Latitude Under Disturbed Magnetic Conditions (Kp > 3.5) Separated into Night and Daytime Periods

Table 3. Phase and S_4 Boundaries, Vernal Equinox - Quiet Magnetic Condition (Kp < 3.5)

	Phase		S_4	
	Goose Bay	Anchorage	Goose Bay	Anchorage
Day	70°Λ	64°Λ	70°Λ	65°Λ
Night	58°Λ	60°Λ	57°Λ	63°Λ

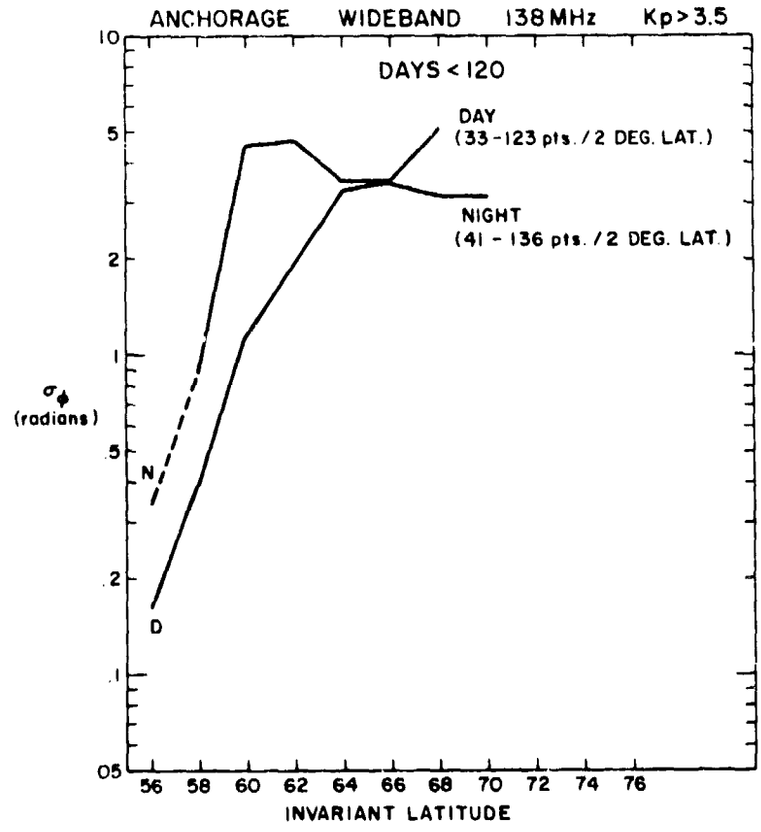

Figure 81. Phase Scintillation Index σ_ϕ Observed During the Vernal Equinox (22 January through 30 April 1979) at Anchorage as a Function of Invariant Latitude Under Disturbed Magnetic Conditions (Kp > 3.5) Separated into Night and Daytime Periods

dip latitude as shown in Figure 86. Rino and Matthews (1980)[9] do not point out that morning scintillation actually exceeds nighttime scintillation at the high-latitude end but, they do state that "a significant amount of daytime morning scintillation does occur".[9] Figure 86 was constructed by combining the nighttime and daytime S_4 plots given in Figures 6 and 7 of Rino and Matthews (1980)[9] and is very helpful in establishing the enhanced level of daytime scintillation occurrence. All data obtained during the year May 1977 through April 1978 were used for the graph, irrespective of the level of magnetic activity. Over most of the latitude interval the exceedance statistics were computed on a large number of 20-sec S_4 values in each 2.5° latitude bin, usually varying between 500-1000. The fact that our small data base at Anchorage follows the trends of the much larger Wideband data bank

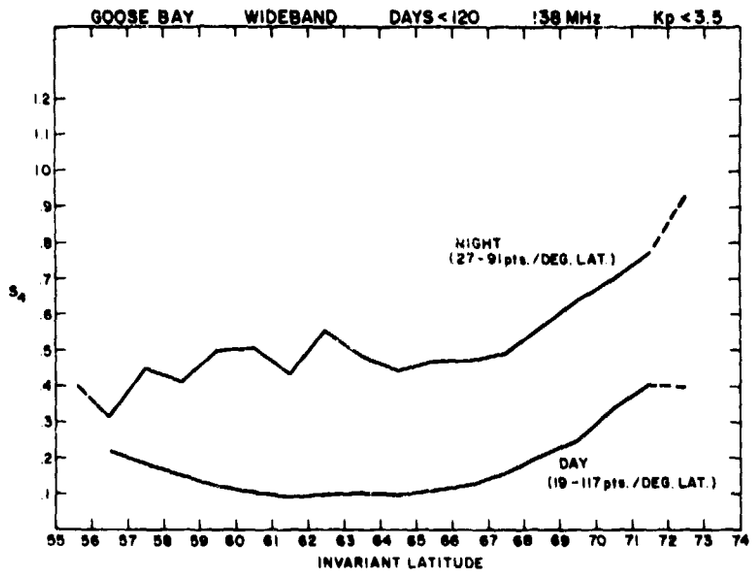

Figure 82. Amplitude Scintillation Index S_4 Observed During the Vernal Equinox (22 January through 30 April 1979) at Goose Bay as a Function of Invariant Latitude Under Quiet Magnetic Conditions (Kp < 3.5) Separated into Night and Daytime Periods

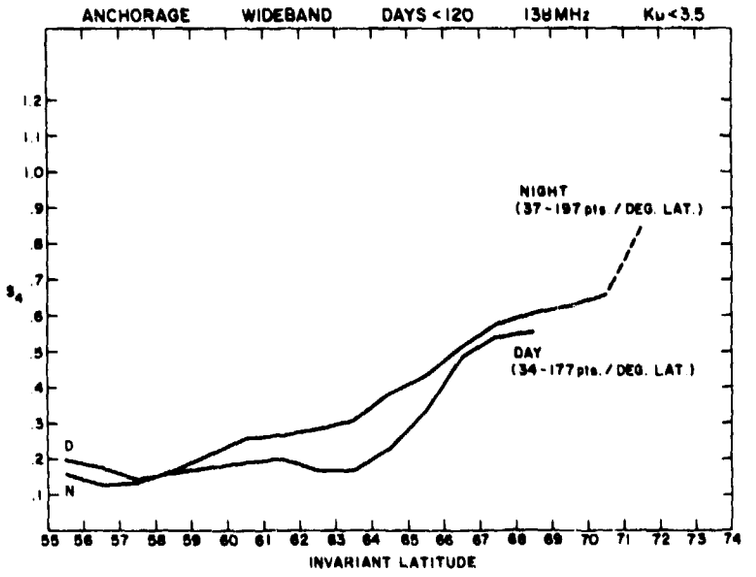

Figure 83. Amplitude Scintillation Index S_4 Observed During the Vernal Equinox (22 January through 30 April 1979) at Anchorage as a Function of Invariant Latitude Under Quiet Magnetic Conditions (Kp < 3.5) Separated into Night and Daytime Periods

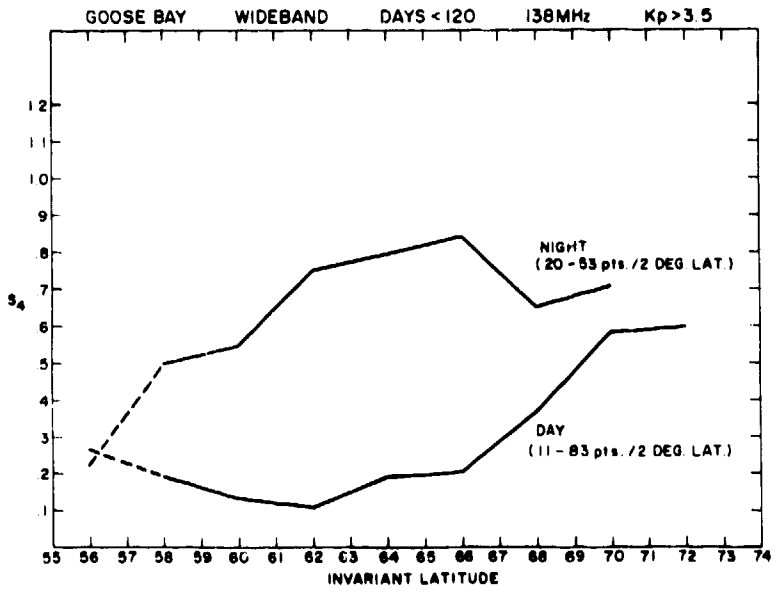

Figure 84. Amplitude Scintillation Index S_4 Observed During the Vernal Equinox (22 January through 30 April 1979) at Goose Bay as a Function of Invariant Latitude Under Disturbed Magnetic Conditions (Kp > 3.5) Separated into Night and Daytime Periods

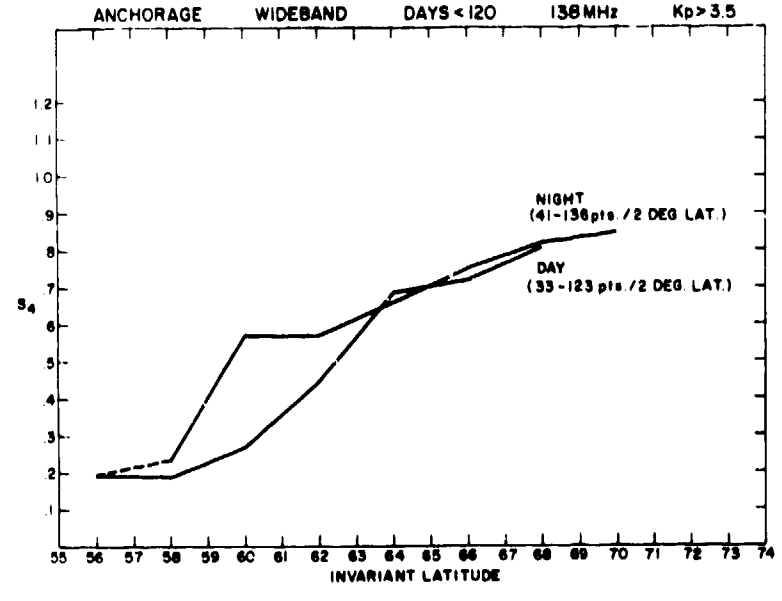

Figure 85. Amplitude Scintillation Index S_4 Observed During the Vernal Equinox (22 January through 30 April 1979) at Anchorage as a Function of Invariant Latitude Under Disturbed Magnetic Conditions (Kp > 3.5) Separated into Night and Daytime Periods

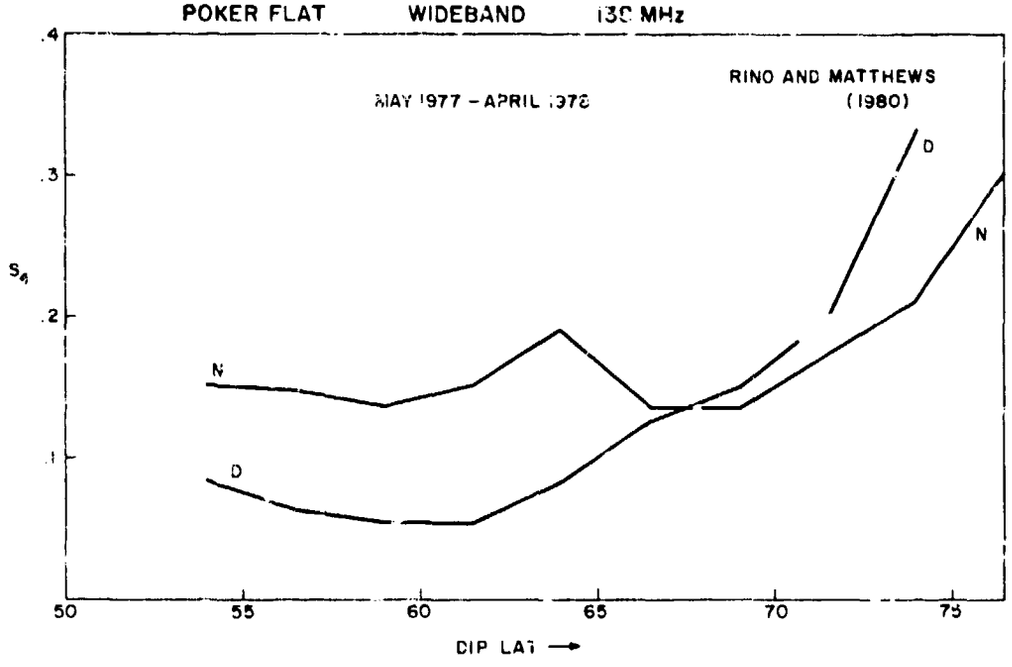

Figure 86. Amplitude Scintillation Index S_4 at Poker Flat During 1977-1978 as a Function of Dip Latitude Separated into Day and Nighttime Periods (Rino and Matthews, 1980)[6]

is very reassuring and actual physical mechanisms for such longitude-dependent morning irregularity generation have to be sought.

The final set of graphs present the summer (May through August, 1979) scintillation pattern observed at Goose Bay. The quiettime phase and amplitude scintillations are shown in Figures 87 and 89 and the disturbed behavior is shown in Figures 88 and 90. Two factors are noticeable in comparison with Goose Bay spring behavior: 1) there is an overall slight decrease in median scintillation values in summer and 2) there is a tendency for the phase scintillations (Figures 87 and 88) to show an increase at the low-latitude end. The decrease in median scintillation values can best be described by determining the boundary location at the two seasons. We have already noted that the amplitude boundary during the vernal equinox at Goose Bay at at $57^{\circ}\Lambda$ by night and $70^{\circ}\Lambda$ by day (Figure 52). In contrast, the corresponding summer boundaries are $59^{\circ}\Lambda$ by night and approximately $73^{\circ}\Lambda$ by day. During disturbed times the boundaries are at 56° and 67°, respectively, while the summer boundaries are at 56° and 69° as given in Table 4. The general shape of the curves in the two seasons remains the same. The low-latitude enhancement during the summer, which was noticeably

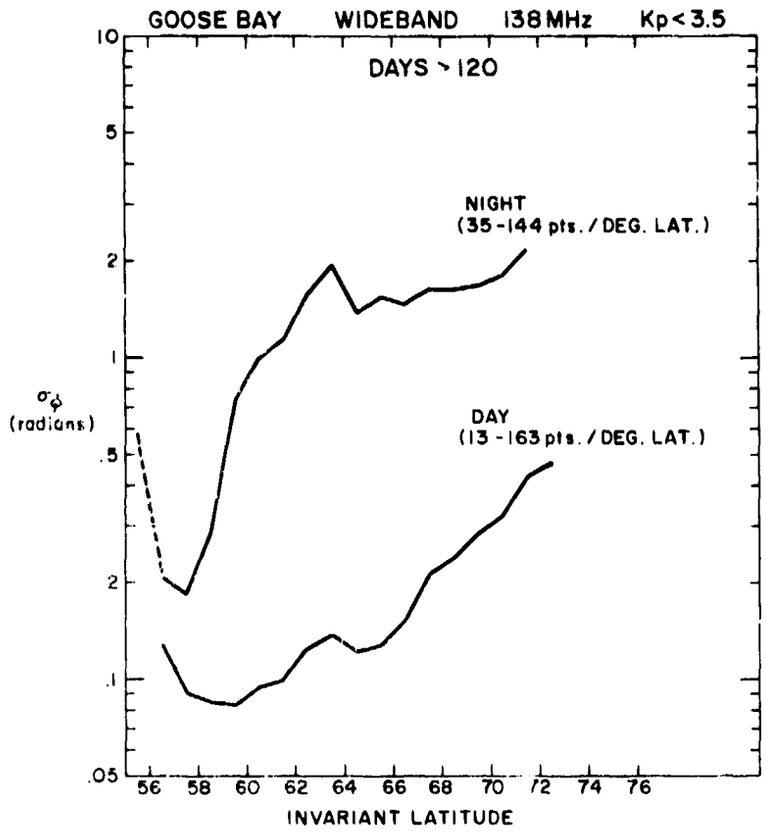

Figure 87. Phase Scintillation Index σ_ϕ Observed During the Summer (May through August) at Goose Bay as a Function of Invariant Latitude Under Quiet Magnetic Conditions (Kp < 3.5) Separated into Night and Daytime Periods

observed from this small data set primarily in phase scintillation, was also observed during the summer of 1976 in Poker Flat data (Rino and Matthews, 1980).[9] However, it was not observed at Poker Flat during either the 1977 or 1978 vernal equinox. Thus, the absence of a low-latitude enhancement at Anchorage during the vernal equinox of 1979 is, at least, consistent with earlier data in the same sector. Further investigations are necessary to determine whether the summer occurrence of enhanced-scintillations near 55°Λ is in anyway related to sporadic-E occurrence at such latitudes (Basu et al, 1973[31]).

---

31. Basu, S., Vesprini, R.L., and Aarons, J. (1973) Field-aligned ionospheric E-region irregularities and sporadic E, Radio Sci. 8:235. AFCRL-TR-73-0258, AD 760 853.

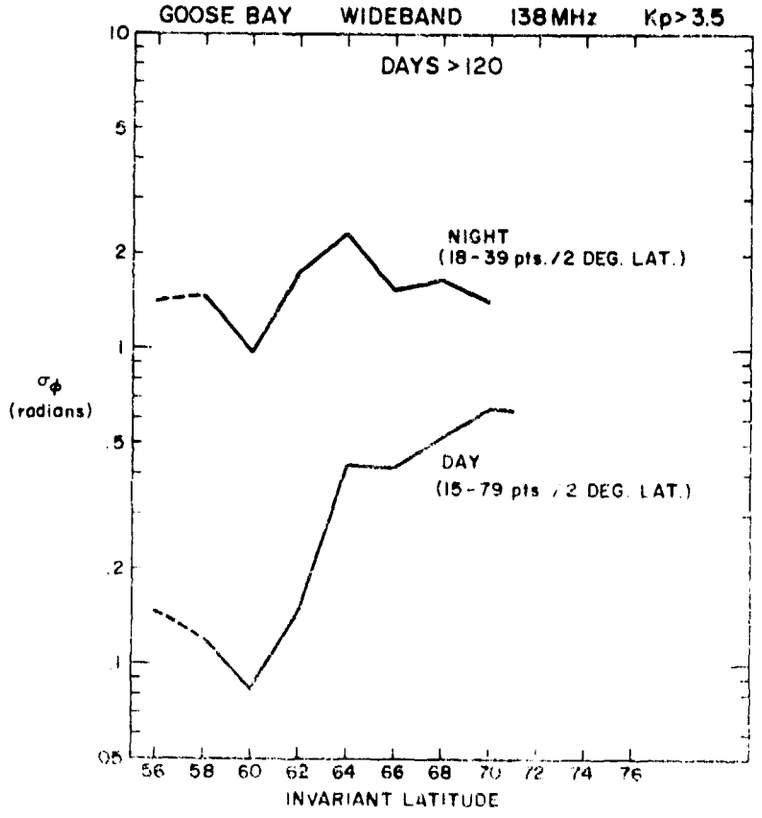

Figure 88. Phase Scintillation Index σ_ϕ Observed During the Summer (May through August) at Goose Bay as a Function of Invariant Latitude Under Disturbed Magnetic Conditions (Kp > 3.5) Separated into Night and Daytime Periods

Table 4. Vernal Equinox vs. Summer S_4 Boundaries at Goose Bay

	S_4			
	Vernal		Summer	
	Day	Night	Day	Night
Quiet	$70^{O}\Lambda$	$57^{O}\Lambda$	$73^{O}\Lambda$	$59^{O}\Lambda$
Disturbed	$67^{O}\Lambda$	$56^{O}\Lambda$	$69^{O}\Lambda$	$56^{O}\Lambda$

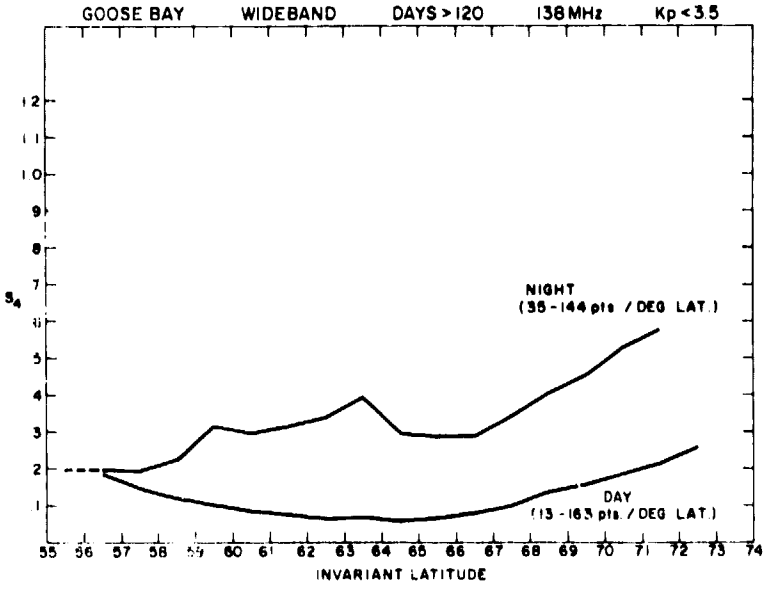

Figure 89. Amplitude Scintillation Index S_4 Observed During the Summer (May through August) at Goose Bay as a Function of Invariant Latitude Under Quiet Magnetic Conditions (Kp < 3.5) Separated into Night and Daytime Periods

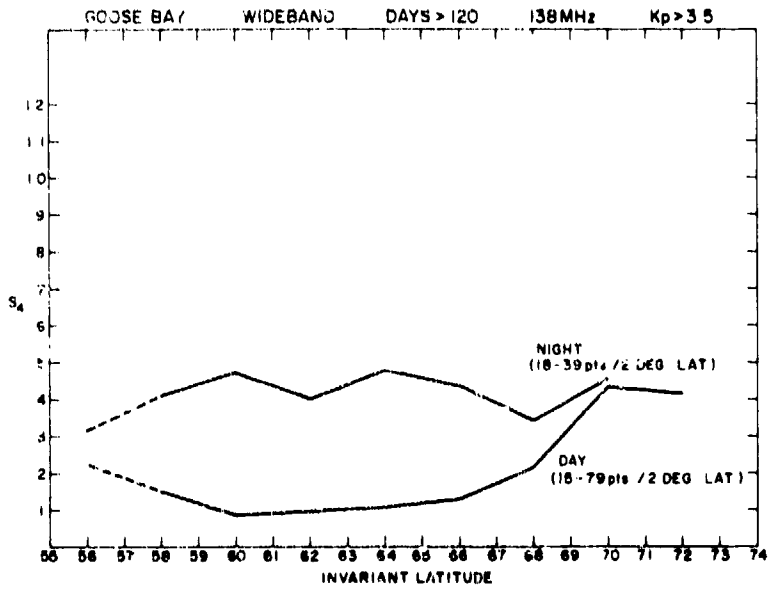

Figure 90. Amplitude Scintillation Index S_4 Observed During the Summer (May through August) at Goose Bay as a Function of Invariant Latitude Under Disturbed Magnetic Conditions (Kp > 3.5) Separated into Night and Daytime Periods

7. CONCLUSIONS

Phase and amplitude scintillation measurements from two widely separated auroral stations have been presented. While the primary objective of this report was to determine the scintillation statistics at the two stations, which would be helpful to users in planning their individual system requirements, features of considerable scientific interest were also observed which need further study. The findings which fall in this latter category are: 1) the existence of L-shell aligned sheets in the daytime and 2) the existence of a significant amount of daytime scintillations in the Alaskan sector at latitudes $\sim 65^{\circ}\Lambda$. To emphasize these findings we show in Figure 91 the phase scintillations observed during four individual daytime passes in the western corridor of the Alaskan sector that show large geometrical enhancements as well as large "source" enhancements at latitudes greater than $61^{\circ}\Lambda$. The large values of the Briggs-Parkin (BP) angle clearly indicate that these passes are off the magnetic meridian plane. Such enhancements were observed in more than half of the passes in the western corridor as mentioned earlier. Goose Bay sector passes also clearly showed evidence of such off-overhead geometrical enhancements when irregularities were present equatorward of the station, particularly in the eastern sector.

The existence of a longitudinally varying daytime irregularity source approximately 10° equatorward of the dayside auroral oval is quite intriguing. In the Alaskan sector, coordinated Chatanika radar and scintillation measurements using 250-MHz beacons and the GPS constellation of satellites are planned for November, 1981, to study these problems further. It will be quite important to determine whether the current-convective instability (Ossakow and Chaturvedi, 1979[32]; Chaturvedi and Ossakow, 1979[33]; Vickrey et al, 1980[34]) and the $\vec{E} \times \vec{B}$ instability that have been postulated to explain nighttime scintillations (Rino and Owen, 1980[30]; Rino, 1981[35]) are also valid mechanisms for daytime irregularity generation.

As far as the user is concerned, the most notable feature has been the longitudinal difference observed during the same season (vernal equinox) of the relative daytime and nighttime levels of phase and amplitude scintillations at the two

---

32. Ossakow, S. L., and Chaturvedi, P. K. (1979) Current convective instability in the diffuse aurora, Geophys. Res. Lett. 6:332.

33. Chaturvedi, P. K. and Ossakow, S. L. (1979) Nonlinear stabilization of the current convective instability in the diffuse aurora, Geophys. Res. Lett. 6:957.

34. Vickrey, J. F., Rino, C. L., and Potemra, T. A. (1980) Chatanika Triad observations of unstable ionization enhancements in the auroral F-region, Geophys. Res. Lett. 7:789.

35. Rino, C. L. (1981) Private communication.

stations. The differences are large enough to warrant more measurements of this kind to provide realistic inputs to user-oriented models currently under development (Aarons et al, 1980[36]; Fremouw and Lansinger, 1981[29]). Finally, it ought to be pointed out that these measurements were carried out at the highest part of the current sunspot cycle. It is important to estimate the effect of the sunspot cycle on scintillations with the help of long-term measurements.

A sequel to this report will present phase and amplitude scintillation statistics obtained at Goose Bay with the geostationary satellite Fleetsatcom transmitting at 244 MHz. The geostationary orbit will allow the determination of a complete diurnal pattern of such statistics.

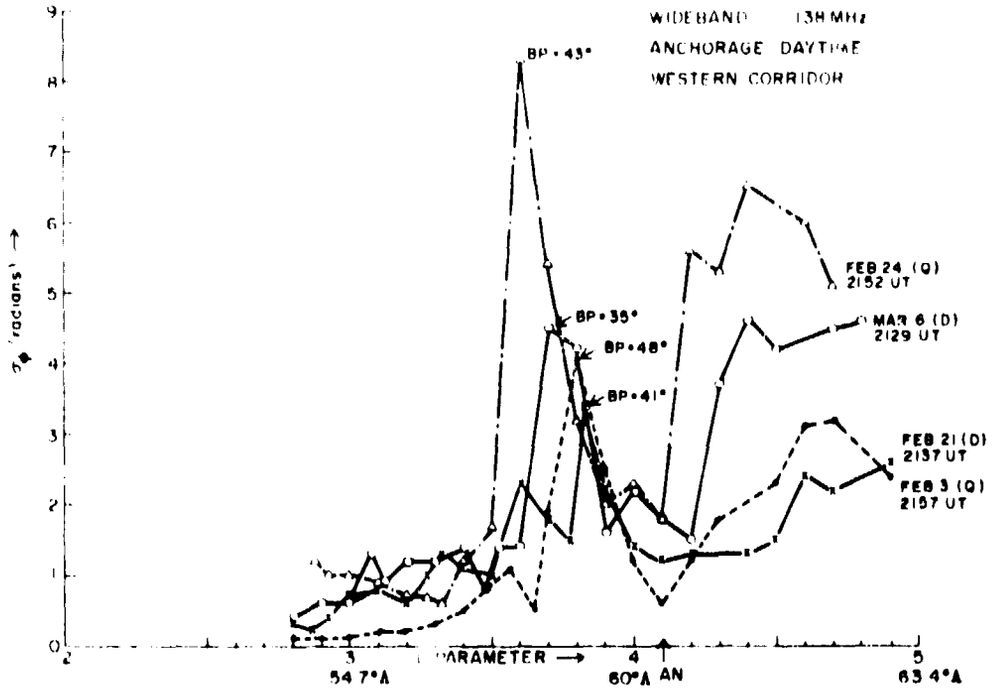

Figure 91. Individual Daytime Passes in the Western Corridor from Anchorage Showing Daytime Geometrical Enhancement

36. Aarons, J., MacKenzie, E., and Bhavnani, K. (1980) High latitude analytical formulas for scintillation levels, Radio Sci. 15:115, AFGL-TR-80-0144, AD A084 299.

References

1. Basu, S. and Kelley, M.C. (1979) A review of recent observations of equatorial scintillations and their relationship to current theories of F-region irregularity generation, Radio Sci. 14:471.
2. Basu, S. and Basu, S. (1981) Equatorial scintillations — a review, J. Atmos. Terr. Phys. 43:473.
3. Aarons, J., Mullen, J.P., and Whitney, H.E. (1969) The scintillation boundary, J. Geophys. Res. 74:884.
4. Aarons, J. and Allen, R.S. (1971) Scintillation boundary during quiet and disturbed magnetic conditions, J. Geophys. Res. 76:170. AFCRL-71-0101, AD 718 923.
5. Brown, W.D. (1976) Effects of atmospheric induced phase errors in synthetic aperture radar, Report SAND76-0520, Sandia Laboratory, Albuquerque, New Mexico.
6. Wand, R.H. and Evans, J.V. (1975) Morphology of ionospheric scintillation in the auroral zone, Proceedings of Symposium on Effect of the Ionosphere on Space Systems and Communications, J.M. Goodman (ed.), U.S. Govt. Printing Office, Washington, D.C.
7. Crane, R.K. (1976) Spectra of ionospheric scintillation, J. Geophys. Res. 81:2041.
8. Fremouw, E.J., Leadabrand, R.L., Livingston, R.C., Cousins, M.D., Rino, C.L., Fair, B.C., and Long, R.A. (1978) Early results from the DNA Wideband satellite experiment — complex-signal scintillation, Radio Sci. 13:167-187.
9. Rino, C.L. and Matthews, S.J. (1980) On the morphology of auroral zone radio wave scintillation, J. Geophys. Res. 85:4139.
10. Fremouw, E.J., Lansinger, J.M., and Miller, D.A. (1980) Further geophysical analysis of coherent satellite scintillation data, Annual Report, PD-NW-81-237R, Contract No. F49620-78-C-0014, Physical Dynamics, Inc., Bellevue, Washington.

11. Fremouw, E.J., Rino, C.L., Livingston, R.C., and Cousins, M.D. (1977) A persistent subauroral scintillation enhancement observed in Alaska, Geophys. Res. Lett. 4:539.

12. Rino, C.L., Livingston, R.C., and Matthews, S.J. (1978) Evidence for sheet-like auroral ionospheric irregularities, Geophys. Res. Lett. 5:1039.

13. Fremouw, E.J. and Lansinger, J.M. (1979) Continued geophysical analysis of coherent satellite scintillation data, Annual Report, PD-NW-79-213R, Contract F49620-78-C-0014, Physical Dynamics, Inc., Bellevue, Washington.

14. Basu, Sunanda (1975) Universal time seasonal variations of auroral zone magnetic activity and VHF scintillations, J. Geophys. Res. 80:4725-4728. AFGL-TR-76-0114, AD A025 579.

15. Basu, S., and Aarons, J. (1980) The morphology of high-latitude VHF scintillation near 70°W, Radio Sci. 15:59. AFGL-TR-80-0145, AD A084 298.

16. Davis, T.N. and Sugiura, M. (1966) Auroral electrojet activity index AE and its universal time variations, J. Geophys. Res. 71:785-001.

17. Boller, B.R. and Stolov, H.L. (1970) Kelvin-Helmholtz instability and the semi-annual variation of geomagnetic activity, J. Geophys. Res. 75:6073.

18. Boller, B.R. and Stolov, H.L. (1974) Investigation of the association of magnetopause instability with interplanetary sector structure, J. Geophys. Res. 79:673.

19. Martin, E. and Aarons, J. (1977) F-layer scintillations and the aurora, J. Geophys. Res. 82:2717-2722. AFGL-TR-77-0182, AD A043 623.

20. Livingston, R.C. (1979) Micro-Wideband analysis summary output —Wideband beacon, Technical Memorandum, SRI International, Menlo Park, California.

21. Feldstein, Y.I. and Starkov, G.V. (1967) Dynamics of auroral belt and polar geomagnetic disturbances, Planet. Space Sci. 15:209.

22. Briggs, B.H. and Parkin, I.A. (1963) On the variation of radio star and satellite scintillation with zenith angle, J. Atmos. Terr. Phys. 25:339.

23. McIlwain, C.E. (1961) Coordinates for mapping the distribution of magnetically trapped particles, J. Geophys. Res. 66:3681.

24. Dyson, P.L., McClure, J.P., and Hanson, W.B. (1974) In-situ measurements of the spectral characteristics of ionospheric irregularities, J. Geophys. Res. 79:1497.

25. Phelps, A.D.R. and Sagalyn, R.C. (1976) Plasma density irregularities in the high-latitude top side ionosphere, J. Geophys. Res. 81:515. AFGL-TR-76-0077, AD A024 248.

26. Rino, C.L. (1979) A power law phase screen model for ionospheric scintillation. 1. Weak scatter, Radio Sci. 14:1135.

27. Whitney, H.E. and Basu, S. (1977) The effect of ionospheric scintillation on VHF/UHF satellite communications, Radio Sci. 12:123. AFGL-TR-77-0067, AD A037 520.

28. Rufenach, C.L. (1975) Ionospheric scintillation by a random phase screen: spectral approach, Radio Sci. 10:155.

29. Fremouw, E.J. and Lansinger, J.M. (1981) Recent high latitude improvement in a computer based scintillation model, Proceedings of Ionospheric Effects Symposium, Alexandria, Virginia.

30. Rino, C.L. and Owen, J. (1980) The structure of localized nighttime auroral zone scintillation enhancements, J. Geophys. Res. 85:2941.

31. Basu, S., Vesprini, R.L., and Aarons, J. (1973) Field-aligned ionospheric F-region irregularities and sporadic E, Radio Sci. 8:235. AFCRL-TR-73-0258, AD 760 853.

32. Ossakow, S.L. and Chaturvedi, P.K. (1979) Current convective instability in the diffuse aurora, Geophys. Res. Lett. 6:332.

33. Chaturvedi, P.K. and Ossakow, S.L. (1979) Nonlinear stabilization of the current convective instability in the diffuse aurora, Geophys. Res. Lett. 6:957.

34. Vickrey, J.F., Rino, C.L., and Potemra, T.A. (1980) Chatanika Triad observations of unstable ionization enhancements in the auroral E-region, Geophys. Res. Lett. 7:789.

35. Rino, C.L. (1981) Private communication.

36. Aarons, J., MacKenzie, E., and Rhoneard, K. (1980) High latitude analytical models for scintillation levels, Radio Sci. 15:115. AFGL-TR-80-0161, AD A090 499.

DNA Distribution List

Berkeley Research Assoc.
Attn: Clifford W. Prettie
P.O. Box 983
Berkeley, CA 94701

ESL, Inc.
Attn: J. Marshall
495 Java Drive
Sunnyvale, CA 94086

Def. Nuclear Agency
Attn: STTL Tech. Library
Washington, D.C. 20305

Mission Research Corp.
Attn: R. Bogush
735 State St.
Santa Barbara, CA 93101

Naval Research Lab.
Attn: Dr. John Goodman
Code 4110
Washington, D.C. 20375

Major R. Babcock
AWS/DNDP
Scott AFB, IL 62225

Major G. Wortham
AFGWC/WSE
Offutt AFB, NE 68113

Lt. P. Styczek
SACCA/CSS
Offutt AFB, NE 68113

Ed Skomal
Aerospace Corp.
Box 92957
Los Angeles, CA 90009

Allen L. Johnson
Air Force Avionics Lab
AFAL/AAAI
Wright Patterson AFB
Ohio 45433

Dow Evelyn
Def Nuclear Agency/RAAE
Washington, D.C. 20305

Major L. Wittwer
Def Nuclear Agency/RAAE
Washington, D.C. 20305

Major R. Sutton
SD/YKX
P.O. Box 92960
Worldway Postal Center
Los Angeles, CA 90009

Dr. H. Soicher
US Army Communication Res. and
Development Commons
Fort Monmouth, NJ 07703
(DRDCO-COM-RH-4)

SRI International
333 Ravenswood Ave.
Menlo Park, CA 94025
Attn: C. Rino

SRI International
333 Ravenswood Ave.
Menlo Park, CA 94025
Attn: R. Livingston

Physical Dynamics, Inc.
P.O. Box 3027
Bellevue, WA 98009
Attn: E.J. Fremouw

Dr. K. Davies
NOAA
Boulder, CO 80302

Dr. H. Mullaney
Code 427
Dept. of the Navy
Office of Naval Research
Arlington, VA 22217

Dr. George Millman
General Electric Co.
Building 9, Room 46
Court Street Plant
Syracuse, NY 13201

Prof. K.C. Yeh
University of Illinois
Dept. of Electric Engineering
Urbana, IL 61801

Dr. Warren Brown
Sandia Lab
ORG 5410A
Albuquerque, NM 87115

Dr. C.H. Liu
60 Electrical Engineering Building
University of Illinois
Urbana, IL 61801

Dr. S. Ossakow
Plasma Dynamics, Code 7750
U.S. Naval Research Lab
Washington, D.C. 20390

Dr. Phil McClure
U. of Texas at Dallas
Richardson, TX 75080

Prof. H.G. Booker
Dept. of Applied Physics
U. of Calif. at San Diego
La Jolla, CA 92037

Prof. Michael Kelley
Dept. of Elect. Engineering
Cornell University
Ithaca, NY 14850

Prof. W.B. Hanson
U. of Texas at Dallas
Richardson, TX 75080